Department of Geomatics Engineering

Interference Effects on GPS Receivers in Weak Signal Environments
(URL: http://www.geomatics.ucalgary.ca/links/GradTheses.html)

by

Nyunook Kim

January 2006

UNIVERSITY OF CALGARY

Interference Effects on GPS Receivers

in Weak Signal Environments

by

Nyunook Kim

A THESIS

SUBMITTED TO THE FACULTY OF GRADUATE STUDIES

IN PARTIAL FULFILMENT OF THE REQUIREMENTS FOR THE

DEGREE OF MASTER OF SCIENCE

DEPARTMENT OF GEOMATICS ENGINEERING

CALGARY, ALBERTA

January, 2006

Abstract

This thesis investigates how GPS receivers react to Radio Frequency interference. Many interference sources such as active TV antennas and ultra wideband devices are present all around the world. Interference effects depend on receiver design and types of interference, making the analysis of interference effects a multi-dimensional task.

In this research, known interference sources and GPS standards for interferences are first discussed. Then, a software receiver and a software GPS signal simulator are used to conduct selected investigations as they provide flexibility by their nature, e.g. the receiver parameters can easily be changed and interference can be simulated under specific and controlled conditions. The impact of selected receiver parameters are investigated, namely the number of quantization bits, the code tracking loop bandwidth and correlator spacing. Also, two commercial GPS receivers are tested under interference using a hardware GPS signal simulator. One of the two receivers is a high sensitivity unit that can operate under attenuated signal conditions and that is designed primarily for mobile phone location. Finally, a receiver autonomous integrity monitoring (RAIM) method is discussed to deal with continuous wave interference effects on position solutions.

Table of Contents

List of Tables

List of Figures and Illustrations

List of Symbols, Abbreviations and Nomenclature

AGPS	Assisted Global Positioning System
AMPS	Analog Mobile Phone Service
BLWNI	Band-Limited White Noise Interference
C/A	Coarse Acquisition
C/N$_0$	Carrier-to-Noise density ratio
CDMA	Code Division Multiple Access
CW	Continuous Wave
CWI	Continuous Wave Interference
dB	Decibel
dBc	Decibels relative to unmodulated Carrier power
dBW	Decibels with respect to 1 Watt
DOP	Dilution Of Position
DLL	Delay Lock Loop
E-911	Enhanced-911
EIRP	Effective Isotropic Radiated Power
EMC	Electro-Magnetic Compatibility
FCC	Federal Communications Commission
FDE	Fault Detection and Exclusion
FIR	Finite Impulse Response
FM	Frequency Modulation
GBAS	Ground-Based Augmentation System
GDOP	Geometric Dilution Of Position
GPS	Global Positioning System
GSM	Global System for Mobile communications
HDOP	Horizontal Dilution Of Position
HSGPS	High Sensitivity GPS
I&D	Integration and Dump
I/S	Interference to Signal power ratio

ITU	International Telecommunication Union
LOS	Line of sight
MOPS	Minimum Operational Performance Standard
NCO	Numerically Controlled Oscillator
PC	Personal Computer
PCS	Personal Communication Services
PLAN	Position Location And Navigation
PLL	Phase Locked Loop
PRF	Pulse Repetition Rate
RAIM	Receiver Autonomous Integrity Monitoring
RFI	Radio Frequency Interference
RTCA	Radio technical commission for aeronautics
SBAS	Space-Based Augmentation System
SNR	Signal-to-Noise power Ratio
TDMA	Time Division Multiple Access
UHF	Ultra High Frequency
UWB	Ultra Wide Band
VDOP	Vertical Dilution Of Position
WAAS	Wide Area Augmentation System
WN	White Noise

CHAPTER ONE: INTRODUCTION

1.1 Background

GPS has become an integral part of navigation for many applications, both military and civilian, for which accuracy and reliability are important user considerations. Applications on the civilian side include Enhanced-911 (E-911) location services. However, the operation of a GPS receiver can be severely limited or completely disrupted in the presence of radio frequency interference. As consumer demand for personal mobile communication system utilization increases and the radio frequency spectrum becomes more occupied, the threat of interference to GPS increases (Zhodzishsky et al 2002). Furthermore, the U.S. Federal Communications Commission (FCC) approved the commercial use of ultra wide band (UWB) technology, which is another potential interference source for GPS.

With advances in receiver technology, high sensitivity receivers can track weak signals, e.g., in the range of -180 dBW; however, the E-911 mandate requires GPS receivers to provide a position solution under any kind of environment (FCC Report 2003). At a low level of signal power, jamming may originate, for instance, in low power sources associated with normal operations such as plant operations inside a building. Also, emissions close to the receiver result in a high level of interference power at the receiving antenna (Phocas et al 2004).

Interference effects are a function of the types of interference as well as receiver characteristics (Forsell et al 2003). Since the GPS frequency bands are protected by FCC, most of the unintentional disruptions occur due to the harmonics coming from broadcasting antennas, personal electronic devices and UWB applications. In a GPS C/A code receiver, a source of interference whose bandwidth is larger than 1 kHz is regarded as wideband interference because of the repetition rate of the C/A code. The harmonics from AM/FM/CDMA transmissions are considered as a source of wideband interference, while emissions from UWB applications will generate a continuous wave (CW) or CW-like signal (Phocas et al 2004).

Owing to the intrinsic characteristics of a software program, a software receiver and software GPS signal generator provide flexibility in system design. The receiver parameters including front-end parameters can be easily changed to investigate algorithms to combat interference. Thus, this flexibility enables the study of interference effects based on the receiver parameters (Ma et al 2004).

Most modern receivers employ an integrity monitoring technique to improve receiver performance in terms of accuracy and reliability. The two methods commonly used for GPS integrity monitoring are: (i) receiver autonomous integrity monitoring (RAIM); and (ii) the wide area augmentation system (WAAS) (Kaplan 1996). The RAIM technique is designed for over-determined solutions to identify and exclude blunders in the data by means of a consistency check. Since

GPS signals subjected to interference result in degraded GPS accuracy and reliability, this scheme offers practical improvements in environments where interference is a significant concern.

1.2 Relevant Research

The Volpe report (2001) on GPS vulnerability identified real worldwide interference problems caused by unintentional disruptions such as harmonics from TV transmitters as well as intentional disruptions such as GPS jammers. The report concluded that GPS is vulnerable to interference effects that can be reduced but not entirely eliminated. The potential consequences on navigation operations can be severe in terms of safety and environmental and economic damage.

Research has also been conducted on UWB interference and its impacts on GPS receiver performance. Titus et al (2002) provided a simple and straightforward technical method for analyzing UWB interference effects on GPS and conducted a series of UWB interference tests using three commercial receivers. Luo et al (2000) presented UWB interference test results that show that the impact of UWB is strongly dependent on the location of the UWB spectral lines relative to the GPS spectrum around the carrier frequency.

Forsell & Olson (2003) carried out performance tests on three commercial receivers for seven different types of interference and showed that the jammer-to-signal ratio values causing loss of navigation capability are quite distinct for different receiver models.

Betz (2002) developed expressions to describe the effect of narrowband interference on code tracking accuracy and carrier-to-noise ratio, which shows that interference at a frequency mid-way between the carrier and the first null has the greatest overall effect. Also, the expressions depend on the early-late spacing, the integration time, the unjammed carrier-to-noise density ratio, and the tracking loop's equivalent rectangular bandwidth.

Deshpande (2004) analyzed the interference effects on the acquisition process. RF interference distorts the autocorrelation peak and leads to false acquisition. However, the power required to prevent or jam the acquisition process largely depends on the type of interference. A relative continuous wave interference (CWI) power of 15 dB (-145 dBW) is needed to jam this process, while a relative FM power of 35 dB is needed.

Karunanayeke et al (2005) investigated acquisition and tracking performance of an assisted GPS receiver (AGPS), SiRFLoc[TM] along with a high sensitivity (HS) receiver (SiRF XTrac) under three types of in-band interference: CW, AM, FM. In tracking mode, the AGPS and High Sensitivity (HS) receivers were able to track

up to 40 dB relative CW (at L1) interference power. However, the tracking thresholds were 10 dB and 20 dB higher than the acquisition thresholds for the AGPS and HS receiver, respectively.

Ma et al (2004) implemented a post-mission GPS software receiver, GNSS_SoftRx™. Dong et al (2004) developed a simulator, GPS_IFGen™ based on a mathematical model geared for the intermediate frequency. The performance of the software GPS signal simulator was verified along with the GNSS_SoftRx™, using a hardware GPS signal simulator, namely the GSS 6560 by Spirent Communications Co. Such software approaches offer many advantages in studying GPS signal characteristics and receiver performance as they can be reconfigured at will. On the other hand, data size and speed are limited, so that the software approach can, at best, model specific discrete cases of receiver operation.

Kuusniemi & Lachapelle (2004) analyzed reliability testing schemes for degraded GNSS signals in urban environments with the use of a high-sensitivity GPS (HSGPS) receiver (SiRF XTrac-LP™). Fault detection and exclusion (FDE) techniques were observed to improve overall accuracy, especially when using a HDOP cut-off. These results also show the difficulty of implementing FDE methods in urban environments due to the lack of redundancy.

1.3 Research objectives

The overall objective of this thesis is the analysis of interference effects on L1 C/A code GPS receivers in tracking mode. If any interference signal exists in acquisition, this may cause a false acquisition of Doppler frequency and chip delay. This is discussed in detail by Deshpande (2004). When the initial values of the tracking loops are not correct due to false acquisition, the tracking loop may lose the ability to track those satellites. If the required redundancy of available satellites is achieved, falsely acquired satellites are not used in position calculation. On the other hand, if any interference signal is initiated in tracking mode, this degrades the accuracy and introduces uncertainties into the determination of a position solution.

Because the effects of interference will differ depending on the origin and characteristics of the particular type of interference experienced, continuous wave interference (CWI) with various centre frequencies are investigated herein, as well as narrowband interference with a selection of bandwidths. In the selection of these particular explorations, the analyses focus on the effects of different types of interference with respect to signal integration time, the number of quantization bits, the code tracking loop bandwidth, correlator spacing in static mode using a software receiver and software GPS signal simulator.

Also, this thesis includes an analysis of interference effects on a commercial off-the-shelf HSGPS receiver. The receiver parameters are determined by application. The XTrac from SiRF Technology inc. is a high-sensitivity receiver with a distinct tracking threshold, which means that it allows measurements of attenuated signals with respect to line of sight (LOS) signals in environments where measurements were previously unavailable (MacGougan 2003). A low cost (several hundred $US) CMC Allstar receiver is also used to compare this standard L1 C/A code receiver to the high sensitivity receiver.

An additional topic warranting investigation herein is indoor applications where signal blockage may occur while the receiver may experience high dynamics. Since the hardware simulator provides the tools for changing dynamics conveniently, these tests are performed using both a hardware simulator and a hardware receiver. In summary, the research contribution of this thesis can be described as the analysis of interference effects on two commercial GPS receivers developed for distinct purposes. This analysis includes different signal power levels in static mode.

Finally, accuracy and reliability assessments are discussed under CWI interference environments through the use of the RAIM technique based on a least-squares residual check. Pseudorange measurements from the XTrac receiver are used in this analysis.

1.4 Thesis outline

Chapter 2 describes interference effects at each stage of the receiver. This also includes a presentation of tracking loop errors and a carrier-to-noise ratio analysis. Chapter 3 describes possible interference sources from licensed transmitters. Measurements of interference levels in both laboratory conditions and downtown Calgary are also included. Chapter 4 contains an analysis of the interference effects using a software receiver and software simulator. This chapter presents a comparison of tracking loop errors, and carrier-to-noise ratio and quantization effects for different types of interference. Chapter 5 presents the analysis of test results of two models of commercial receivers under: (i) weak signal and interference; and (ii) dynamic mode and interference environments. Chapter 6 presents the assessment of position accuracy under CWI using the RAIM technique. Finally, conclusions drawn from this work, and recommendations for future research, are presented in Chapter 7.

CHAPTER TWO: INTERFERENCE EFFECTS ON GPS
RECEIVERS

The GPS signal employs direct sequence spread spectrum signal through the use of a pseudo random noise C/A code. This feature provides a processing gain with respect to the RF interference component, especially to narrow band interference. This chapter begins with a description of the interference effects on the receiver at each stage. Next, the carrier-to-noise ratio due to non-white interference is described, with respect of its role as an indicator of signal quality. Finally, tracking loop errors which determine the tracking thresholds are discussed under both white noise and coloured noise interference conditions.

2.1 Interference Effects during Signal Processing

Figure 2.1 shows the simplified block diagram of a generic hardware receiver. The key functions of a GPS receiver are to acquire and track the GPS signal in order to estimate the Doppler shift and pseudorange based on the transmission time from each satellite to the receiver antenna. The functional behaviour of the receiver is described in detail in Kaplan (1996) and Van Dierendonck (1996).
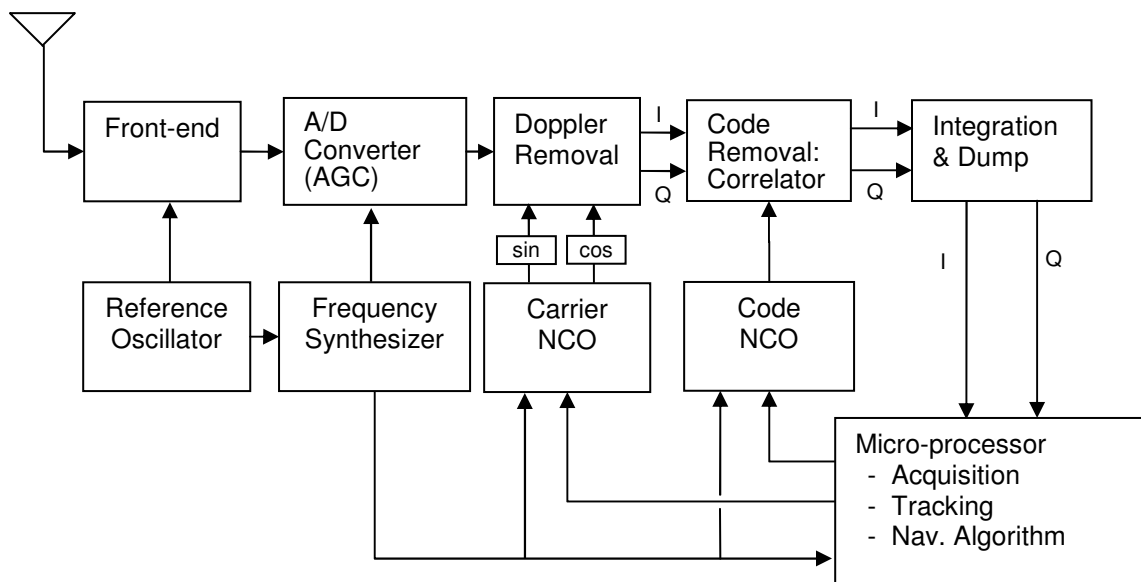
Figure 2.1: Generic Receiver Block Diagram (after Van Dierendonck 1996)

2.1.1 Interference at antenna

The RF interference signal from the transmission antenna suffers the effects of free-space loss. The effective noise power density at the receiver is defined as (Titus et al 2002):

$$J_r = ERPD_j - L_p \text{ [dB/Hz]} \tag{2.1}$$

where $ERPD_j$: Effective radiated power density of the jamming signal,

[dB/Hz]

$$L_p = 20 \log \left(\frac{4\pi d}{\lambda_j} \right) : \text{Free-space Loss, [dB]}$$

Path loss is a function of the frequency of the signal and separation distance and produces an increase in the noise floor. The noise floor increase is given by:

$$NF_{INC} = 10\log(10^{J_r/10} + 10^{NF_{GPS}/10}) - NF_{GPS} \qquad (2.2)$$

where NF_{INC} : Noise floor increase due to RF interference, [dB]

NF_{GPS} : GPS noise floor with no interference, [dB/Hz]

The out-of-band signal is rejected by the antenna and front-end bandpass filter. On the other hand, the in-band signal passes through the antenna and front-end band pass filter. Also, white noise interference becomes band-limited white noise due to this filter.

2.1.2 Sampling and Quantization

Sampling and quantization are essential elements of the digital processing of the signal. Sampling frequency is determined by Nyquist's theorem based on the front-end bandwidth in order to eliminate aliasing effects. To avoid the effects of aliasing, the sampling rate must be larger than twice the bandwidth of the front-end bandpass filter. Since band-limiting rounds the correlation peak, the performance of a narrow correlator is influenced by the pre-correlation bandwidth. Hence, a faster sampling rate should lower the correlator spacing.

Figure 2.2 shows a quantization mechanism for a 3-bit quantizer, where L denotes the maximum quantization threshold and Δ is the quantization interval. In order to minimize the quantization loss, the L value is set based on the standard deviation of the thermal noise under the assumption of Gaussian white noise. Thus, if a multi-bit quantizer is used in the receiver, automatic gain control is required to optimize the L value and to suppress the level of interference. In the case of a 1-bit quantizer, the signal-to-noise ratio (SNR) degradation after quantization is 1.96 dB while, in the case of a 3-bit quantizer, the minimum degradation is 0.16 dB with $L = \sqrt{3} * \sigma$ (Spliker & Natali 1996).
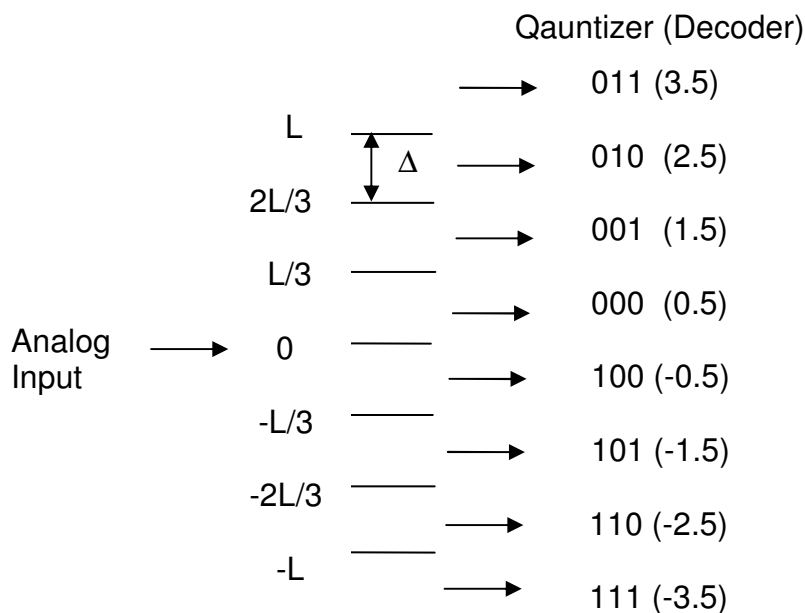
Figure 2.2: Quantization Mechanism for 3-bit Quantization

The expected value, E[m(t)], and mean square, Var[m(t)], of the quantizer and correlator output m(t) is, according to Spliker & Natali (1996):

$$E[m(t)] = \sum_{n=-M}^{M-1} \left(n + \frac{1}{2}\right)\left\{\mathbf{P}\left(Q = n + \frac{1}{2}, D = +1\right) - \mathbf{P}\left(Q = n + \frac{1}{2}, D = -1\right)\right\}\frac{1}{2}$$

$$\text{(2.3)}$$

$$\text{Var}[m(t)] = \sum_{n=-M}^{M-1} \left(n + \frac{1}{2}\right)^2 \left\{\mathbf{P}\left(Q = n + \frac{1}{2}, D = +1\right) + \mathbf{P}\left(Q = n + \frac{1}{2}, D = -1\right)\right\}\frac{1}{2}$$

where $\mathbf{P}\left(Q = n + \frac{1}{2}, D = +1\right)$: probability that Q=n+1/2 given that D= +1

M : Number of quantization bits

Q[·] : Quantizer output

D : Data bit =+/- 1 with equal probability

The degradation in quantizer-correlator output vs. input signal-to-thermal noise ratio is then

$$\text{Degradation} = \frac{\dfrac{[E(m)]}{\sqrt{\text{Var}(m) - [E(m)]^2}}}{\dfrac{1}{\sigma_0}}$$

$$\text{(2.4)}$$

where σ_0 : Variance of the thermal noise

Figure 2.3 depicts the degradation in the presence of frequency offset interference, u(t)=Kcos(ωt+θ) with Δ=0 for 1 bit, $\Delta = \sqrt{\sigma^2 + K^2}$ for 2 bits, $\Delta = \sqrt{\sigma^2 + K^2}/\sqrt{3}$ with Gaussian white noise with σ =10 when θ is uniformly distributed. The difference in the SNR degradations between 1-bit and 3-bit

quantizers escalates with an increase in the amplitude of interference, K, especially when the amplitude of interference is less than 50. For a 3 bit quantizer, the optimal quantizer interval for the frequency offset interference has a value of $\Delta = \sqrt{\sigma^2 + K^2}$ (Spilker & Natali 1996). With this optimal spacing, the 3 bit quantizer shows a similar trend of SNR degradation to that of the 2 bit quantizer. However, this spacing is not good for white noise only.
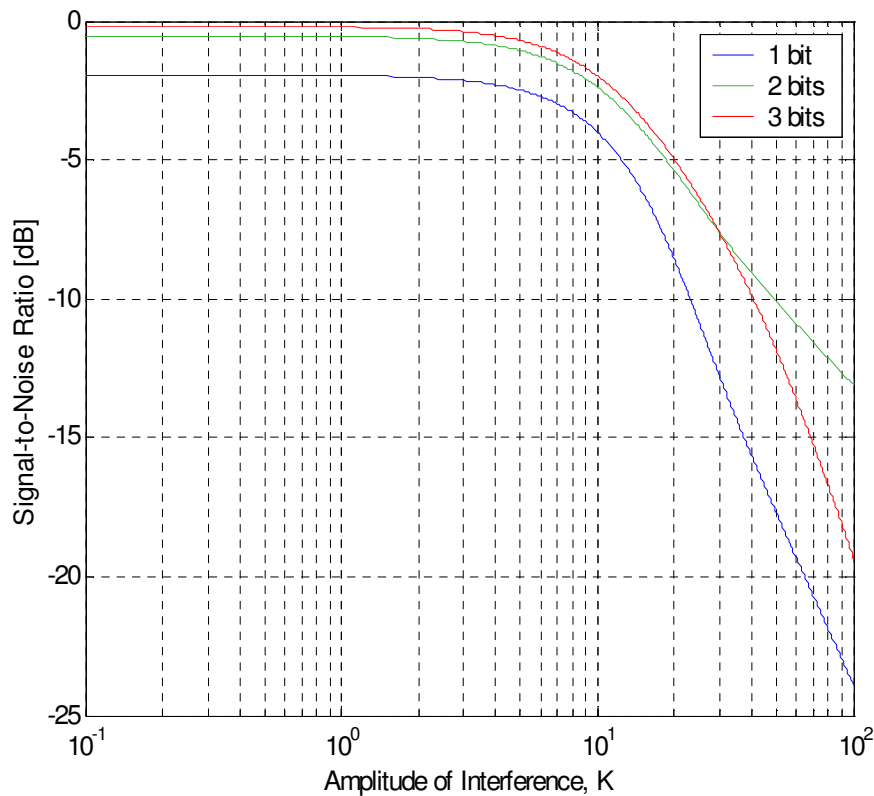
Figure 2.3: Quantizer-correlator Degradation vs. Amplitude for Frequency Offset Interference. Gaussian noise is present with σ_0 =10. Quantizer spacing =0 for 1 bit; Quantizer spacing = $\sqrt{\sigma^2 + K^2}$ for 2 bits; and Quantizer spacing = $\sqrt{\sigma^2 + K^2}/\sqrt{3}$ for 3 bits.

2.1.3 Interference after Doppler removal and correlation processes

Where a non-white interference signal is present, the expression of the incoming signal at the down-converter output, neglecting sampling and quantization, V(t) is:

$$V(t) = A \times D(t - \tau)C(t - \tau)\cos(2\pi(f_I + f_D)t + \theta) + u(t) + n(t) \qquad (2.5)$$

where   A : Signal amplitude

τ : Propagation delay

D(t-τ) : Navigation message

C(t-τ) : C/A code

f_I : Intermediate frequency

f_D : Doppler frequency

θ : Carrier phase

u(t) : Unwanted non-white interference signal

n(t) : White noise

If the estimations of τ, θ are exact and an ideal front-end filter is assumed, the in-phase component of the second term after the correlation process is (Hegarty 2002):

$$m_{uI}(t) = \frac{1}{\sqrt{2}}u_I(t)C(t) \qquad (2.6)$$

The autocorrelation of $m_{ul}(t)$ is:

$$
\begin{aligned}
R_m(\tau) &= E[m_{ul}(t+\tau)m_{ul}(t)] \\
&= \frac{1}{2}E[u_l(t+\tau)u_l(t)c(t+\tau)c(t)] \\
&= \frac{1}{2}R_u(\tau)R_c(\tau)
\end{aligned}
\tag{2.7}
$$

The autocorrelation of (2.7) is:

$$
\begin{aligned}
S_m(f) &= \frac{1}{2}S_u(f) * S_c(f) \\
&= \frac{1}{2}\int_{f_1=-\infty}^{f_1=\infty} S_u(f_1)S_c(f-f_1)df_1
\end{aligned}
\tag{2.8}
$$

As shown in equation (2.8), the power spectrum of the non-white interference signal is the convolution integral of the power spectrum of u(t) and the C/A code spectrum. Figure 2.4 shows simplified spectra of the interference and correlator output for different interference bandwidths. As the C/A code spectrum are comprised of spectral lines that are 1 kHz apart due to the repetition rate, RFI energy can pass through the correlation process when one of the C/A spectral lines coincides with the RFI spectrum in a case of narrowband interference, e.g., bandwidth < 10 Hz. In addition, since the C/A code line spectrum is not a perfect sinc curve, it has a strong frequency line, the so-called worst line spectrum. If the narrow-band interference signal spectrum reaches this worst line, the interference signal is multiplied by this power spectrum, thus causing severe degradation of performance. However, this is a rare occurrence.
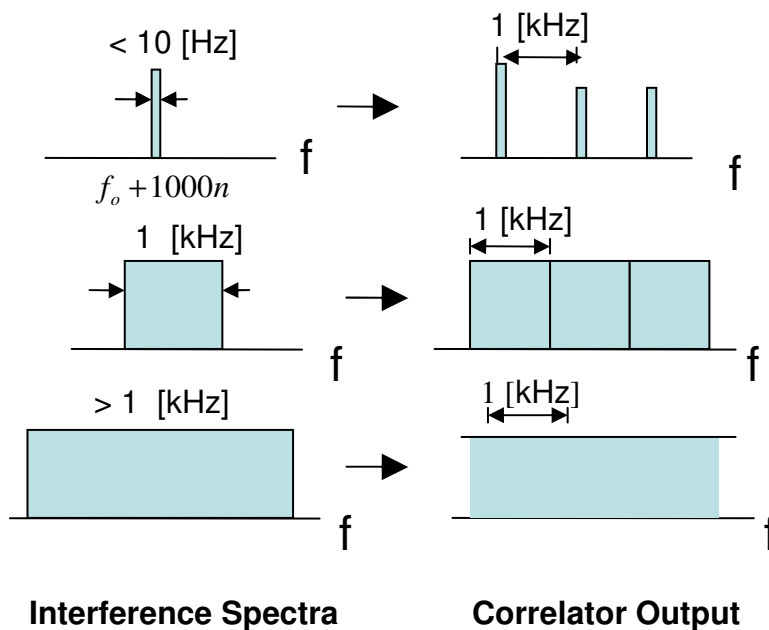
Figure 2.4: Simplified spectra of the interference input and correlator output for various interference bandwidths (after Spilker & Natali 1996)

In the case of continuous wave interference, $u(t) = A_J \cos(2\pi f_J t)$, we can rewrite the integration and dump (I&D) output (Macabiau et al 2001) as

$$m_{uI}(t) = \frac{A}{2} D(t) R(\tau - \hat{\tau}) \cos(\theta - \hat{\theta})$$

$$+ \frac{A_J}{2} T_{int} |C_{sinc}(k_0)| \frac{\sin(\pi \delta f T_{int})}{\pi \delta f T_{int}} \cos(2\pi k_0 f_R \hat{\tau} + \varphi(t)) \qquad (2.9)$$

$$+ n_I(t)$$

where f_R : 1 kHz

$\delta f : k_o f_R - \Delta f$

$C_{\sin c}(k_o)$ (or C_I) : Magnitude of $k_o{}^{th}$ C/A code line spectrum

k_o : Index of the C/A code spectrum line such that

$$k_0 f_R \in \left[\Delta f - \frac{f_R}{2}, \Delta f + \frac{f_R}{2} \right]$$

$$\Delta f = f_{L1} - f_J$$

$$\varphi(t) = 2\pi(\Delta f - k_o f_R)\frac{t}{2} - (\theta_J - \hat{\theta}) + \varphi(k_0)$$

According to the second term in equation (2.9), the multiplexer output due to interference is a function of the magnitude of the nearest C/A code line spectrum, $C_{sinc}(k_0)$, to the centre frequency of the jammer as well as the frequency difference between this line spectrum and the centre frequency of the jammer, δf. This will be at its maximum within 1 kHz of the frequency at which the interference line spectrum hits the C/A code line spectrum. The interference-to-signal power ratio (I/S) at the correlator input to the I/S at the correlator output is the so called processing gain which is achieved by the spread spectrum signal. The processing gain against CWI from (2.9) is (Godefroy 2004):

$$PG = \frac{1}{|C_I|^2 \sin c(\pi \cdot \delta f \cdot T_{int})} \tag{2.10}$$

Figure 2.5 shows the actual processing gain of PRN 6 whose worst line occurs at 227 kHz under CWI, with a different centre frequency following the fixing of the

Doppler frequency. As shown in this figure, the processing gain has a 20-30

dB difference within 1 kHz. Since the Doppler shifts can be different for each

satellite, the signal for one satellite in view may be affected by the CWI, while

others are not. If the falsely locked satellite is used in the position solution in the

absence of a RAIM algorithm (or lack of redundancy), misleading or hazardous

information may result.
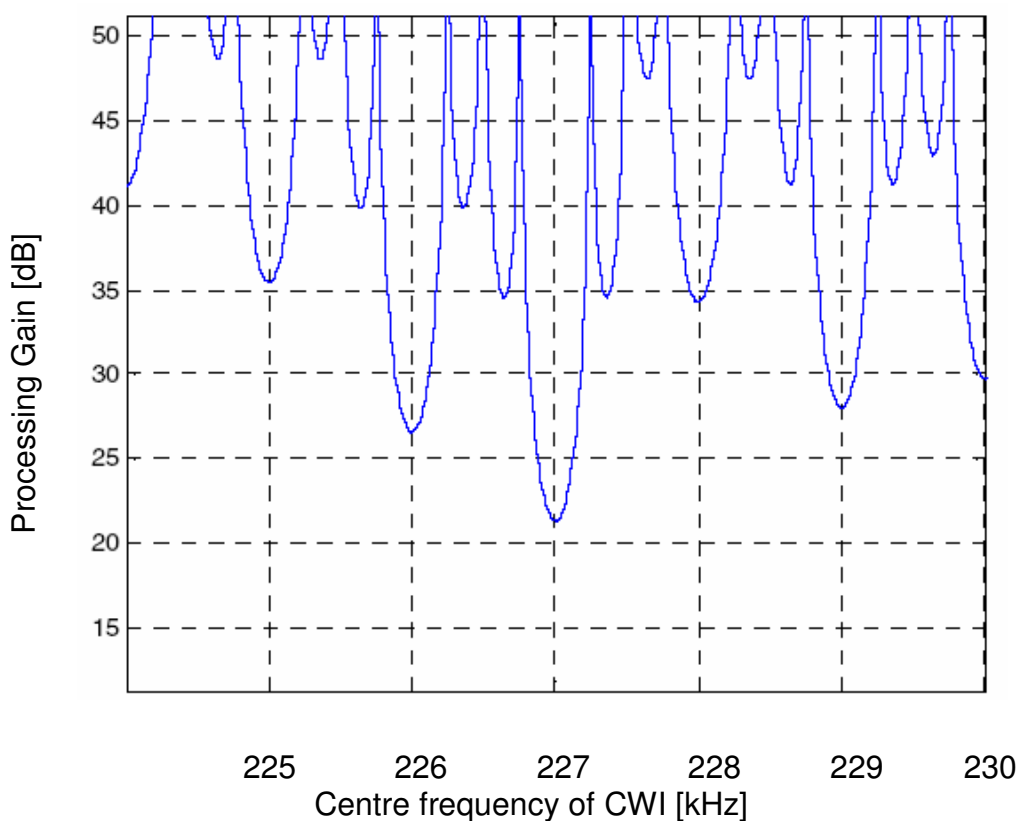
Figure 2.5: Processing Gain for PRN 6 under CWI (from Godefroy 2004)

On the other hand, if the bandwidth of the interference is 1 kHz or wider, the

interference signal is replicated by the C/A spectrum, resulting in a wide-band

signal. Thus, if the bandwidth of the interference is 1 kHz or wider, this can be regarded as wideband interference in a GPS receiver. Table 2.1 shows the effective noise power in case of wide-band interference.

Table 2.1: Effective Noise Power in case of Wide-band Interference

(from Spilker & Natali 1996)

Interference BW	Effective Noise Due to Wide-band Interference
1 kHz	$P_u P_n /10^3$
10 kHz	$\sim= P_u /10^6$
100 kHz-1 MHz	$P_u /10^6$

P_u : Interference Power

P_n : Relative power of the n-th line component of C/A code

2.2 Interference Effects on Carrier-to-Noise Ratio

The carrier-to-noise density ratio (C/N_0) is an important parameter which indicates the signal quality at the receiver. The C/N_0 is a ratio of carrier power to the noise density level, expressed in dB-Hz. In theory, the carrier-to-noise density ratio is independent of the receiver type.

It is well established that RF interference degrades the C/N_0. When a GPS receiver displays an unexpected C/N_0 at a certain location, this could be the result of RF interference. The effective C/N_0 under the assumption of ideal power spectrum of the signal is (Betz 2004):

$$\left(\frac{C}{N_0}\right)_{eff} = \frac{\left(\dfrac{C_S}{N_0}\right)\displaystyle\int_{-\frac{\beta_r}{2}}^{\frac{\beta_r}{2}} sinc^2(\pi fT_c)df}{\displaystyle\int_{-\frac{\beta_r}{2}}^{\frac{\beta_r}{2}} sinc^2(\pi fT_c)df + \frac{C_I}{N_0}\int_{-\frac{\beta_r}{2}}^{\frac{\beta_r}{2}} G_I(f)G_s(f)df} \tag{2.11}$$

where $G_s(f)$: Normalized power spectrum of the signal

$G_I(f)$: Normalized power spectrum of the interference

C_S : Signal power

C_I : Interference power

N_0 : Power spectral density of noise

β_r : Front-end bandwidth (one-sided)

Figure 2.6 shows the C/N_0 estimation for the different unjammed C/N_0 values in the case of wide-band interference when the bandwidth of the interference is larger than 2 MHz. As shown in this figure, when the interference signal is relatively low, the unjammed C/N_0 contributes to the effective C/N_0, while an interference power level of above 40 dB of I/S dominates the effective C/N_0.
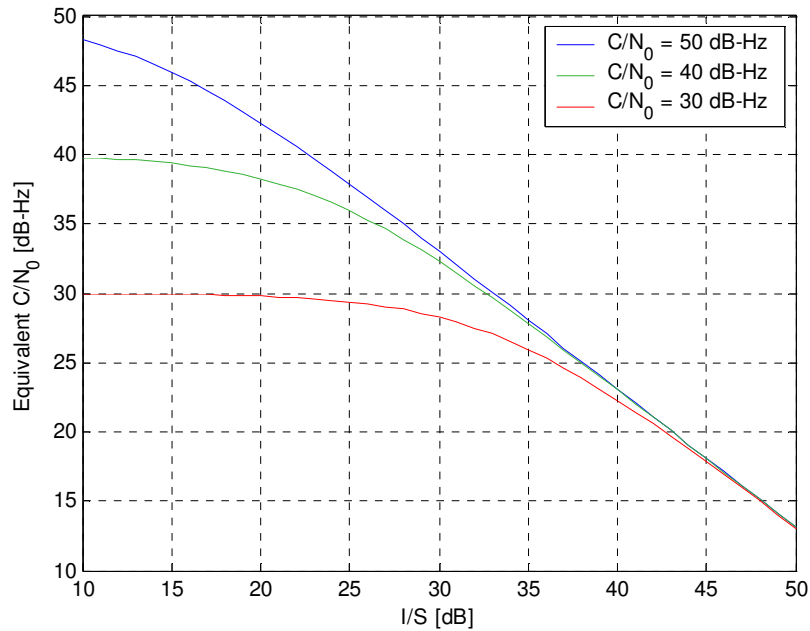
Figure 2.6: Equivalent C/N$_0$ for different unjammed C/N$_0$

Figure 2.7 shows the effective C/N$_0$ estimation for pure tone interference for different centre frequencies over the range of the main lobe of the C/A code spectrum under the assumptions of an ideal 2 MHz bandwidth of the front-end band-pass filter and an ideal signal spectrum. As shown in this figure, a CWI whose centre frequency is close to that of the L1 degrades the effective C/N$_0$ most readily due to correlation.
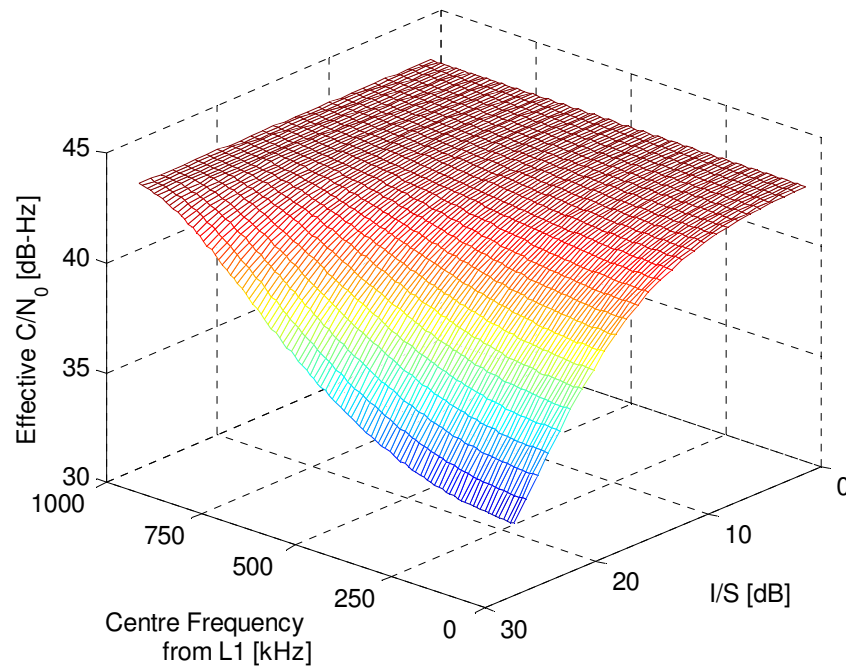
Figure 2.7: Effective C/N$_0$ for Continuous Wave Interference

2.3 Interference Effects on Tracking Loops

A GPS receiver has two tracking loops: a carrier tracking loop and a code tracking loop. The phase-locked loop (PLL) is used for carrier tracking, and the delay-locked loop (DLL) is used for code tracking. The errors of the tracking loop are reflected in the pseudorange and Doppler frequency estimations, respectively, which are used to calculate position and velocity. The tracking loop errors are well defined in the case of white noise (Kaplan 1996):

$$\sigma_{PLL} = \sqrt{\sigma_{PLLt}{}^2 + \sigma_v{}^2 + \theta_A^2} + \frac{\theta_e}{3} \leq 15°$$

$$\sigma_{PLLt} = \frac{360}{2\pi} \sqrt{\frac{B_L}{c/n_0}[1 + \frac{1}{2T_{int}c/n_0}]} \qquad [degree]$$

(2.12)

where σ_{PLLt} : Thermal noise jitter

σ_v : Vibration Induced jitter

θ_A : Allan variation-induced jitter

θ_e : Dynamic stress error (bias-like)

B_L: Bandwidth

T_{int}: Integration time

The thermal noise jitter is proportional to the square root of the bandwidth, while the Allan variation-induced jitter is inversely proportional to the bandwidth. Also, the dynamic stress error is proportional to the $1/(B_n)^k$ for a kth order loop. The bandwidth of the PLL should be determined based on the Allan variance of the reference clock and the dynamics of a loaded vehicle in order to maintain the tracking loop. However, the thermal noise jitter is treated as the only source of carrier tracking error because other sources are either transient or negligible.
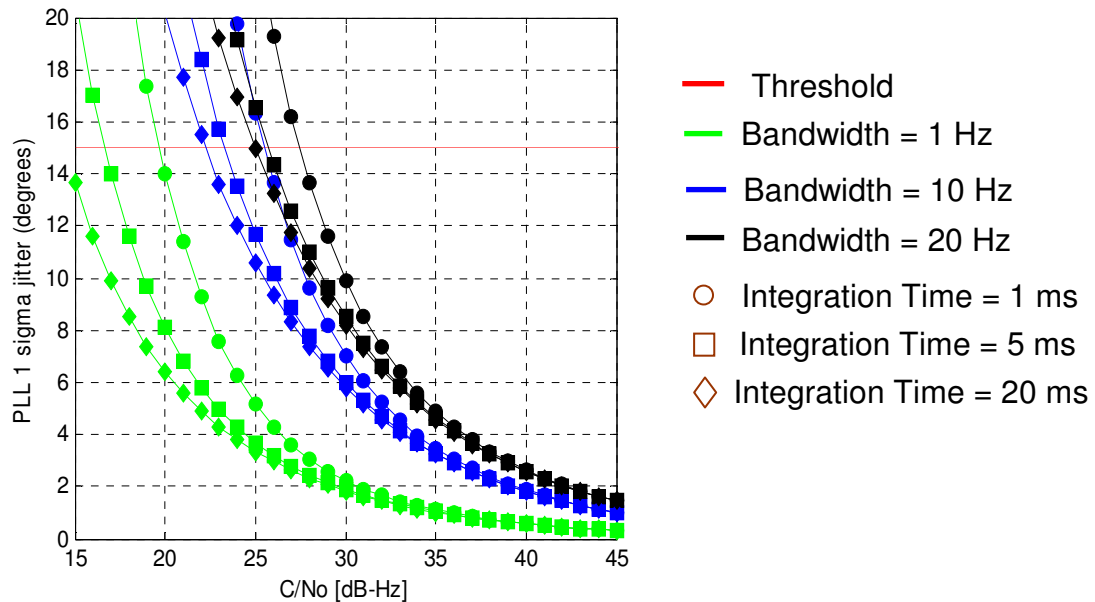
Figure 2.8: PLL 1-Sigma Jitter due to Thermal Noise

Figure 2.8 shows the PLL 1-sigma jitter due to thermal noise, as a function of bandwidth, integration time and C/N_0. For a digital loop approximation, the update rate should be larger than 5 to 10 times the loop bandwidth. As a result, if the integration time is 20 ms, the corresponding maximum bandwidth is 5-10 Hz.

The tracking threshold of the DLL is given by the following rule of thumb (Kaplan 1996):

$$\sigma_{DLL} \leq \frac{D}{6} \qquad \text{[Chips]} \qquad\qquad (2.13)$$

where D : Correlator spacing between early-late

The variance of DLL tracking loop error for non-coherent early-late processing is (Betz 2000):

$$\sigma_\tau^2(\text{Chip}) = \begin{cases} \dfrac{B_L\left(1-0.5B_L T_{int}\right)}{2\dfrac{C}{N_0}}D\left(1+\dfrac{2}{T_{int}\dfrac{C}{N_0}(2-D)}\right) & Db \geq \pi \\[3em] \dfrac{B_L\left(1-0.5B_L T_{int}\right)}{2\dfrac{C}{N_0}}\left(\dfrac{1}{b}+\dfrac{b}{\pi-1}\left(D-\dfrac{1}{b}\right)^2\right)\left(1+\dfrac{2}{T_{int}\dfrac{C}{N_0}(2-D)}\right) & 1 < Db < \pi \\[3em] \dfrac{B_L\left(1-0.5B_L T_{int}\right)}{2\dfrac{C}{N_0}}\left(\dfrac{1}{b}\right)\left(1+\dfrac{1}{T_{int}\dfrac{C}{N_0}}\right) & Db \leq 1 \end{cases}$$

(2.14)

where $b : T_C\beta_r$

T_c: Chipping Time

B_L: DLL Bandwidth

T_{int}: Integration Time

Figure 2.9 and Figure 2.10 show the DLL 1-sigma jitter when correlator spacing equals 1 chip and 0.1 chips, respectively.
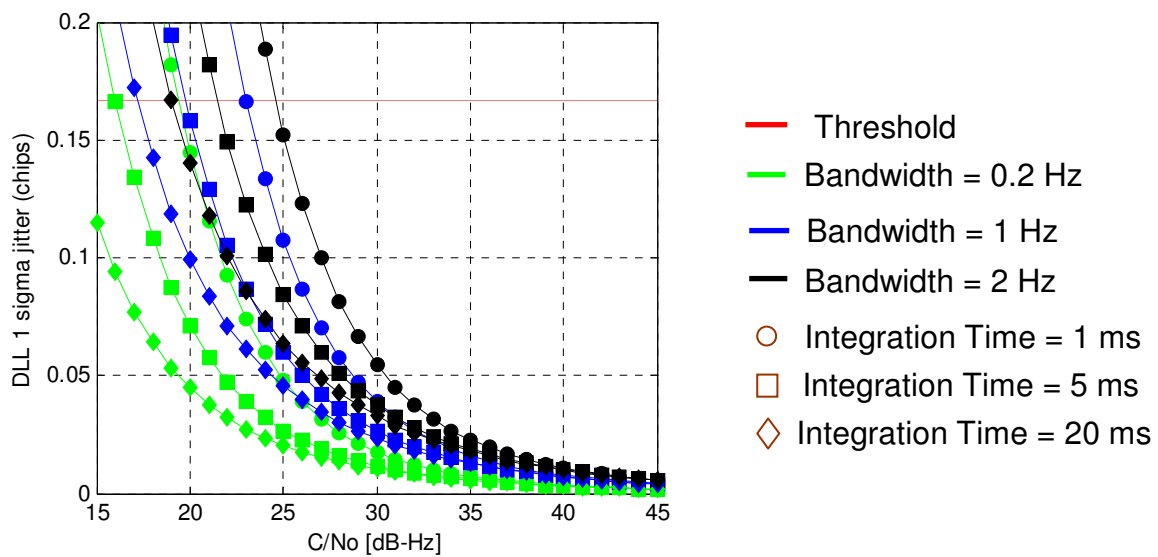
Figure 2.9: DLL 1-Sigma Jitter when E-L = 1 Chip
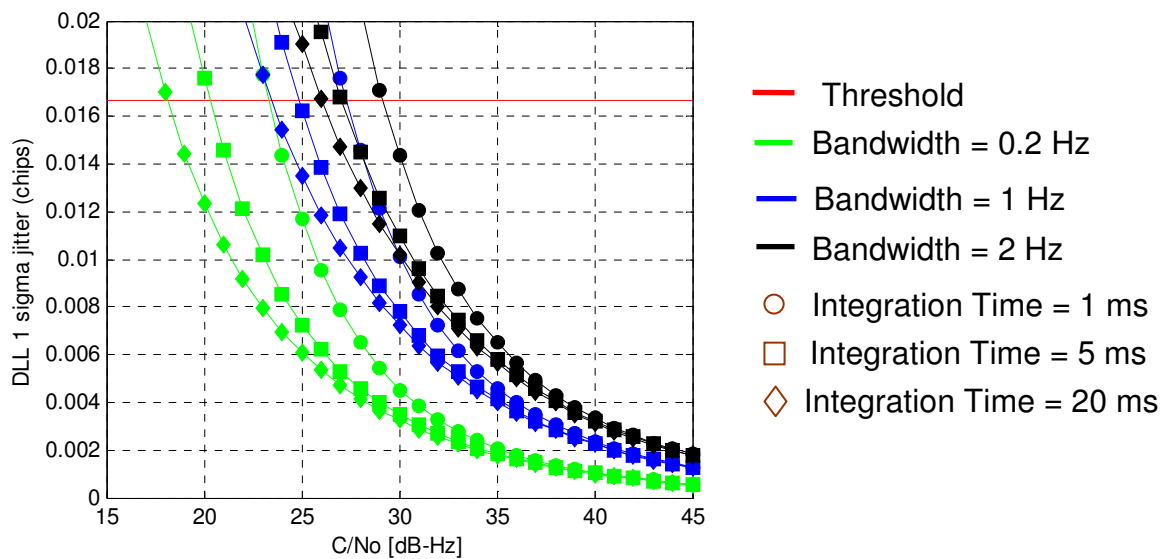
Figure 2.10: DLL 1-Sigma Jitter when E-L=0.1 chips

Also, the variance of code tracking errors associated with narrow band interference for coherent early-late processing are, as derived by Betz (2002):

$$\sigma^2_{CELP} = 2B_L T_{int}(1 - 0.5B_L T_{int}) \times \left[\frac{\int_{-\frac{\beta_r}{2}}^{\frac{\beta_r}{2}} G_s(f)\sin^2(\pi fD)df + \frac{C_I}{N_0}\int_{-\frac{\beta_r}{2}}^{\frac{\beta_r}{2}} G_I(f)G_s(f)\sin^2(\pi fD)df}{2(2\pi)^2 T_{int}\frac{C_s}{N_0}\left(\int_{-\frac{\beta_r}{2}}^{\frac{\beta_r}{2}} fG_s(f)\sin^2(\pi fD)df\right)^2} \right] \quad (2.15)$$

where $G_s(f)$: Normalized power spectrum of the signal

$G_I(f)$: Normalized power spectrum of the interference

C_S : Signal power

C_I : Interference power

N_0 : Power spectral density of noise

β_r : Front-end bandwidth (one-sided)
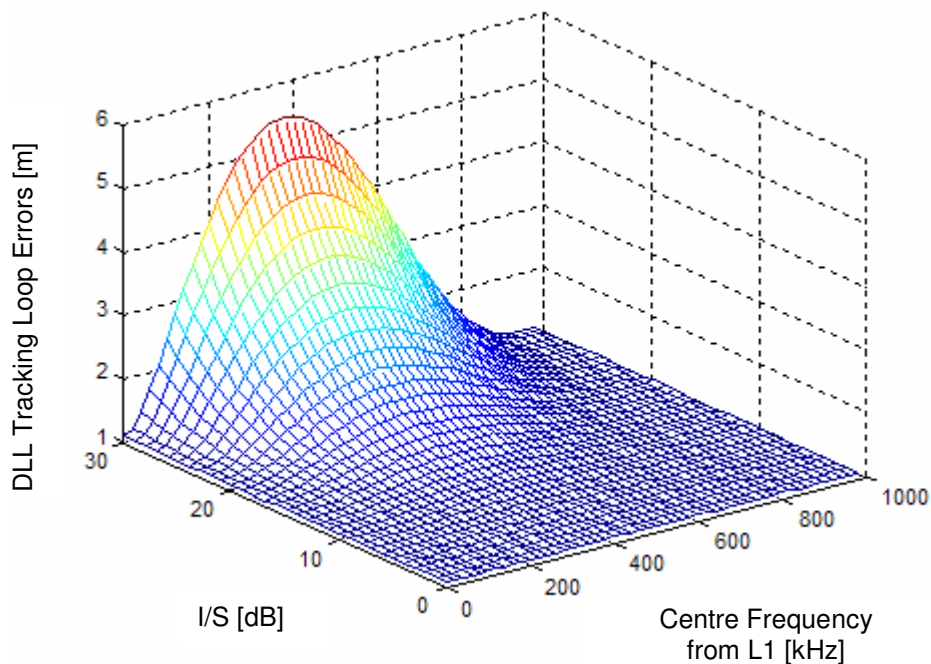
Figure 2.11: DLL 1-Sigma Jitter with CWI

Figure 2.11 shows the DLL 1-sigma jitter estimation for pure tone interference for different centre frequencies over the range of the main lobe of the C/A code spectrum under the assumptions of an ideal signal spectrum, an ideal 2 MHz bandwidth of the front-end band-pass filter and 1 chip correlator spacing. This figure shows that the CWI with a centre frequency mid-way between the carrier and the first null has a greater effect on code tracking, while the interference near the carrier frequency has little effect on the code tracking error.

CHAPTER THREE: INTERFERENCE SOURCES

Most of the interference associated with the GPS signal is unintentional, originating in transmitters built for communication purposes. This chapter describes sources of GPS interference reported in the literature. First, the GPS standards are described, followed by a discussion of the interference sources and their impacts on the receiver. This chapter also includes the interference measurements taken to classify and validate the interference sources in both the indoor environment and in the downtown area of Calgary.

3.1 GPS standards for interference

Receiver susceptibility thresholds defined by International Telecommunication Union (ITU) are summarized in Table 3.1 (Nguyen & Ely 2004). Also, Minimum Operational Performance Standards (MOPS) for the airborne antenna developed by RTCA Inc. indicates -110.5 dBm/MHz for broadband noise and -150.5 dB within L1 +/- 10 MHz (Nguyen & Ely 2004). Both standards have higher thresholds with larger bandwidth. However, since GPS Block II satellites have a 1.5 dB increase in the minimum user received GPS signal power, i.e. -158.5 dBW (IS-GPS-200D 2004), this provides more resistance to jamming signal.

Table 3.1: GPS Susceptibility Threshold at antenna

(from Nguyen & Ely 2004)

	SBAS	GBAS	Semi-codeless Receiver
Narrowband (Tracking mode)	-120.5 dBm	-120.5 dBm	-124.5 dBm
Narrowband (Acquisition mode)	-126.5 dBm	-126.5 dBm	-126.5 dBm
Wideband (Tracking mode)	-110.5 dBm/MHz	-110.5 dBm/MHz	-116.5 dBm/MHz
Wideband (aquisition mode)	-116.5 dBm/MHz	-116.5 dBm/MHz	-116.5 dBm/MHz

SBAS : Space-based Augmentation System
GBAS : Ground-based Augmentation System

3.2 Interference Sources from Licensed Transmitters

Potential sources of interference include offending sources at L1, or sources operating on a frequency well below or above that of GPS but having harmonic terms in the GPS band (Klinker & Piertersen 2000). A 1-Watt jammer causes lock loss within 10 km. However, this can be protected by using a P-code signal for high security missions such as military applications. For a dual frequency receiver, if an acceptable carrier-to-noise ratio on one frequency and a low value on the other frequency are observed at the same time, one may reasonably suspect the existence of RF interference (Butsch et al 2002).

Possible sources of unwanted interference include any RF signal from broadcasting and communication systems. Spurious emission is limited by ITU convention. The limitation on spurious emissions between 960 MHz and 17.7

GHz consists of a minimum 60 dB attenuation with respect to the level of the signal of interest (ITU 2002). In the case of high powered transmission, this may not be enough to protect against jamming of the GPS signal.

Portable wireless communication systems may have a significant impact on GPS reception over large areas. Since such electronic devices can be easily carried, the distance between the receiver and interference sources may be close. Also, many harmonic combinations of wireless devices (as shown in Table 3.2) that fall in the GPS band may cause interference (Nguyen & Ely 2002). These harmonics may be generated by the interaction of different wireless technology devices. NASA reported that a wide-band emission at a power level of -54 dBm from a CDMA mobile phone caused complete loss of GPS signal when the phone is on (Nguyen & Ely 2002).

Table 3.2: Mobile Operating Frequency

Wireless Technology	Handset Transmit Frequency [MHZ]
CDMA/TDMA/AMPS	824-849
GSM	880-915, 1710-1785
PCS	1850-1910
Bluetooth/802.11b	2400-2497, 2400-2483

AMPS: Analog Mobile Phone Service

TDMA: Time Division Multiple Access

CDMA: Code Division Multiple Access

GSM: Global System for Mobile communications

PCS: Personal Communication Services

Interference from TV signals has been observed in GPS operations worldwide. The U. S. Coast Guard, for instance, reported that an active UHF/VHF marine television antenna caused operational degradation in the performance of GPS receivers (USCG 2002). In Australia, a UHF channel 27 whose 3rd harmonic term falls in the GPS band is considered a source of interference with respect to GPS reception. The UHF antenna, whose effective isotropic radiated power (EIRP) is 480 kW, affects GPS signal reception at a distance of approximately 3.5 km, while the EIRP of some UHF transmitters exceeds 900 kW (AGNSSCC 2001). In addition, digital TV which employs an entirely different signal from analog TV should be taken into consideration (Volpe 2001)

UWB technology, which is envisaged for a variety of applications such as radar, imaging and communication fields, lays claim to 1.5 GHz or more of spectrum including the bands used by GPS (Titus et al 2002). Interference due to UWB is often considered as noise-like or CW-like interference. According to the FCC's Report and Order, the most strict emission levels are -75.3 dBm/Hz for noise and -85.3 dBm for CWI. The impact on GPS depends on UWB signal characteristics such as the pulse repetition rate (PRF) and duty cycle. Variations

in impacts on GPS can be explained by the location of UWB spectral lines with respect to the GPS spectrum around L1. As an example, UWB with a PRF of 19.94 MHz and a duty cycle of 100% causes loss of lock with the UWB power of -93.5 dBm when the simulated GPS power is -161 dBW, since one of its harmonics is located at 1575.26 MHz which is close to the L1 carrier frequency (Luo et al 2000). On the other hand, UWB with PRF of 100 kHz needs a power level of -55 dBm to jam the receiver under test.

An indoor receiver is required to operate at a signal power of -180 dBW or less. Owing to the operation of communication systems within occupied buildings, the antenna housed inside the building is likely to be close to sources of interference. Phocas et al (2004) indicated that electronic equipment that contains micro-processors and display screens are the most obvious interference sources to GPS. Furthermore, electromagnetic compatibility (EMC) measurements are made with less than 10 kHz bandwidth, thereby spreading the energy much wider and allowing a higher level of effective radiated power to by-pass the EMC regulations. In addition, typical EMC regulations limit the strength of radiated interference at a range of 10 metres. For indoor applications, there is a higher chance that the receiver will approach the interference sources within this distance.

3.3 Measurement of Interference Sources

This section intends to classify and validate the effects of interference sources in both the indoor environment and in the downtown area of Calgary. First, the test setup and validation of this test are discussed, followed by interference measurements.

3.3.1 Test settings

In order to measure the intensity of interference from the various sources, and since only GPS bands are of interest, a spectrum analyzer (Agilent E4402B) and NovAtel GPS-600-LB-GPS L1/L2 antenna were used, as shown in Figure 3.1. A two-way splitter was used to provide the power from the receiver to the antenna. Table 3.3 shows the summary from the specifications of the antenna used for this test.
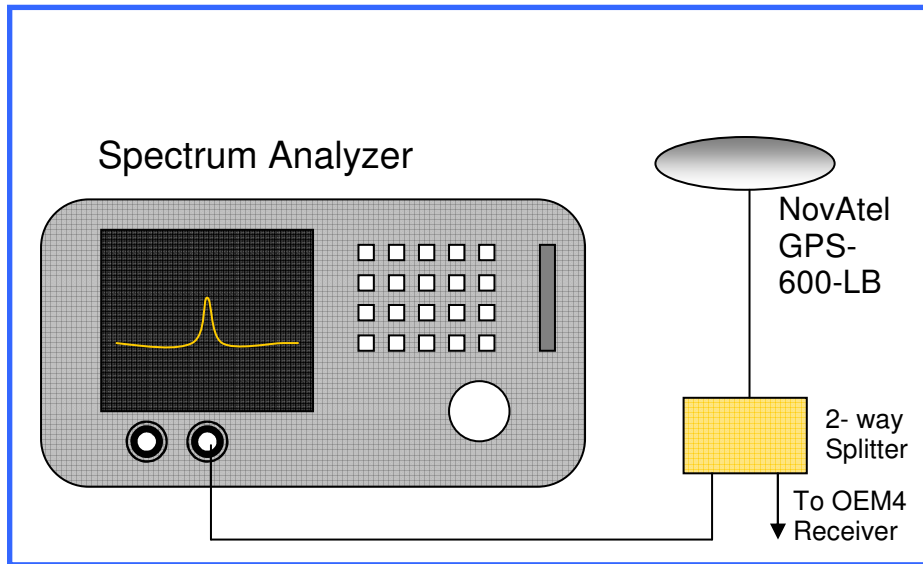
Figure 3.1: Interference Measurement Test Setup

Table 3.3: GPS-600-LB Specification

3 dB Pass Band	L1 : 1575 ±10 MHz (typical) L2 : 1228 ±10 MHz (typical)
Out-of-Band Rejection	L1 : 1420 MHz 40 dBc (typical) 1470 MHz 20 dBc (typical) 1635 MHz 20 dBc (typical) 1675 MHz 45 dBc (typical) L2 : f_c – 100 MHz 50dBc (typical) f_c – 50/+100 MHz 30dBc (typical) f_c + 50 MHz 50dBc (typical)

dBc : Decibels relative to unmodulated Carrier power

3.3.2 Interference measurement

Four locations were selected for investigation of existing sources of RF interference. The results of interference measurements are provided in the form of screen plots from the spectrum analyzer. The results are discussed in respect of whether bursts of power spectral density are detected or not.

The first measurement was made near a personal computer in the Navigation Laboratory, CCIT, University of Calgary, as a typical venue for ambient indoor interference sources. The antenna was located very close to a PC with the cover open, as shown in Figure 3.2. Spurious emissions were found inside the GPS band as shown in Figure 3.3, at a magnitude of -73.2 dBm. If a GPS antenna was located 1 m away from this source, the resultant interference power is -109.6 dBm. Since the GPS CWI margin from Table 3.1 is -120.6 dBm in tracking mode, the resultant safety margin is -11 dB. However, as shown in Figure 3.4, this peak disappeared when the cover was closed.

Figure 3.2: Interference Measurement near a PC
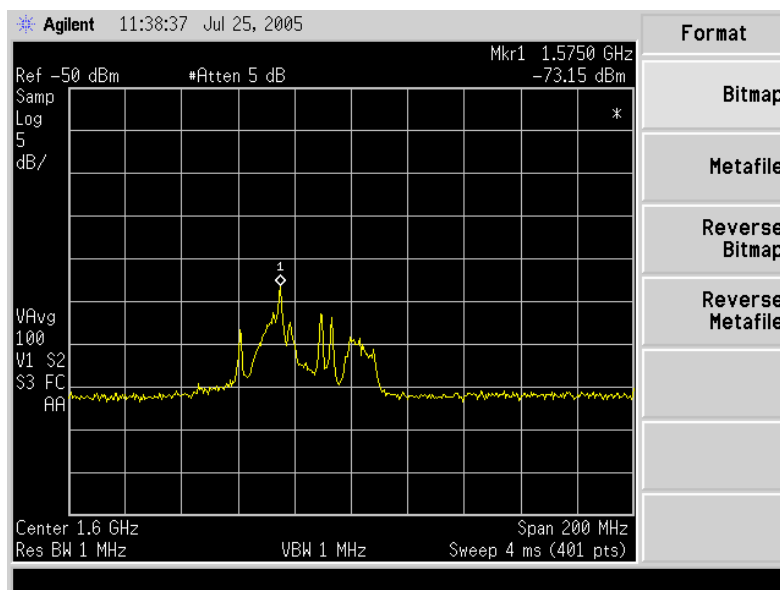
Figure 3.3: Interference Measurement near a PC with the cover open in the Laboratory
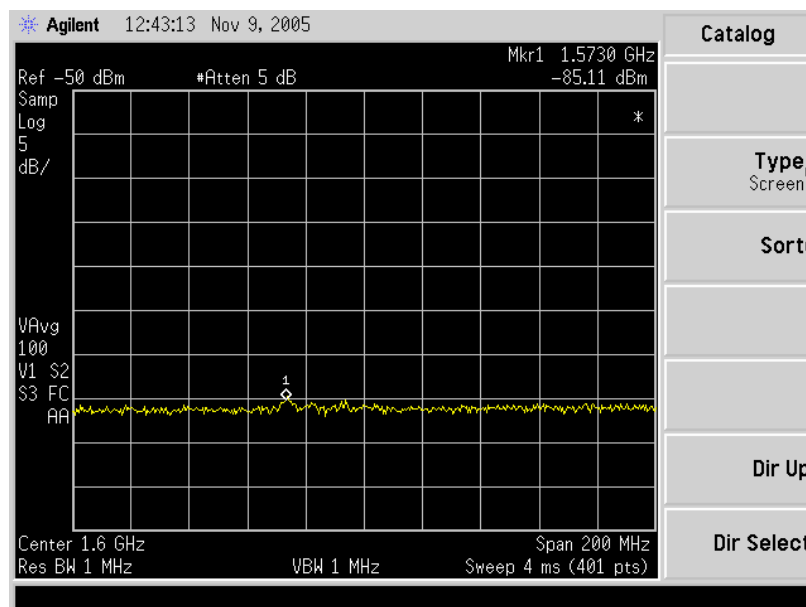
Figure 3.4: Interference Measurement near a PC with the cover close in the Laboratory

The next location selected for testing was a student lounge located in the ICT Building at the University, which provides wireless internet service for students. As shown in Figure 3.5, strong signals at a level of -20 dBm were detected around the 500 MHz - 900 MHz bands which are used for TV channels 36-68 and for cellular phone service. Also, several signal peaks were located at around 1.95 GHz which is used for PCS 2.4 GHz wireless internet signals, as attenuated by the antenna since this signal was rejected by the antenna pass band. As shown in Figure 3.6, no peaks were measured in the GPS L1 band.
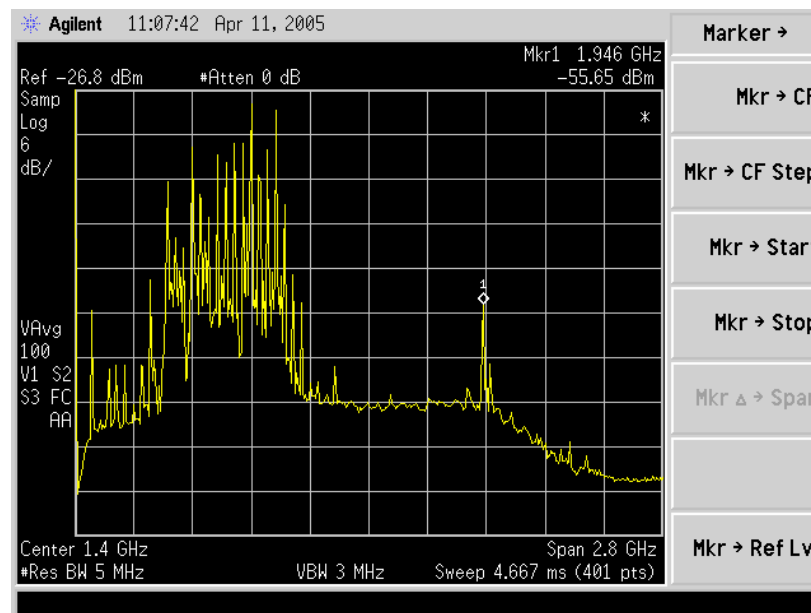
Figure 3.5: Interference Measurement in the ICT Building

Figure 3.6: Interference Measurement in ICT Building - Enlarged Scale of Frequency Span

Also, two other measurements were performed in the downtown core of Calgary. The first test location was the Citytv broadcasting station located on 6th Ave, 2nd St. SW; the other location on 9th Ave. SW Calgary was approximately 300 m away from the first site and was selected for purposes of comparison. As shown in Figure 3.7 and Figure 3.8, no peaks were measured in the GPS L1 band.
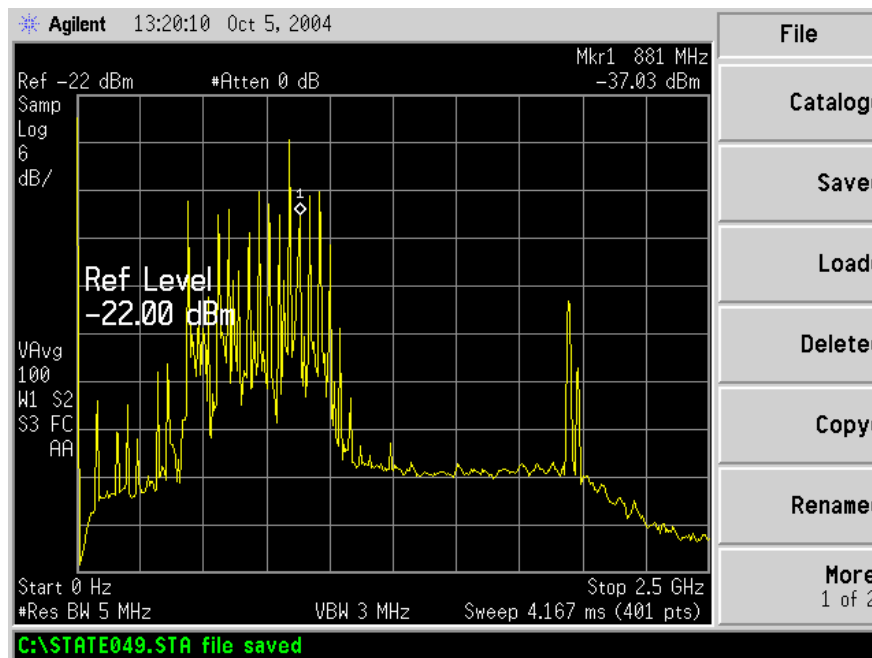
Figure 3.7: Interference Measurement in 9th Ave, 2nd St. SW in Downtown Calgary

Figure 3.8: Interference Measurement in 6th Ave, 2nd St. SW near a Broadcasting Station

3.4 Summary

Interference with the GPS signal has been experienced in both tactical and civil application environments across the globe. The performance of a GPS receiver could be degraded by electronic devices around the antenna. The interference measurement tests conducted herein show that EMC from personal computers can possibly degrade the GPS performance. In this investigation, the observed maximum power of interference from the PC was above the GPS CWI threshold. However, this interference disappeared when the cover was closed. Since interference emissions are typically non-deterministic, they may have any form in the spectral domain. Thus, their impacts can be analyzed in terms of the spectral property with respect to the signal spectrum.

CHAPTER FOUR: ANALYSIS OF INTERFERENCE EFFECTS

USING BOTH SOFTWARE RECEIVER AND SIMULATOR

This chapter includes interference tests using a software receiver and software simulator developed by the PLAN group at the University of Calgary. The purpose of this research is to verify the interference effects in relation to the integration time, correlator spacing, bandwidth of the DLL and the number of quantization bits.

4.1 GPS_IFGen™ and GNSS_SoftRx™

GPS_IFGen™ generates the digitized IF GPS signal based on a mathematical model of the GPS signal at the intermediate frequency. The software simulator outputs a file which provides a quantized bit stream at the sampling frequency. The signal model used in GPS_IFGen™ is (Dong et al 2003, Ma et al 2004):

$$S_{IF} = \sum_{i=1}^{N} AD_i(t - T_d)C_i(t - T_d)\cos((\omega_{IF}t - \omega_{L1}T_d) + \varphi_0) \tag{4.1}$$

$$\text{where } T_d = \delta t_{SV} + \delta t_{eph} + t_p + \delta t_{tropo} + \delta t_r - \delta t_{iono}$$

δt_{SV} : Satellite clock error

δt_{eph} : Ephemeris error

t_p : Propagation time

δt_{tropo} : Tropospheric delay

δt_r : Receiver clock error

δt_{iono} : Ionospheric delay

Since this software simulator is reconfigurable, errors such as atmospheric delay and satellite clock errors can be implemented based on the user-defined parameters. Also, different values of front-end bandwidth, sampling rate, as well as quantization schemes, are available for implementation at the user's option. After the signal is digitally generated, it is filtered by a software finite impulse response (FIR) band-pass filter to simulate the front-end filter.

Interference signals are generated and added to the satellites' signal at the intermediate frequency. The signal model for the continuous wave interference is

$$u(t) = \sqrt{2A} * \cos(\omega_{IF} + \omega_{fl})t \tag{4.2}$$

where A : Interference power

ω_{IF} : Intermediate frequency

ω_{fl} : Interference frequency offset from L1

The simulation of band-limited white noise interference (BLWNI) is implemented using a 50th order digital FIR filter. The signal spectrum generated at the output

of the software signal simulator, having 1 kHz of bandwidth band-limited white noise interference centred at L1, is shown in Figure 4.1. Interference power is determined by:

$$P_u = E[u^2(t)] \tag{4.3}$$
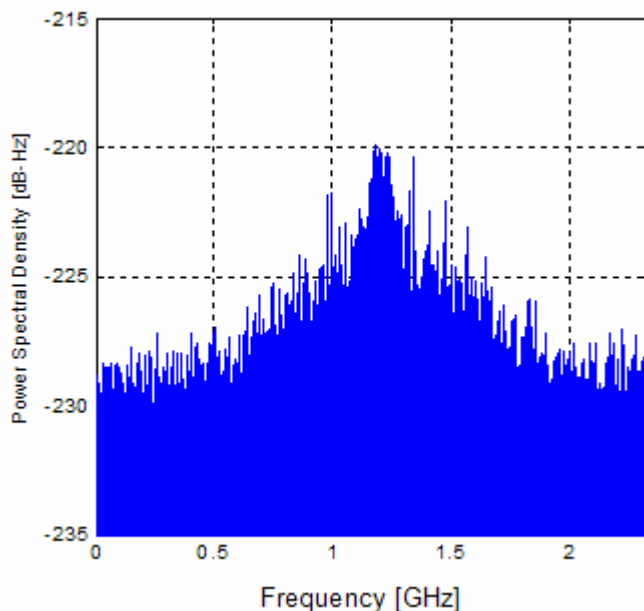
Figure 4.1 : Power Spectrum of the Signal Simulator Output

with Band-Limited White Noise Interference

The main role of the tracking loop of the receiver is to maintain the phase error and code delay error between the incoming and locally generated signals at a level of zero. Generally, the order of the tracking loop and bandwidth are chosen based on the anticipated dynamics of the receiver. During selection of the loop bandwidth, one should take two factors into account. First, the digital loop is valid when the sampling rate is larger than the Nyquist frequency. Second, the update

rate of the tracking loop must be higher than 5 to 10 times the loop bandwidth. Typically, the code tracking loop bandwidth is in the range of 1-4 Hz, while the carrier tracking loop bandwidth is in the range of 5-15 Hz (Jwo 2001).

Figure 4.2 shows a 3rd order PLL which is used in this research, whose associated error is sensitive to jerk stress. An arctan discriminator is used to calculate the phase of the incoming signal. This type of discriminator is known to be optimal at high and low levels of the signal-to-noise ratio, since it is not sensitive to the signal amplitude. However, this type of discriminator has a drawback in that false locks may occur, as this discriminator has a zero point at any multiple of 90 degrees. For a 3rd order PLL, the loop remains stable when its bandwidth is lower than 18 Hz (Kaplan 1996). The bandwidth of the PLL also limits the lock-in and pull-in range of the tracking loop. The bandwidth of the PLL of the software receiver continuously adapts according to the phase lock detector proposed by Van Dierendonck (1996).
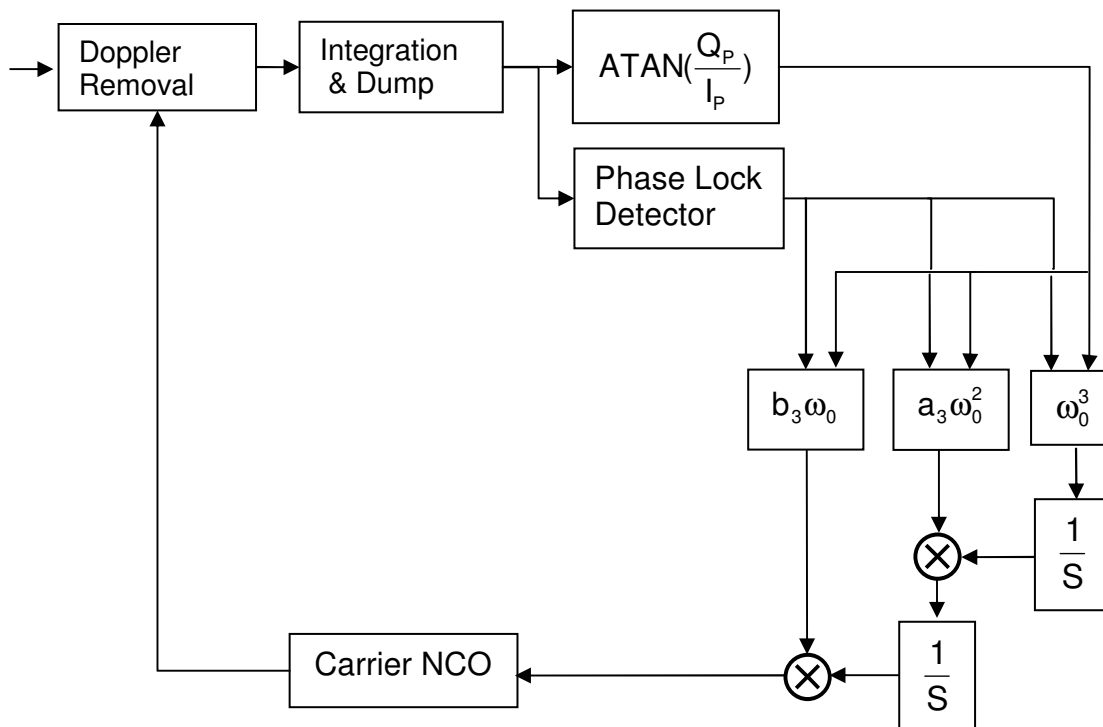
Figure 4.2: Phase-Locked Loop

Figure 4.3 shows a 2nd order DLL. Since the DLL is aided by the PLL, the 2nd order DLL is required to track the difference between the code and carrier-phase dynamics, allowing a small noise bandwidth (Raquet 2004). A normalized non-coherent early minus late envelope discriminator is used in the software receiver. This type of discriminator is not sensitive to the magnitude of the signal-to-noise ratio.
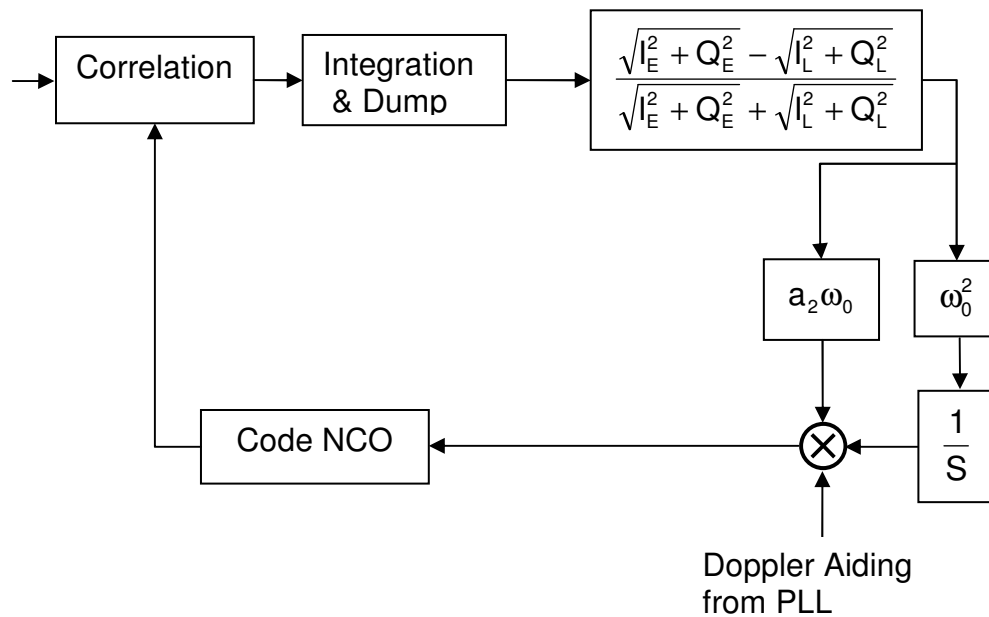
Figure 4.3: 2nd Order Delay Lock Loop

The C/N$_0$ is estimated every second by the method proposed by Van Dierendonck (1996) with M=20 and K=50:

$$\frac{\hat{C}}{N_0} = 10\log_{10}\left(\frac{1}{T} \cdot \frac{\hat{\mu}_{NP} - 1}{M - \hat{\mu}_{NP}}\right) \qquad (4.4)$$

$$\text{where } \hat{\mu}_{NP} = \frac{1}{K}\sum_{k=1}^{K} NP_k$$

$$NP_k = \frac{NBP_k}{WBP_k}$$

$$NBP_k = \left(\sum_{i=1}^{M} I_i^2\right)_k + \left(\sum_{i=1}^{M} Q_i^2\right)_k \quad \text{(narrow-band power)}$$

$$WBP_k = \left(\sum_{i=1}^{M} (I_i^2 + Q_i^2) \right)_k \quad \text{(wide-band power)}$$

The pseudorange is estimated using the following equation (Kaplan 1996):

$$\rho(t) = c[t_u(t) - t^{(s)}(t - \tau)] \qquad (4.5)$$

where c : speed of light

$t_u(t)$: receive time of the GPS receiver's clock

$t^{(s)}(t\text{-}\tau)$ = Z-count

+ number of navigation bits*20 ms

+ number of C/A code * 1ms

+ number of C/A code chips * Tc

+ fraction of C/A code chips in second

The Doppler frequency is estimated directly from the carrier NCO. The epoch-by-epoch least-squares method is used to obtain the position.

4.2   Test Setup

The receiver and simulator parameter settings were:

- Simulation Time: 2003. Oct. 26 15:00 for 30 s
  (GPS Time: 226800 – 226830)

- Position: 51º 04' 48", -114º 08' 01", 1118.5 (LLH)

- Elevation cutoff: 5 [deg]

- Front-end bandwidth: 2 MHz

- Sampling rate: 4.75 MHz

- Intermediate frequency: 15.42 MHz
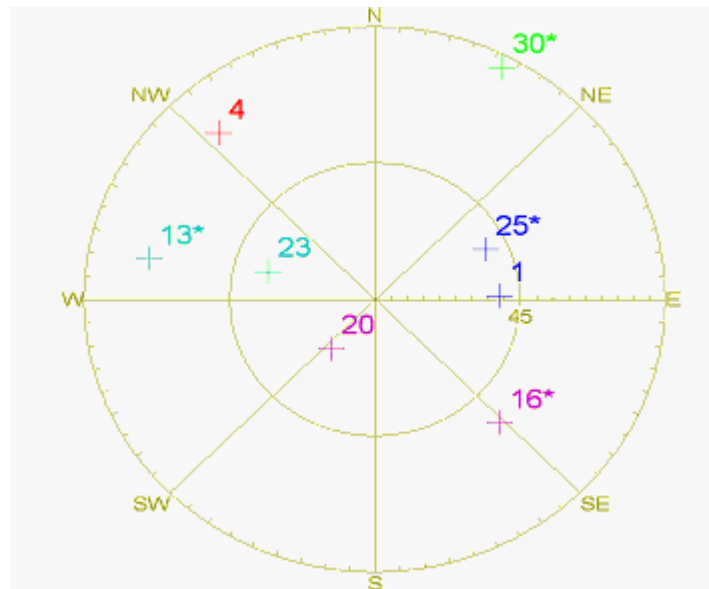
Figure 4.4: Sky plot at the beginning of simulation

Figure 4.4 shows the sky plot at the beginning of the simulation. No other disruptions - such as atmospheric effects, orbital errors, receiver clock error and multipath - were added to the GPS signal in order to isolate interference effects from other disruptions. Since most of the interference signal is unintentional,

three types of interference are investigated: white noise, CWI and BLWNI. For the white noise, the C/N_0 was varied from 46 dB-Hz to 22 dB-Hz. For the CWI, the unjammed C/N_0 was maintained at a level of 46 dB-Hz while interference power was gradually increased from 15 to 55 dB in 5 dB steps relative to the signal power. The centre frequencies were 5 kHz, 500 kHz, and 1 MHz from the L1 frequency. These frequencies were selected on the basis of the locations of spectral lines with respect to the C/A code's main lobe. For the BLWNI, a 1 kHz bandwidth centred at L1 was used. The unjammed C/N_0 was maintained at 46 dB-Hz. The level of interference power was varied from 20, 30, 35, 40 and 45 dB relative to the signal power.

4.3 Test Results

The term, 'tracking threshold' in this chapter means the threshold of loss of true lock. All available pseudorange measurements are used to compute positions. No mitigation algorithm is applied to the receiver. The parameters used are: 0.2 Hz of DLL bandwidth for the wide correlator, and 3 bits quantization, unless otherwise specified.

4.3.1 Dependency of Types of Interference

C/N$_0$

As shown in Table 4.1, in the case of white noise, the measured C/N$_0$ values were approximately 0.6 dB lower than the simulated value, which was a result of quantization loss. The C/N$_0$ values were maintained within $\pm$0.1 dB of the average value for all of the satellites tracked.

Table 4.1: Measured C/N$_0$ with white noise

Simulated C/N$_0$ [dB-Hz]	PRN 1	PRN 4	PRN 10	PRN 16	PRN 20	PRN 23	PRN 25	Average
46	44.6	44.7	44.7	44.7	44.7	44.9	44.7	**44.7**
36	35.5	35.6	35.5	35.5	35.5	35.5	35.5	**35.5**
34	33.5	33.6	33.5	33.6	33.5	33.6	33.6	**33.5**
32	31.6	31.6	31.6	31.5	31.5	31.6	31.5	**31.6**
30	29.6	29.5	29.5	29.5	29.5	29.6	29.6	**29.5**
28	27.4	-	27.6	27.5	27.5	27.4	27.6	**27.5**
26	25.5	25.5	-	-	25.6	25.5	25.4	**25.5**
24	23.5	-	23.6	23.5	23.6	-	-	**23.5**

The measured C/N$_0$ values differed for satellites under the same power of CWI at L1+5 kHz, as shown in Figure 4.5. The measured C/N$_0$ of PRN 13 for the CWI is shown in Figure 4.6. The measured C/N$_0$ with CWI at L1+5 kHz deviated from the trend when I/S = 35, 45 and 50 dB, which indicates that the interference power leaked through the correlation process and the tracking loop filter and

appeared to be treated as carrier power. The measured values of C/N_0 were quite different from the theoretical value. However, since most of the interference power is concentrated on the centre frequency, it is expected that the measured C/N_0 is degraded most readily with CWI near the L1 frequency.
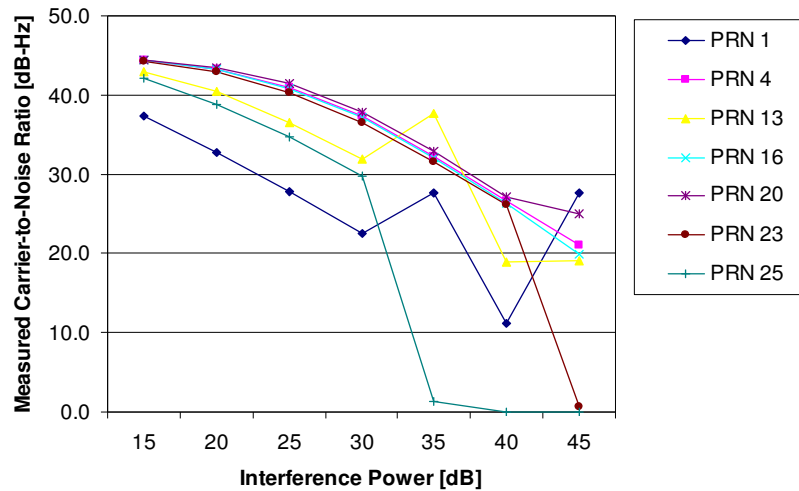
Figure 4.5: Measured C/N_0 for CWI at L1+5 kHz
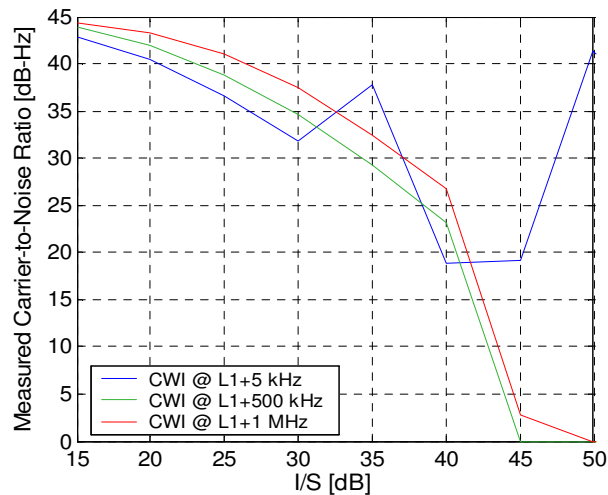
Figure 4.6: Measured C/N_0 for CWI (PRN 13)

Table 4.2 shows the measured carrier C/N_0 under the BLWNI centred at L1. The variances between the satellites were smaller than those seen for CWI, but larger than those seen for white noise. As discussed in chapter 2, the effective jamming power under the BLWNI is only effected by the interference power and relative power of the n-th line component of C/A code, while the effective jamming power under the CWI is effected by the interference power, the relative power of the n-th line component of C/A code, and the distance from this line.

Table 4.2: Measured C/N_0 for BLWNI

I/S[dB]	PRN 1	PRN 4	PRN 13	PRN 16	PRN 20	PRN 23	PRN 25	Average
20	43.8	44.1	43.9	43.9	43.7	43.9	43.9	**43.9**
30	37.7	38.4	37.8	38.0	37.4	37.6	37.8	**37.8**
35	33.2	33.9	33.3	33.4	32.8	33.1	33.3	**33.3**
40	28.4	29.1	28.4	28.5	28.0	28.3	28.5	**28.5**
45	23.2	-	22.4	-	-	23.0	23.5	**23.0**

Tracking loop errors

The DLL tracking errors of PRN 13 with white noise and CWI are shown in Figure 4.7. In all cases of CWI, the tracking errors were smaller than those seen with white noise (WN). The DLL errors with CWI at L1+500 kHz were the highest amongst the three types of interference; this error approached its threshold of 1/6 chips when I/S = 40 dB under CWI at L1+500 kHz. The DLL errors were not the

same for all satellites in view under CWI; however, the averages of the DLL errors of the satellites had a maximum for 500 kHz under CWI, as shown in Table 4.3.
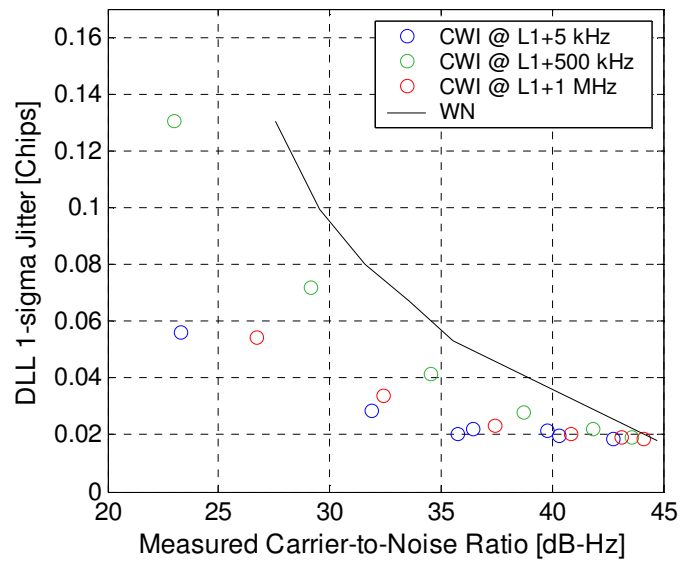
Figure 4.7: DLL Tracking Errors of PRN 13 for CWI

Table 4.3: Averages of DLL Tracking Loop Errors for CWI

Interference Power [dB]	CWI at L1+ 5 kHz [Chips]	CWI at L1+ 500 kHz [Chips]	CWI at L1+ 1 MHz [Chips]
15	0.019	0.020	0.019
20	0.020	0.022	0.020
25	0.022	0.028	0.021
30	0.029	0.039	0.025
35	0.052	0.060	0.034
40	0.077	0.109	0.057
45	0.099	0.127	0.104

As shown in Figure 4.8, the PLL tracking errors under white noise exhibited a change of trend since the bandwidth of PLL of the software receiver was adaptively changed. Since the phase of the CWI was fixed, the PLL errors under CWI were maintained at the same level when I/S is lower than 30 dB. The maximum PLL tracking error that occurred with CWI at L1+5 kHz was due to false lock.
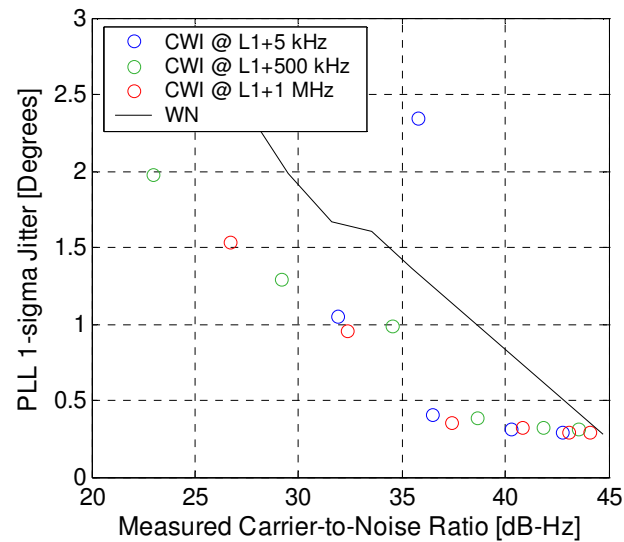
Figure 4.8: PLL Tracking Errors of PRN 13 for CWI

Figure 4.9 and Figure 4.10 show the tracking loop errors for BLWNI. Both DLL and PLL errors were affected to a similar degree for all satellites in view. The DLL errors did not reach their threshold until 23 dB-Hz and they were smaller than those seen for white noise. As a result, better performance is expected as compared to the white noise case for the same C/N_0. However, the tracking thresholds in terms of C/N_0 for BLWNI and white noise were not much different, since the tracking loop errors increased exponentially. The PLL showed no difference between the white noise and BLWNI. No false tracking lock was seen under BLWNI.
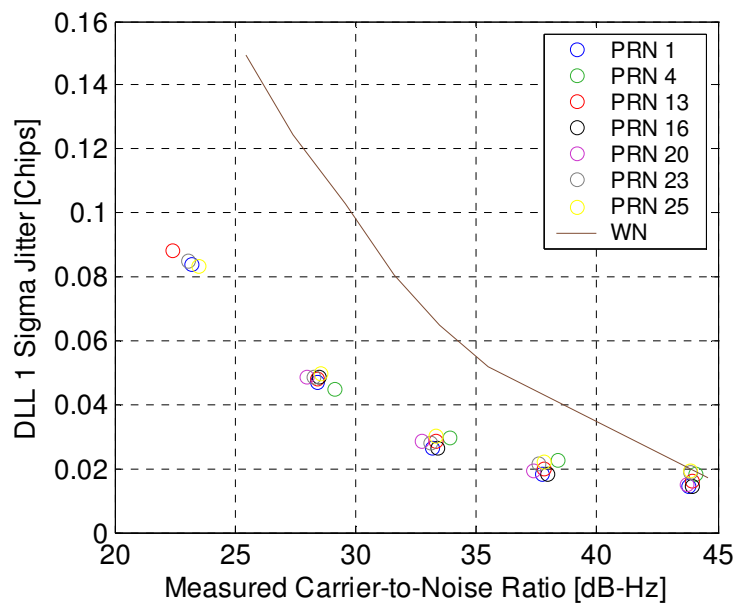
Figure 4.9: DLL Tracking Errors for BLWNI
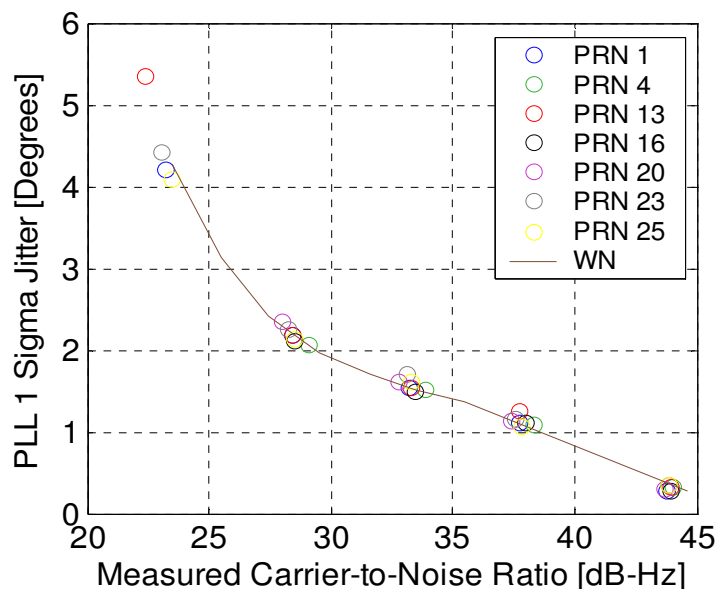
Figure 4.10: PLL Tracking Errors for BLWNI

Tracking thresholds and position errors

Under white noise interference, the software receiver was able to track and provide a position solution until 23.5 dB-Hz of measured C/N_0, as shown in Table 4.4. The position errors tended to increase exponentially with the decrease in C/N_0, which was the same trend observed for the corresponding case involving DLL tracking loop errors.

Table 4.4: 3D RMS Position Errors for White Noise

Simulated C/N_0 [dB-Hz]	Measured C/N_0 [dB-Hz]	3D Pos. Error [m]	Number of Satellites Tracked
46	44.7	34.8	7
36	35.5	101.0	7
34	33.5	120.4	7
32	31.6	147.2	7
30	29.5	164.0	7
28	27.5	214.1	6
26	25.4	235.8	5
24	23.5	608.2	4

Table 4.5 shows the position errors for the three different centre frequencies. When the I/S is less than 30 dB, the CWI at L1 + 500 kHz had the largest position error, as the largest error in the estimation of the pseudorange is expected under these conditions owing to DLL tracking loop errors. When the I/S was equal to and larger than 35 dB, false locks started to occur. The position

errors were no longer a function of the interference power and increase rapidly

in a false lock state, resulting in very large errors in the position domain.

Table 4.5: 3D RMS Position Errors for CWI

I/S [dB]	L1+5 kHz [m]	L1+500 kHz [m]	L1+1 MHz [m]
15	30.9	38.9	35.2
20	39.8	45.9	41.8
25	43.7	63.8	48.2
30	48.6	99.3	76.2
35	**3182.2***	**431.7***	110.9
40	136.8	335.2	157.8
45	**3257.5***	-	**1162.2***

* : false lock

The software receiver tolerated 45, 45 and 50 dB of I/S for three different centre

frequencies of CWI, respectively. Figure 4.11 shows the number of satellites

tracked for the CWI test as well as the number of false locks. As shown in this

figure, the CWI whose centre frequency was nearest to L1 causes false lock

more frequently. Therefore we may conclude that, although the tolerances

against the CWI at L1+5 kHz and L1+500 kHz were the same as for 45 dB of I/S,

the loss of tracking for CWI at L1+5 kHz was mainly caused by false lock, while

the loss of tracking for CWI at L1+500 kHz was caused by DLL tracking errors.
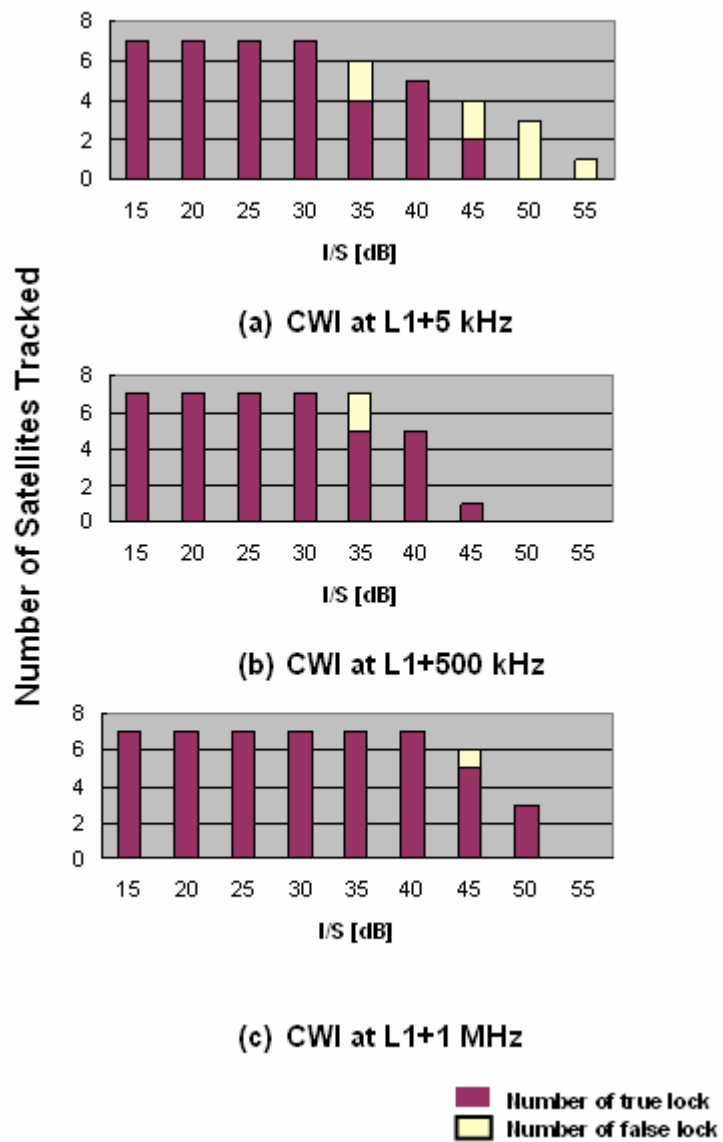
Figure 4.11: Number of Satellites Tracked for CWI

The position errors for BLWNI as a function of I/S are shown in Table 4.6. The errors were smaller than those for white noise for the same level of C/N_0.

Table 4.6: 3D RMS Position Errors for BLWNI

I/S [dB]	Measured C/N_0 [dB-Hz]	3D Pos. Error [m]	Number of Satellites Tracked
20	43.9	29.4	7
30	37.8	36.4	7
35	33.3	68.0	7
40	28.5	95.1	7
45	23.0	363.8	4

4.3.2 Receiver Parameter Dependency

Integration time

Two values of integration time were investigated, namely 5 ms and 20 ms. The software receiver was able to provide the position solution down to 30 dB-Hz of simulated C/N_0 under white noise interference with 5 ms of integration time, which was 6 dB lower than with an integration time of 20 ms, as the SNR of 20 ms integration is 6 dB higher gain than the SNR of 5 ms under white noise. The 3D position errors under white noise interference conditions were larger for 5 ms than for 20 ms of integration time due to DLL tracking loop errors, as shown in Table 4.5 and Table 4.7.

Table 4.7: 3D Position Errors Under White Noise With an Integration Time of 5 ms

Simulated C/N_0 [dB-Hz]	Measured C/N_0 [dB-Hz]	3D Pos. Error [m]	Number of Satellites Tracked
46	44.7	47.5	7
36	35.4	128.4	7
34	33.5	126.4	7
32	31.5	142.7	7
30	25.9	304.4	6

Table 4.8 shows the position errors for the different centre frequencies of CWI when the integration time is 5 ms. Position errors were also larger than those resulting from a 20 ms integration time.

Table 4.8: 3D Position Errors under CWI With an Integration Time of 5 ms

I/S [dB]	L1+5 kHz [m]	L1+500 kHz [m]	L1+1 MHz [m]
15	59.1	70.0	59.8
20	55.8	86.2	56.3
25	95.7	125.2	71.2
30	114.9	142.2	95.7
35	583.4	2370.5	107.0
40	5085.2	33,284.5	123.5
45	-	-	358.4

False lock started to occur when I/S = 25 dB with CWI at L1+5 kHz, which was

10 dB lower than that resulting from an integration time of 20 ms, as shown in

Figure 4.12. The tracking threshold under CWI at L1+5 kHz was the same as the

20 ms integration time case, while the tracking thresholds under CWI at L1+500

kHz and L1+1 MHz were 40 dB, 45 dB , which were 5 dB lower than those

resulting from an integration time of 20 ms.
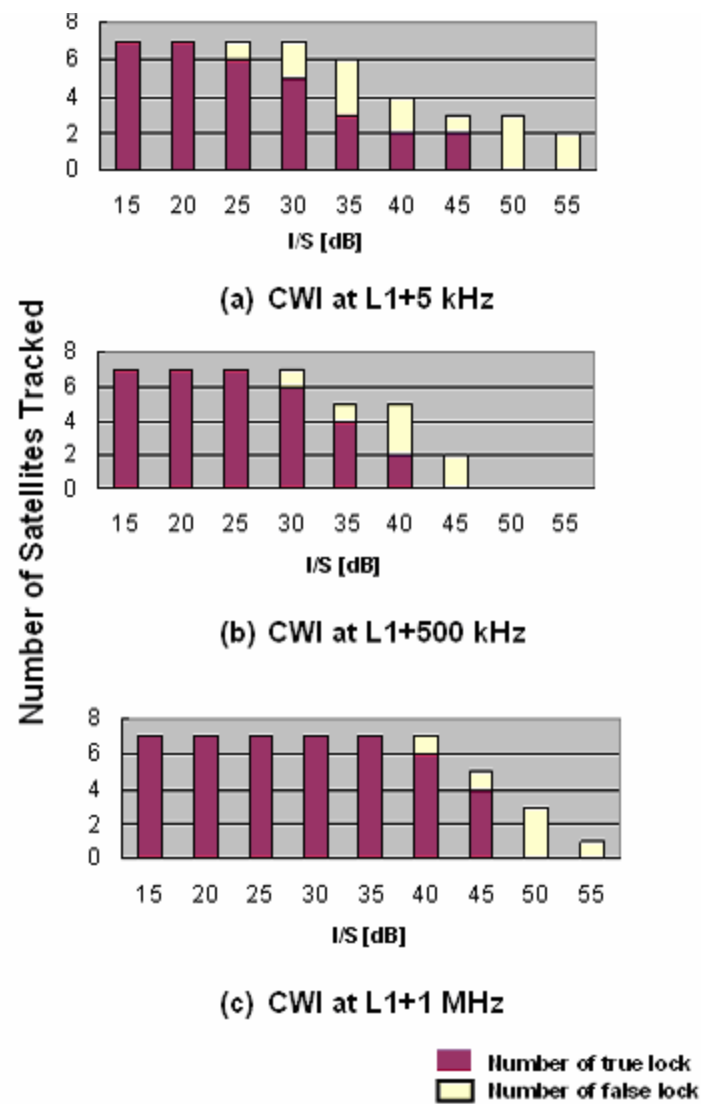
Figure 4.12: Number of Satellites Tracked for CWI With an Integration Time of 5 ms

The tracking thresholds for both integration times were the same as 45 dB in terms of I/S. The position errors under BLWNI are shown in Table 4.9. The position errors were larger than in a case of 20 ms of integration time when I/S is less than 35 dB.

Table 4.9: 3D RMS Position Errors under BLWNI with an Integration Time of 5 ms

I/S [dB]	Measured C/N$_0$ [dB-Hz]	3D Pos. Error [m]	Number of Satellites Tracked
20	43.9	41.2	7
30	37.8	51.2	7
35	33.3	81.8	7
40	27.2	82.7	5
45	22.1	266.9	4

Correlator spacing and bandwidth of DLL

As shown in Figure 4.13, the mean DLL tracking loop errors were affected by the correlator spacing, rather than by the bandwidth of the DLL as in the case of white noise. Also, this figure demonstrates that the DLL tracking loop errors have reached their tracking threshold for all receiver parameter settings. The DLL parameter changes do not appear to affect the tracking threshold.
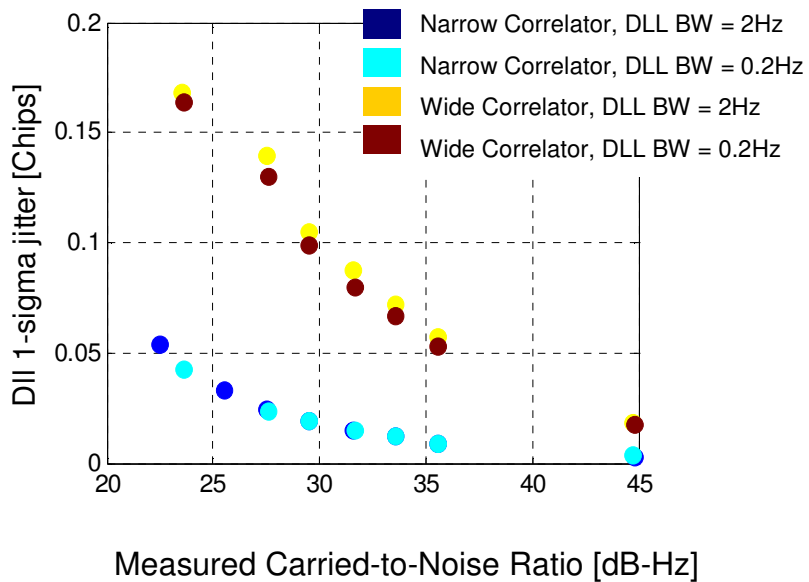
Figure 4.13: DLL Tracking Errors for White Noise for Different Receiver Parameters

Figure 4.14 shows the PLL tracking errors for the white noise case. They did not change with the DLL parameter changes. Also, the Doppler frequency errors did not change in relation to those changes.
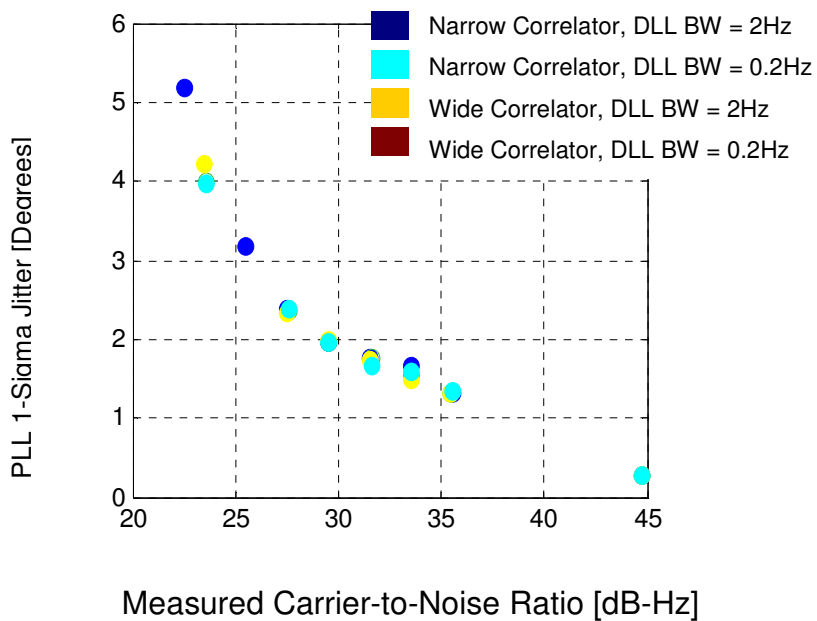
Figure 4.14: PLL Tracking Errors for White Noise for Different Receiver Parameters

Since the DLL tracking loop error was low when the bandwidth of the DLL was narrow, the receiver with a narrow DLL bandwidth tolerated more interference under CWI at L1+500 kHz and CWI at L1+1 MHZ, as shown in Table 4.10. However, since the loss of tracking with CWI at L1+5 kHz was mainly caused by false lock, the tracking thresholds between different bandwidths were the same in terms of I/S.

Table 4.10: Tracking Threshold (I/S [dB]) of CWI

Centre Frequency	N, 2 Hz*	N, 0.2 Hz*	W, 2 Hz*	W, 0.2 Hz*
L1+5 kHz	45	45	45	45
L1+500 kHz	40	45	40	45
L1+1 MHz	45	50	45	50

* Correlator Spacing (N: 0.1, W:1), Bandwidth of DLL

The percentages shown in Table 4.11 were calculated as the percentage of the false lock to the total number of satellites tracked. The table indicates that the probability of false lock was low when the correlator spacing and the bandwidth of the DLL were narrow.

Table 4.11: Percentage of False Lock for CWI

Centre Frequency	N, 2 Hz*	N, 0.2 Hz*	W, 2 Hz*	W, 0.2 Hz*
L1+5 kHz	34	31	35	31
L1+500 kHz	8	7	20	4
L1+1 MHz	16	2	22	20

* Correlator Spacing (N: 0.1, W: 1), Bandwidth of DLL

Figure 4.15 shows the 3D RMS position errors for white noise for different receiver parameters. Although the front-end bandwidth was not wide enough for the case of a narrow correlator, it is obvious that the correlator spacing affected the accuracy of position estimation, while the DLL bandwidth did not.
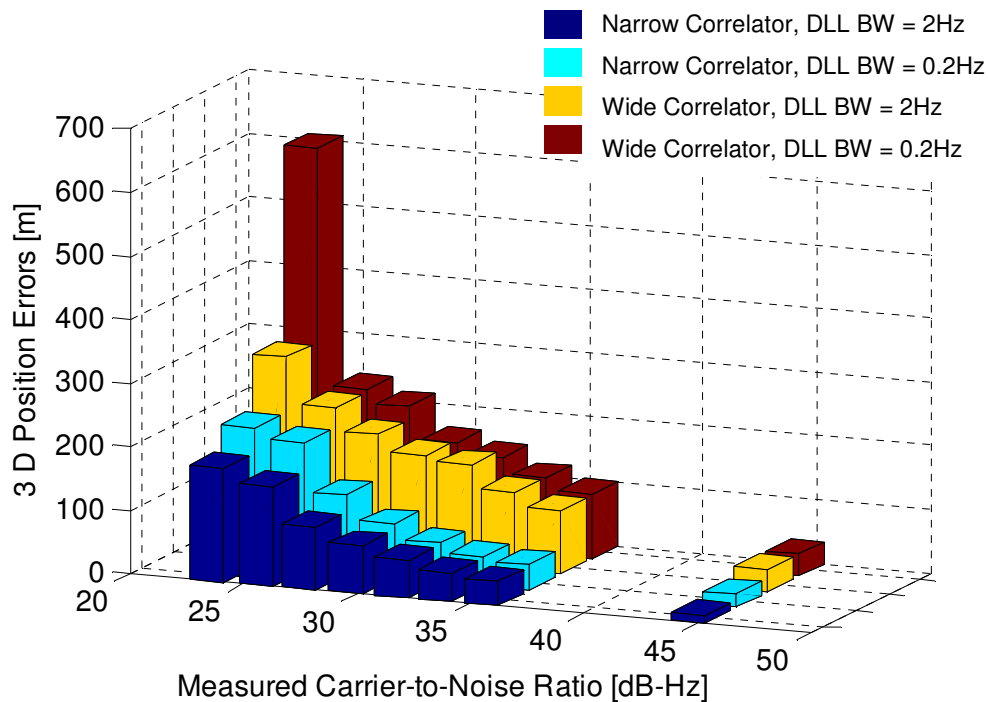
Figure 4.15: 3D RMS Position Errors for White Noise for Different Receiver Parameters

Table 4.12 shows the position errors for CWI. The maximum position error occurred with the CWI at L1+5 kHz for all receiver parameter settings; the correlator spacing improved the position accuracy in the case of CWI as well. However, the difference between wide and narrow correlators in position domain under CWI was smaller than for the corresponding white noise case.

Table 4.12: 3D RMS Position Errors for CWI for Different Receiver Parameters

I/S [dB]	N, 2 Hz* [m]	N, 0.2 Hz* [m]	W, 2 Hz* [m]	W, 0.2 Hz* [m]
L1+5 kHz				
15	12.2	20.3	31.1	30.9
20	16.0	21.1	39.7	39.8
25	18.0	25.6	44.0	43.7
30	32.3	38.8	47.8	48.6
35	4,116.4	413.4	90.1	3,182.2
40	-	144.6	3,121.3	136.7
L1+500 kHz				
15	14.2	22.4	39.8	38.9
20	20.8	26.0	47.0	45.9
25	32.1	33.8	65.2	63.8
30	53.5	53.8	102.9	99.3
35	132.9	121.2	-	431.7
40	-	-	-	335.2
L1+1 MHz				
15	15.3	22.4	35.3	35.2
20	18.1	24.0	41.4	41.8
25	30.2	32.8	48.9	48.2
30	52.1	48.8	75.6	76.2
35	99.4	90.9	106.6	110.9
40	188.5	174.7	174.5	157.8
45	-	229.0	232.3	358.4

* Correlator Spacing (N: 0.1, W: 1), Bandwidth of DLL

The position errors depending on the receiver parameters in the case of BLWNI are shown inFigure 4.16. The maximum position error appeared with a wide correlator and a 0.2 Hz bandwidth for the DLL, which was the same as the white noise interference. Once again, correlator spacing affected the position errors rather than the DLL bandwidth. The differences between the correlator spacing results in position domain were smaller than in the white noise case.
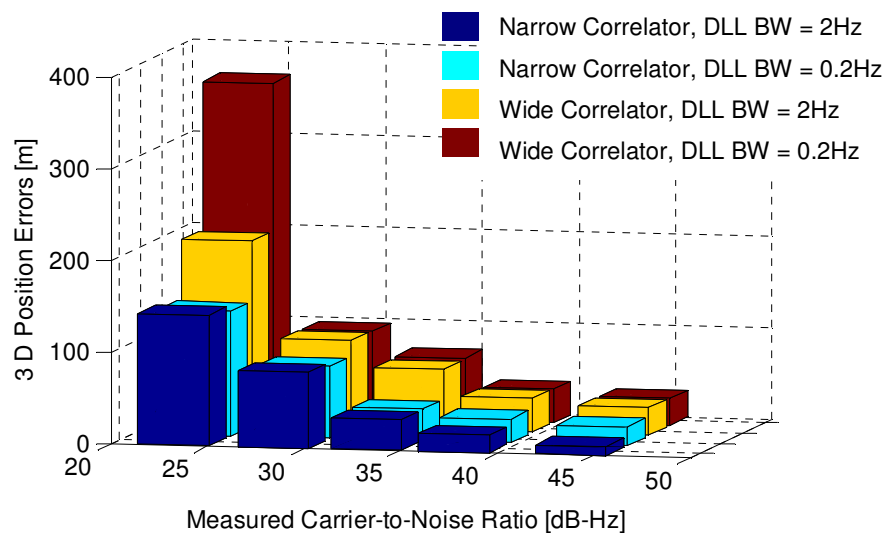
Figure 4.16: 3D RMS Position Errors for BLWNI for Different Receiver Parameters

Number of quantization bits

Table 4.13 shows the degradation of C/N_0 in the white noise case, which is comparable to the value of -1.8 dB between 1-bit and 3-bit quantizers. As a result, the tracking threshold had a 2 dB difference between two quantization bits. The position errors as a function of measured C/N_0 are shown in Figure 4.17. In the case of CWI, the larger the interference power, the bigger the degradations due

to the change of quantization bit, as shown in Table 4.14. As a result, the 3-bit quantization tolerated 5 to 10 dB more in terms of interference power than did the 1-bit quantization case. Also, the position error difference between 2 quantization bits increased with an increase in interference power, as shown in Table 4.15. The degradation of C/N_0 under BLWNI was lower than those seen under white noise, as shown in Table 4.16. The position errors were maintained in a similar trend with respect to the measured C/N_0 as shown in Figure 4.18.

Table 4.13: C/N_0 Comparison between 1-bit and 3-bit Quantization under White Noise

Simulated C/N_0 [dB-Hz]	3 Bits	1 Bit	3 Bits - 1 Bit
46	44.7	43.0	1.7
36	35.5	33.7	1.8
34	33.5	31.7	1.8
32	31.6	28.8	1.8
30	29.5	27.7	1.8
28	27.5	25.7	1.8
26	25.4	23.6	1.8
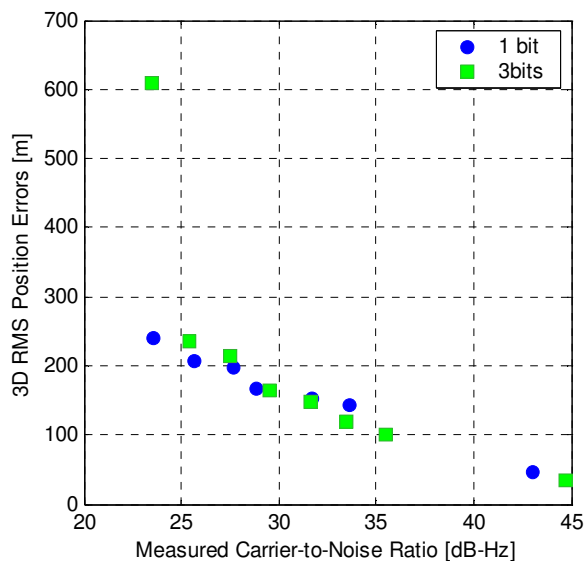
**Figure 4.17: Position Error Comparison between 1-bit and 3-bit
Quantization under White Noise**

Table 4.14: Measured C/N$_0$ for Different Quantization Bits under CWI

I/S [dB]		15	20	25	30
Centre Frequency	**Number of Bits**	**Measured C/N$_0$ [dB-Hz]**			
L1+5 kHz	3 bits	41.9	38.8	34.6	29.7
	1 bit	40.0	35.5	28.8	22.7
	3 bits –1 bit	**1.9**	**3.3**	**5.8**	**7.0**
L1+500 kHz	3 bits	44.0	42.7	40.2	36.6
	1 bit	41.7	39.1	34.6	29.7
	3 bits –1 bit	**2.3**	**3.6**	**5.6**	**6.9**
L1+1 MHz	3 bits	44.2	43.4	41.3	38.0
	1 bit	41.8	39.6	35.5	26.1
	3 bits –1 bit	**2.4**	**3.8**	**5.8**	**7.9**

Table 4.15: Position Error Comparison between 1-bit and 3-bit Quantization under CWI

I/S [dB]		15	20	25	30
Centre Frequency	**Number of Bits**	**3D RMS position Errors [m]**			
L1+5 kHz	3 bits	30.9	39.8	43.7	48.6
	1 bit	46.6	64.2	90.8	127.5
	3 bits –1 bit	**15.7**	**24.4**	**47.1**	**78.9**
L1+500 kHz	3 bits	38.9	45.9	63.8	99.3
	1 bit	57.9	69.7	119.5	335.8
	3 bits –1 bit	**19.0**	**23.8**	**55.7**	**236.5**
L1+1 MHz	3 bits	35.2	41.8	48.2	76.2
	1 bit	48.7	60.6	89.9	172.3
	3 bits –1 bit	**13.5**	**18.8**	**41.7**	**96.1**

Table 4.16: C/N_0 comparison between 1-bit and 3-bit Quantization under BLWNI

I/S [dB]	3 Bits	1 Bit	3 Bits - 1 Bit
20	43.9	42.7	**1.2**
30	37.8	36.3	**1.5**
35	33.3	31.7	**1.6**
40	28.5	26.9	**1.6**
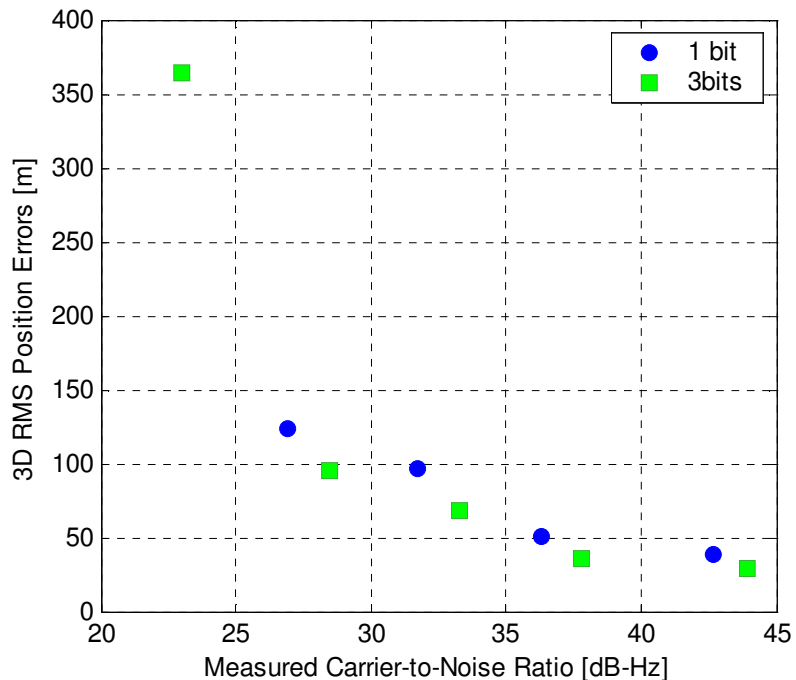
Figure 4.18: Position Errors Comparison between 1-bit and 3-bit Quantization under BLWNI

4.4   Conclusions

This chapter presents an analysis of the interference effects based on the types of interference and selected receiver parameters in tracking mode using a software receiver and software GPS signal simulator. The results indicate that position errors due to narrow-band interference were small in comparison to white noise unless false lock. On the other hand, continuous wave interference centred near the L1 frequency tended to cause false lock, resulting in severe

degradation of position accuracy. This investigation has also shown that interference tolerance was a function of tracking loop errors as well as the probability of false lock. As distinct from the case of continuous wave interference, the band-limited white noise interference with a 1 kHz bandwidth affected all satellites in view to a similar degree.

The estimation of position was affected by correlator spacing. However, the correlator spacing did not affect the PLL tracking errors with a 2 MHz front-end band-pass filter. Furthermore, the probability of false lock was low when the correlator spacing and the bandwidth of DLL were narrow. This study has also shown that the number of quantization bits played an important role under CWI in terms of tracking threshold. The 3-bit quantizer tolerated 10 dB more CWI than did the 1-bit quantizer case. In addition, long integration improved the tracking threshold and position errors with white noise. However, this did not always improve the performance with coloured noise.

CHAPTER FIVE: ANALYSIS OF INTERFERENCE EFFECTS OBSERVED USING A HARDWARE SIMULATOR AND HARDWARE RECEIVERS

5.1 GPS Hardware Simulator

The hardware GPS signal simulator (Spirent GSS6560) and interference signal generator (Agilent E4460) of the University of Calgary's PLAN Group were used to provide repeatable and controllable GPS signal references along with various interference signal replicas. The simulation hardware consists of a control computer, a GPS simulator, an interference combiner unit and an interference signal generator. The GSS6560 is a 12-channel L1 C/A-code simulator. The interference signal, along with the GPS signal parameters, are defined from a Graphical User Interface (GUI) control software, SIMGEN. Summaries of the specifications of the GPS simulator and interference signal generator are given in Table 5.1 and Table 5.2, respectively. Figure 5.1 shows the configuration of the test equipment used in this chapter.

The simulator's main capabilities are outlined below (Spirent 2003):

- Atmospheric Delay Modeling

- Antenna Gain Pattern Control

- Multipath Modeling

- Output of Simulated Pseudorange and Pseudorange Rate

- Vehicle Motion Modeling

- Satellite Constellation Control

- Navigation Data Bit Control
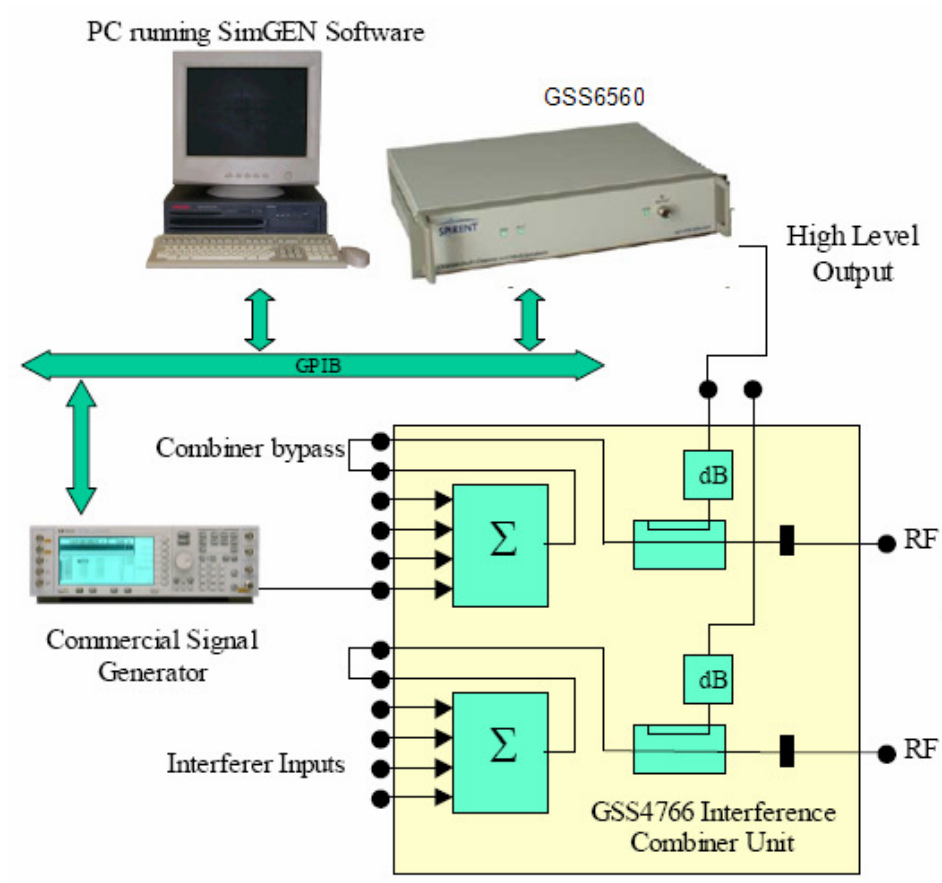
Figure 5.1: Configuration of Test Equipment

Table 5.1: Summary of Performance and Accuracy Specifications of the Hardware GPS Simulator (GSS6560)

Number of Channels	12
Pseudorange Error	±0.002 m(RMS), Dynamics<45 m/s^2,50 m/s^3
Satellite Signal level	Range : -130 dBm +15 dB, -20 dB, Error : ± 2 dB max.
Dynamics	Maximum Relative Velocity : ±15,000 m/s Maximum Relative Acceleration : ±450 m/s^2 Maximum Relative Jerk : ±500 m/s^3

Table 5.2: Summary of Interference Generator (Agilent E4460)

Interference Power	Noise : -172 to -33 dBW All other mode : -172 to -30 dBW
Noise	BW : 50 kHz~20 MHz
CW Interference	Freq. Range : 0.5~2 GHz
AM Interference	AM Depth : 0~100 %
FM Interference	Maximum Deviation : 20 MHz for carrier 1.0~2 GHz 10 MHz for carrier 0.5~1.0 GHz
Pulsed Modulation	Period : 16 µs~30 s, Width : 8 µs~30 s Of any of the above

5.2 Receivers under test

The sensitivity limitation of the receiver poses a major challenge in degraded environments such as indoor settings and urban canyons. A conventional GPS

receiver has a sensitivity of about -130 dBm, while a HSGPS receiver has sensitivity in the order of -150 dBm or lower (Ray 2005). This means that high sensitivity receivers can track a signal 100 times lower than nominal signal power. To accomplish this, longer integration is required to increase the signal-to-noise ratio (SNR). Since the correlation peaks repeat every 1 ms, the signal power increases by N^2 times with a coherent integration time of N ms, while the noise power increases by N under the assumption of Gaussian white noise. This produces a gain of N in terms of SNR. However, coherent integration time is limited by the navigation data modulation of 20 ms. In addition, if a residual frequency error exists during tracking, it also causes the signal power to oscillate between in-phase and out-of phase components, and limits the coherent integration time (MacGougan 2003).

Both a SiRF high sensitivity GPS receiver and a conventional low-cost CMC Allstar receiver were used in testing. Table 5.3 gives a summary of the specifications of these receivers.

Table 5.3: Descriptions of Receivers under Test

	SiRF Technology, Inc.	CMC Electronics Inc.
Model	SiRF XTrac L1 C/A code 12-channel	Allstar L1 C/A code 12-channel
Navigation Accuracy	Position < 5 m (Autonomous)	Position : 30 m (2σ) Velocity : 0.13 m/s (2 σ)
Sensitivity (Min.)	Tracking : 16 dB-Hz	Tracking : 31 dB-Hz
TTFF	Cold Start < 45 s	50 s (95%)
Dynamics (Max.)	Vel. : 514 m/s Accel. : 4 g	Vel. : 514 m/s Accel. : 4 g Jerk : 2 m/s^3
S/W Version	2.4.13.04-XTrac2.0.2	

5.3 Test Details

Figure 5.2 shows the set-up for hardware receiver tests, which were conducted on two receivers simultaneously. The antenna inputs of both receivers were connected to the hardware simulator via the interference combiner unit, low noise amplifier (LNA) and splitter. The LNA effectively decreases the line loss between the receivers and the LNA. Except for the interference signal, no other error sources were added to the GPS signal. The internal position solutions are discussed herein. The main descriptors of the test are as follows:

- Simulation Start Time: 2004. Oct. 26 (GPS Time: 226800)
- Initial Position: 51º 04' 48", -114º 08' 01", 1118.5 (LLH)
- No Atmospheric Delay, No Orbit Error, No multipath

- Elevation Cut-off: 5 degree

- Data Rate: 1 [Hz]

- YUMA Almanac File: YUMA270.txt (GPS week : 1294)
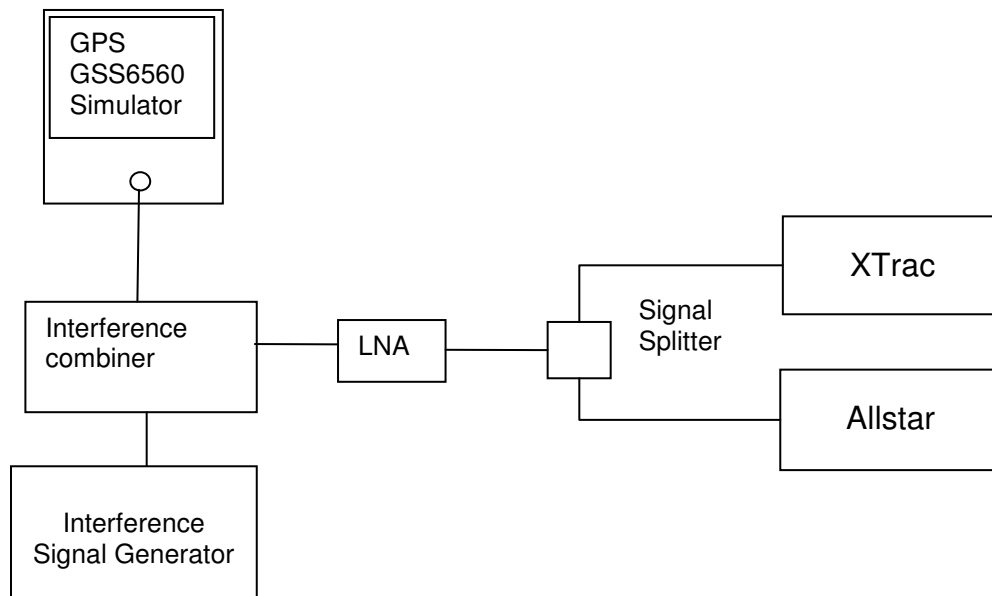
Figure 5.2: Hardware Receiver Test Setup

Pseudorange error calculation

The hardware simulator provides the simulated pseudorange and Doppler frequency. For the pseudorange calculation, the error means (which are regarded as embedded in the receiver clock bias) were removed at every epoch.

Position solutions

To estimate positions, the receiver internal solutions may employ different estimation schemes such as least-squares or a Kalman filter. The type of RAIM

that may be used in the internal solution is not known either. This is proprietary information that is not available to users. Additionally, although no atmospheric delays were simulated, the internal software applies a correction to compensate for trophospheric delays. In order to correctly analyse and compare the position solutions in a consistent manner, the measured pseudoranges were recorded during the tests and processed using C^3NAVG^2™, software developed by the PLAN Group (e.g., Petovello et al 2000). C^3NAVG^2™ uses an epoch-by-epoch least-squares method to estimate the positions. No mitigation or measurement rejection option (i.e. RAIM) was enabled in this case.

5.4 Static Test

A static vehicle was simulated with all error sources turned off. The available satellites during the static test are shown in Figure 5.3. In total, there are 10 satellites available during the static test.
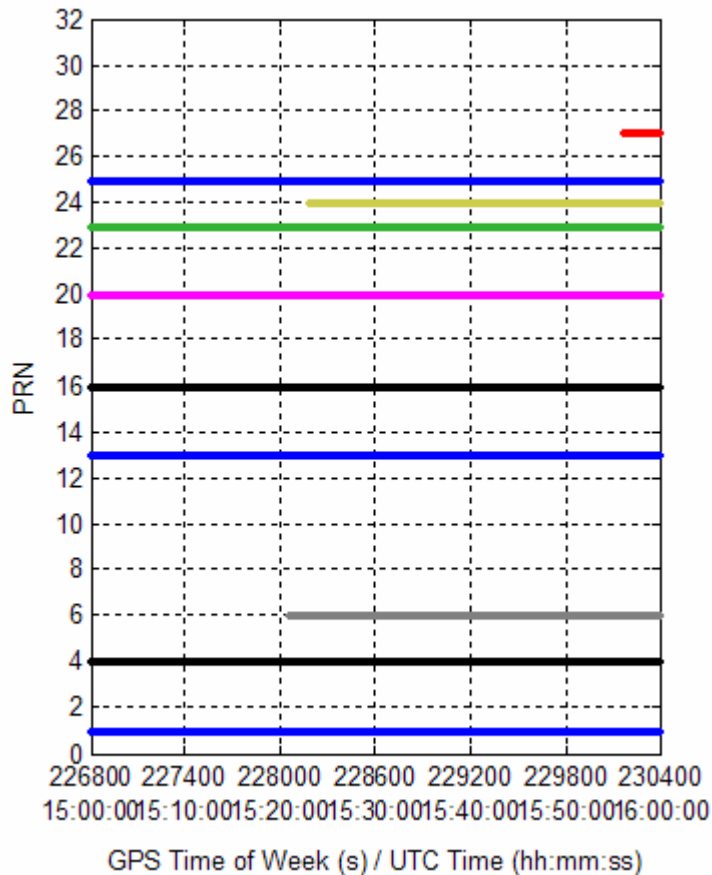
Figure 5.3: PRNs in View during Static Test

5.4.1 Error-free Test

Objective and methodology

The purpose of this test is to characterize the position errors of both receivers without pseudorange errors for purposes of comparison to subsequent interference tests. The remaining errors include background noise and receiver noise and receiver clock error. The GPS signal power was maintained at −155 dBW for 30 minutes.

C/N$_0$

Although the values for SNR were the same at the antenna inputs of both receivers, different C/N$_0$ values due to distinct estimation schemes are shown in Table 5.4. The XTrac's measured C/N$_0$ is 5.6 dB lower than that of the Allstar receiver.

Table 5.4: Measured C/N$_0$ during Error-free Test

C/N$_0$ [dB-Hz]	Average	Min	Max
XTrac	43.4	42.9	44.2
Allstar	49.0	48.8	49.3

Tracking and position errors

Figure 5.4 shows the number of satellites tracked by the receivers, used in the solution and the simulated (available) number of satellites. At the beginning of each static test, the XTrac unit tracked one more satellite that was not in view without providing any raw measurements. Initially, seven satellites were simulated throughout the static test. With a simulated signal of -155 dBW and no errors added, relatively accurate position estimations were measured, as shown in Table 5.5. The HDOP and VDOP were excellent, being below 1.6 and 2.5 during this test. The position errors are caused by measurement noise.
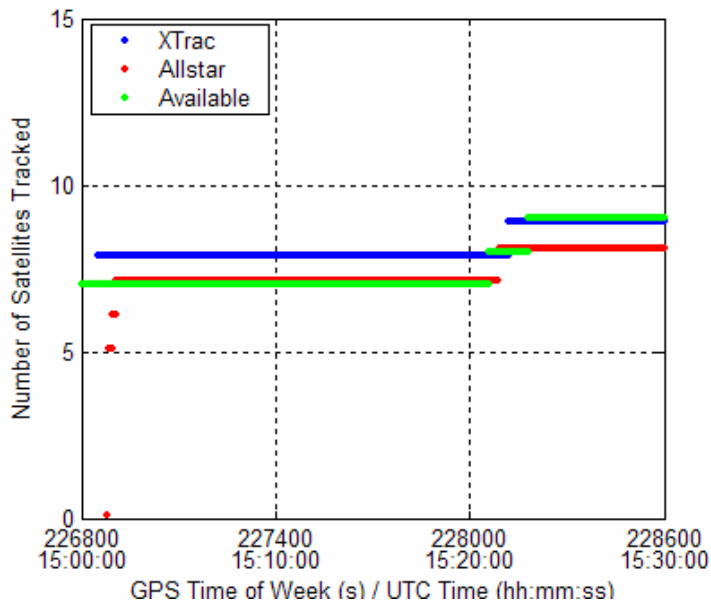
Figure 5.4: Number of Satellites Tracked during Error-free Test

Table 5.5: Statistics of Position Errors during Error-free Test

		Mean [m]	1 σ [m]	RMS [m]
Xtrac	Latitude	0.0	0.6	0.6
	Longitude	0.0	0.3	0.3
	Height	**-0.1**	**1.0**	**1.0**
Allstar	Latitude	-0.2	0.5	0.6
	Longitude	-0.1	0.1	0.1
	Height	**-0.4**	**0.9**	**1.0**

5.4.2 White Noise

Objective and methodology

This test examines performance under white noise conditions. The signal power

of the simulator is changed from +15 to -20 dB with respect to -160 dBW. A 20

dB attenuator was connected between the simulator and LNA to decrease the reference signal power from −160 dBW to −180 dBW. The resulting simulated power ranged from -165 dBW to -200 dBW. The signal power was decreased in steps of 1 dB every 1 minute after a 10-minute warm-up period.

C/N_0

The C/N_0 is a function of the signal strength, as shown in Figure 5.5-(a). Theoretically, since C/N_0 is the ratio of the signal power to noise power density, a decrease of 1 dB in signal power should produce a corresponding decrease of 1 dB-Hz in C/N_0, since the noise power density is assumed constant. MacGougan (2003) described the 'hockey stick effect' for the SiRF HS receiver. The C/N_0 estimation of the SiRFstarIIe receiver closely follows two trends depending on the GPS signal power. The slope of C/N_0 versus signal power with 21 dB-Hz and higher for measured C/N_0 is 0.83 dB-Hz/dB, while for C/N_0 21 dB-Hz and lower, it is 0.35 dB-Hz/dB. However, the slopes of C/N_0 versus signal power from this test are 0.97 dB-Hz/dB, and 0.99 dB-Hz/dB for the XTrac and Allstar units, respectively. The tracking thresholds were −185 dBW and −176 dBW for XTrac and Allstar, respectively, as shown in Figure 5.5-(b). Similarly, the minimum observed C/N_0s were 15.1 and 29.5 dB-Hz for the XTrac and Allstar, respectively, as shown in Table 5.6.

(a) Mean C/N$_0$ (b) Number of Satellites Tracked
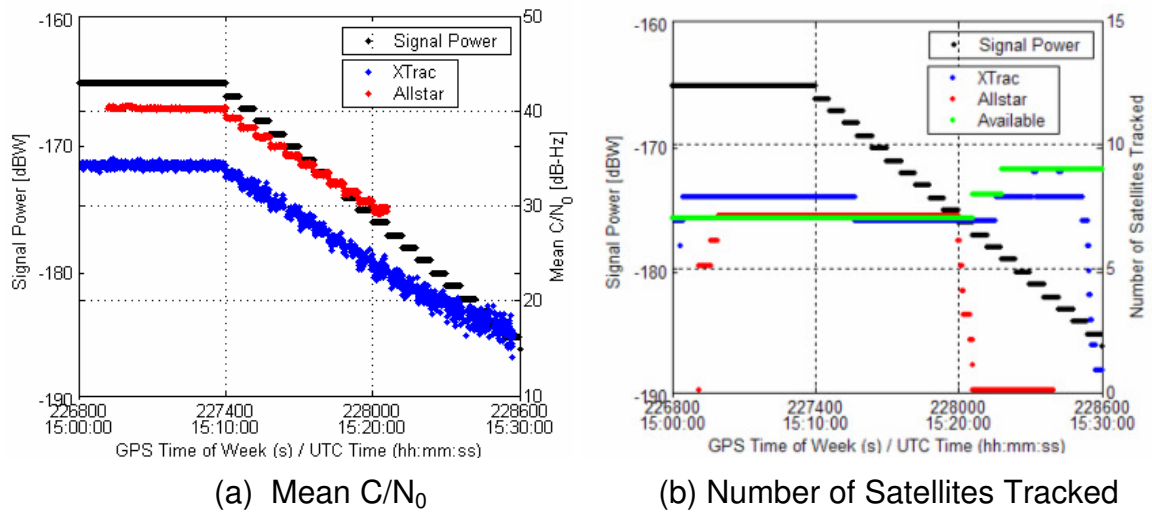
Figure 5.5: Mean C/N$_0$ and Number of Satellites Tracked during White Noise Test

Table 5.6: Minimum C/N$_0$ and Related Signal Power during White Noise Test

	Signal Power [dBW]	Minimum C/N$_0$ [dB-Hz]
XTrac	-185	15.1
Allstar	-176	29.5

(a) XTrac Unit   (b) Allstar Unit

Figure 5.6: Raw Measurements during White Noise Test

Table 5.7: Maximum Pseudorange Errors during White Noise Test

	Max. Pseudorange Error [m]	Signal Power [dBW]
XTrac	24.1	-185
Allstar	2.0	-170

Tracking and raw measurements

XTrac

Exponential increases in the errors of pseudorange and Doppler estimates for PRN 1 and PRN 4 with the decrease in signal strength are shown in Figure 5.7. In addition, both pseudorange and Doppler 1 σ errors decreased when simulated signal power of −182 dBW and −180 dBW for PRN 1 and PRN 4 were reached, respectively. This may be caused by the integration time changes inside the receiver. The maximum pseudorange error is 24.1 m when signal power was -185 dBW, as shown in Table 5.7. The large pseudorange error associated with PRN 6, with −179 dBW of signal power as shown in Figure 5.6-(a), was due to the transience of the tracking loop since that satellite was newly acquired. The maximum Doppler error of 70.4 Hz was observed immediately before the loss of tracking due to the divergent nature of the tracking loop. Except for this aspect of operation, the Doppler errors were within the range of ±15 Hz.

(a) Pseudorange
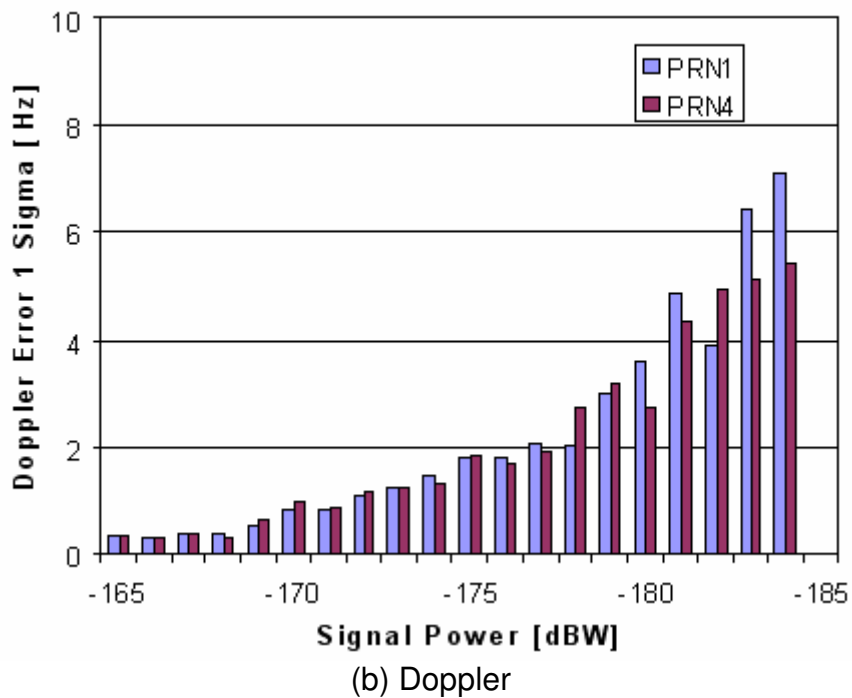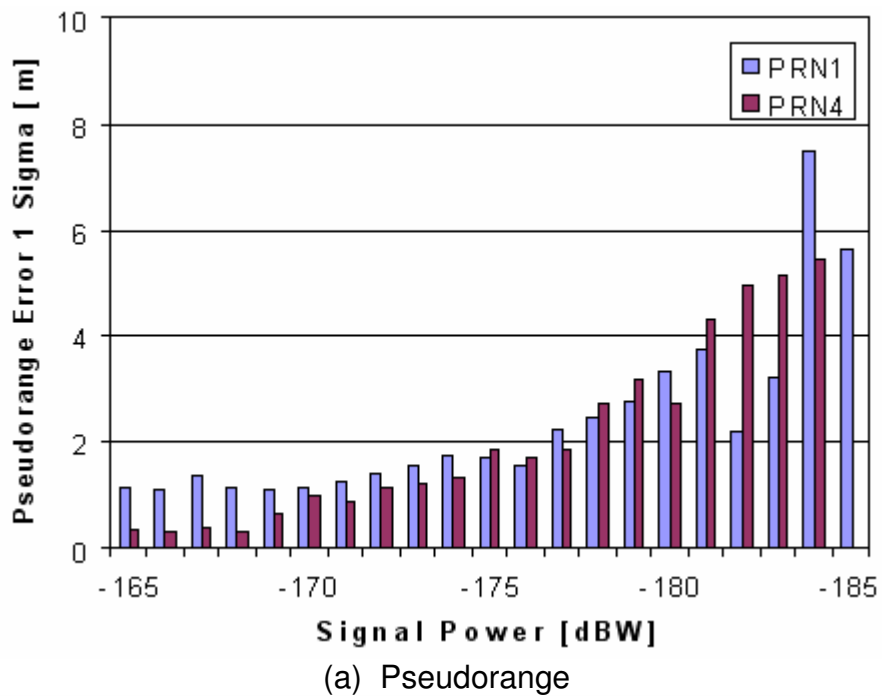
(b) Doppler

Figure 5.7: 1 σ of Pseudorange (a) and Doppler (b) errors - XTrac unit - during White Noise Test

Allstar

The 1 σ tracking loop errors of pseudorange and Doppler estimates of PRN 1 and PRN 4 versus signal strength are shown in Figure 5.8. The pseudorange errors were within ±2 m. When the signal power was lower than −173 dBW,

unusual jumps of Doppler frequency were measured, as shown in Figure 5.6; however, this does not affect the pseudorange measurements. In addition, Doppler frequency errors due to receiver clock estimation were observed, especially when the number of tracked satellites was three.
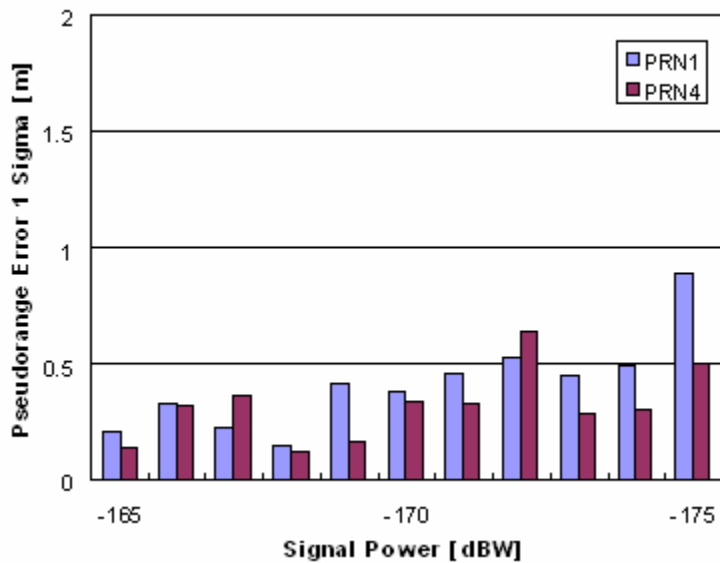
(a) Pseudorange
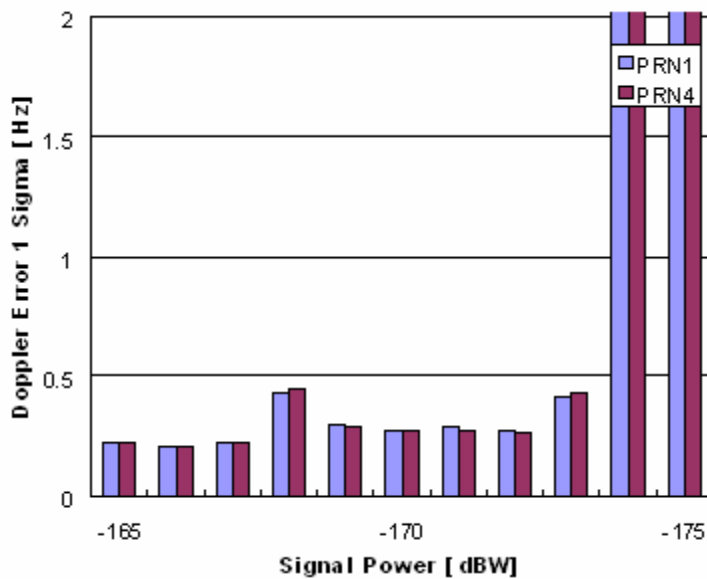
(b) Doppler

Figure 5.8: 1 σ of Pseudorange (a) and Doppler (b) errors - Allstar Unit - during White Noise Test

Position errors

For the XTrac unit, the pseudorange measurements exponentially increased when decreasing the signal power, resulting in an exponential increase in position errors, as shown in Figure 5.9. The maximum errors were 104.9 m and 6.6 m measured with the lowest signal power for the XTrac unit and Allstar unit, respectively, as shown in Table 5.8. It is called herein that the probability level of a 3D RMS position error is about 60%.
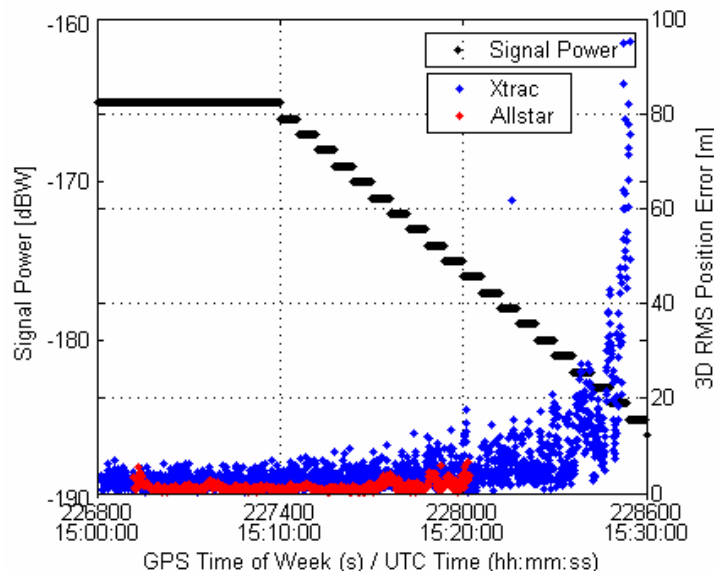
Figure 5.9: Position Errors during White Noise Test

Table 5.8: Maximum 3D RMS Position Errors during White Noise Test

	Max. 3D RMS Error [m]	Signal Power [dBW]
Xtrac	104.9	-185
Allstar	6.6	-175

5.4.3 CWI – Frequency Sweep from L1 to L1+1 MHz

Objective and methodology

This test examines the C/N_0 dependency on the centre frequency under CWI. The centre frequency of the CWI was changed from L1 to L1+1 MHz by 50 Hz every 100 ms after the 10-minute mark of testing. This frequency range approximately covers the main lobe of the L1 C/A code spectrum. The signal power was set to –155 dBW and the interference power was set to –130 dBW after a 10-minute warm-up period. Measurements were collected at a rate of 10 Hz.

Results and discussion

The C/N_0 of the XTrac unit as a function of centre frequency under CWI is shown in Figure 5.10. The theoretical estimation under CWI at L1+5 kHz with the 25 dB of I/S is 34.1 dB-Hz under the assumption of 43 dB-Hz of unjammed C/N_0 with a 2 MHz ideal front-end band-pass filter and ideal signal spectrum, as shown in Figure 2.7. The measured C/N_0 under CWI at L1+5 kHz was distributed from 30 to 35 dB-Hz. When the centre frequency of CWI is located at L1+1 MHz, the theoretical estimation is 42.97dB-Hz. However, the measured C/N_0 was approximately 37.5 dB-Hz. These differences could be caused by:

- Front-end band-pass filter characteristics such as pass band and cut-off, or/and
- a noise floor increase due to interference

The C/N$_0$ of the Allstar unit is changed from 40.8 to 42.3 dB-Hz throughout the test frequency range. The small changes of C/N$_0$ compared to that of the XTrac could be explained by the high unjammed C/N$_0$ of the Allstar for the same signal power as well as the different scheme used to estimate the C/N$_0$.

(a) XTrac Unit   (b) Allstar Unit
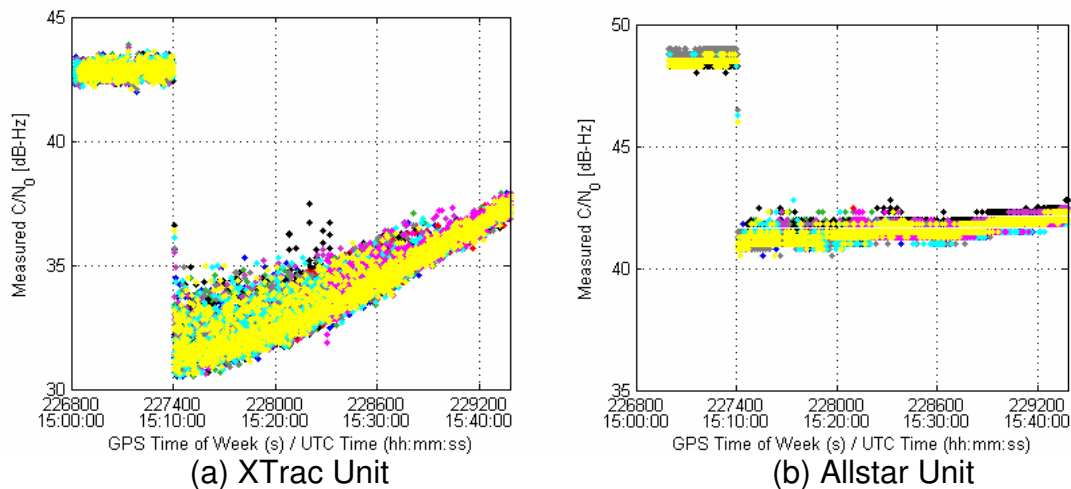
Figure 5.10: C/N$_0$ during Frequency Sweep Test

5.4.4 CWI within 1 kHz of δf

Objective and methodology

The objective of this test is to examine the effects of CWI within 1 kHz of δf, which is the frequency difference between the interference spectral line and a 1 kHz line spectrum of the signal. The interference power was set to −135 dBW after 5.5 minutes. This allows the I/S to range from 20 to 32 dB. The satellite's signal powers were set to levels of 5, 3, 1 −1, -3, -5, -7 dB relative to the −160 dBW for PRN 1, 4, 13, 16, 20, 23, 25, respectively, after a 5-minute warm-up

period. The centre frequency of CWI was L1+5 kHz. The test was performed

for 70 minutes so that the Doppler frequencies of satellites of interest would be

certain to travel more than 1 kHz.

Results and discussion

XTrac

The measured C/N_0, pseudorange error, and Doppler frequency of the XTrac unit

are shown in Figure 5.11. As shown in equation (2.7), the processing gain for the

CWI is a function of the magnitude of the nearest C/A code power spectral line,

frequency difference between the signal spectral line and interference frequency,

δf, and integration time. The processing gain has relatively low values when δf =

0. In this test, the interference frequency was fixed at L1+5 kHz, while the δf was

changing due to satellite motion. In theory, the low processing gain increases the

effective jamming power and results in a low C/N_0. However, as discussed in

Chapter 4, the C/N_0 increases due to the interference power leaking throughout

the correlation process. Increases in C/N_0 are observed when the δf became

small, regardless of the signal power. However, the increments were different

due to the power of the nearest power spectral line, $|C_l|^2$ as well as the

unjammed C/N_0. The second peak of PRN 13 occurred when the δf is relatively

high. This could be explained as cross-correlation between PRN 13 and 23, as

PRN 23 was highly affected by the interference. As shown in Figure 5.11-(b), the

rapid increases of pseudorange errors with false lock of the tracking loop were

observed for PRN 20, 23, 25, whose I/S values were relatively high. The δf of

PRN 20 became zero two times during this test. At the first occurrence, a false tracking loop lock occurred, while not so at the second occurrence – a phenomenon caused by the differing magnitudes of C_l. In addition, PRN 20 and 23 were lost and reacquired, while PRN 25 (whose signal power was the lowest) was not reacquired until the conclusion of this test.
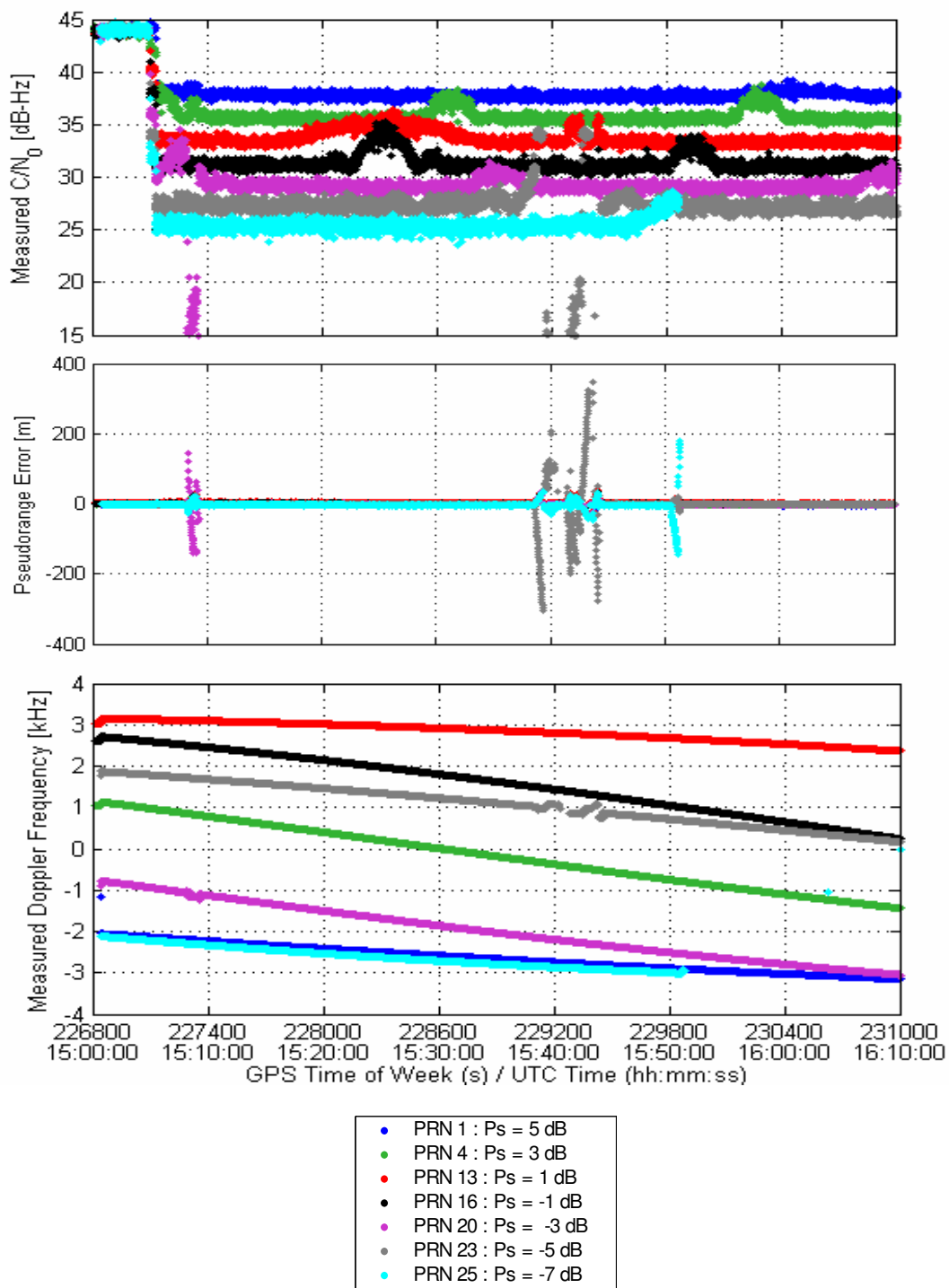
Figure 5.11: C/N$_0$ and Raw Measurements of the XTrac unit during CWI within 1 kHz of δf Test

Allstar

The increases in C/N_0 were also observed during test of the Allstar unit as shown in Figure 5.12, albeit with relatively low changes of C/N_0. PRN 16 and 20 were lost and reacquired, while PRN 23 and 25 were lost and not reacquired. No rapid increases of pseudorange errors due to false lock were observed.
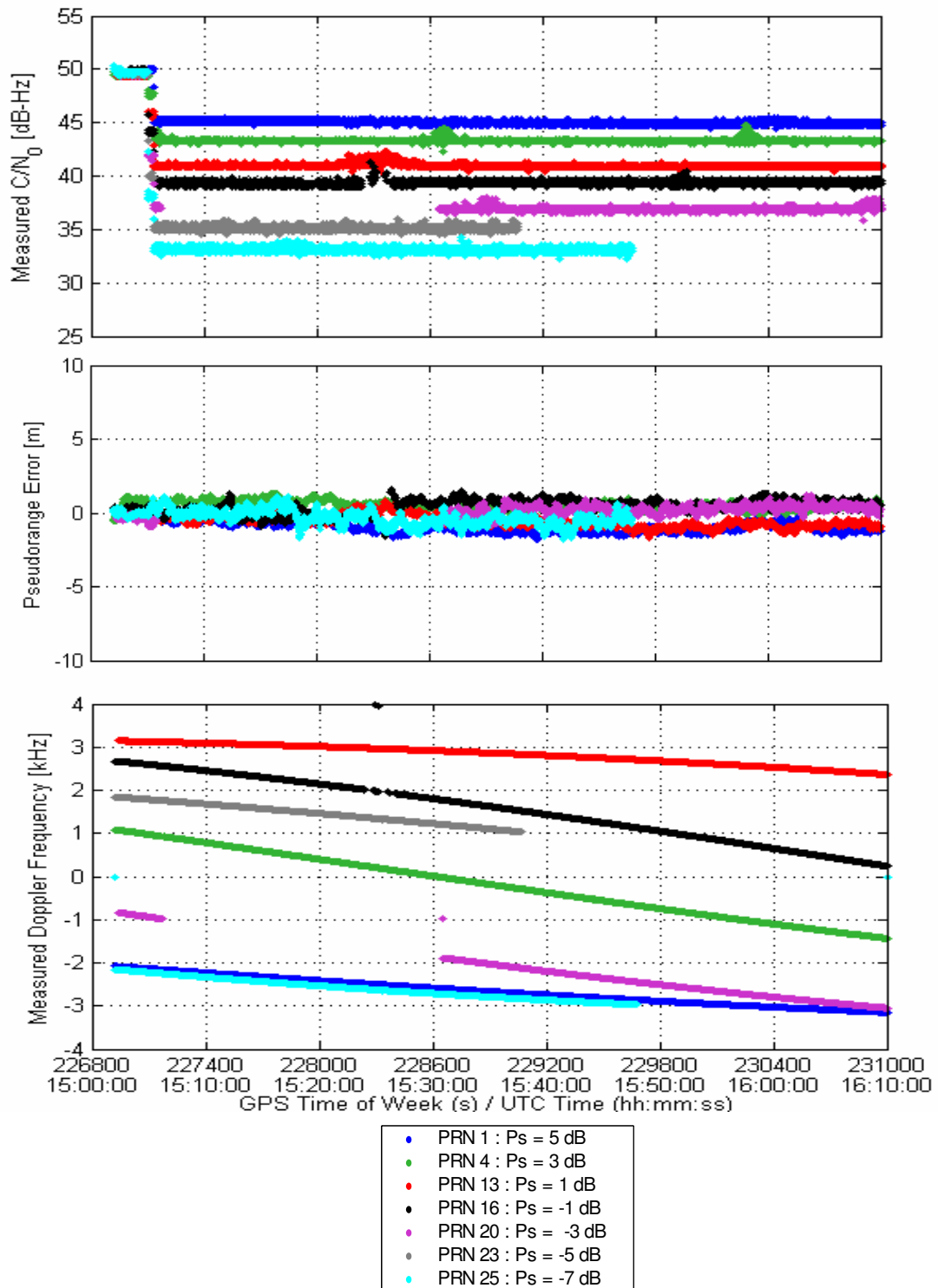
Figure 5.12: C/N$_0$ and Raw Measurements of Allstar unit during CWI within 1 kHz of δf Test

5.4.5 CWI - Centre Frequency Dependency

Objective and methodology

This test verifies the centre frequency dependency of the tracking threshold, raw measurement errors and position errors on CWI. Since the nature and magnitude of CWI effects depend on the relative position of the frequency's spectral line of interference in the C/A code frequency spectrum, three frequencies were selected with respect to the C/A code main lobe: L1+5 kHz, L1+500 kHz and L1+1 MHz. The signal power was maintained at −155 dBW. After the 10-minute warm-up period, the interference generator was switched on at a level of −160 dBW; following a 3-minute delay, the interference power was increased every 3 minutes in steps of 5 dB from an initial level of −145 dBW. Three tests were performed with three selected centre frequencies.

C/N_0

The C/N_0 versus interference power graphs for three different centre frequencies are shown in Figure 5.13. Both C/N_0 estimates are different from the theoretical estimates shown in Chapter 2. However, for the XTrac receiver, the centre frequency dependency on measured C/N_0 was observed until the measured C/N_0 values were higher than 20 dB-Hz. The lowest C/N_0 values under CWI at L1+5 kHz are 7.6 dB-Hz and 26.3 dB-Hz for the XTrac and Allstar units, respectively, which are lower than those under white noise interference conditions. Since the tracking is limited by the tracking loop jitter, this may indicate that the tracking loop errors under CWI are smaller than those under white noise for the same

C/N$_0$. The XTrac's C/N$_0$ values were available until 45 dB, 50 dB and 55 dB for CWI at L1+5 kHz, L1+500 kHz and L1+1 MHz, respectively, while the Allstar C/N$_0$ values were available until I/S = 40 dB, 45 dB, 45 dB for CWI at L1+5 kHz, L1+500 kHz, L1+1 MHz, respectively.

(a) XTrac Unit   (b) Allstar Unit
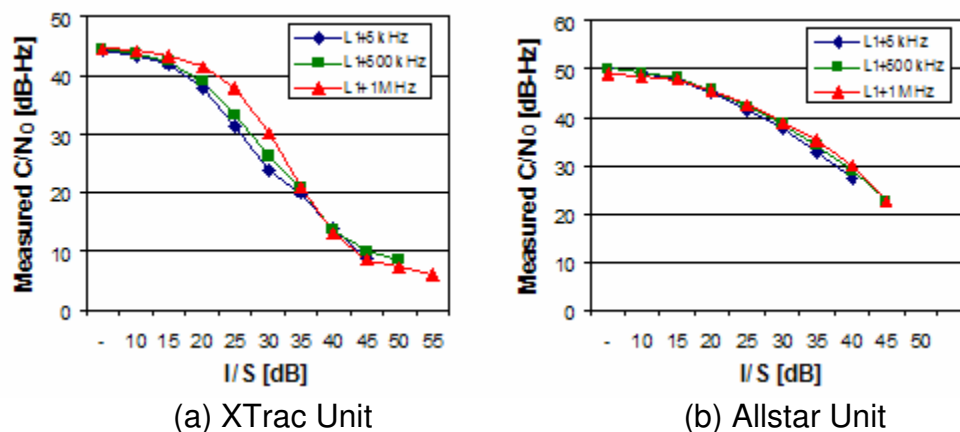
Figure 5.13: C/N$_0$ for three Different Centre Frequencies of CWI

Tracking and raw measurements

Table 5.9 shows the first loss of satellite and tracking thresholds in terms of I/S. The first false lock and loss of lock for the XTrac unit tracking loops were observed at 30 and 35 dB of I/S for CWI at 5 kHz and 500 kHz, respectively; similarly, the Allstar unit lost the satellites at the same power levels and CWI values, respectively. Under CWI at L1+1 MHz, the XTrac unit did not lock on the interfered signal. In addition, the tracking thresholds show 5 dB to 10 dB differences between the centre frequencies, since the XTrac unit reacquired the satellites with interfered signals. As shown in Table 5.10, pseudorange errors

were the maximum with a CWI of 500 kHz for both receivers, as this type of

interference contains the most DLL tracking loop error amongst the three centre

frequencies, as shown in Section 2.3. In addition, maximum pseudorange errors

were not observed as having the highest interference powers due to the

processing gain changes with Doppler shift under CWI. Figure 5.14, Figure 5.16

and Figure 5.18 illustrate the number of satellites tracked and Figure 5.15, Figure

5.17 and Figure 5.19 show the pseudorange errors and Doppler measurements

under CWI at L1+5 KHz, L1+500 kHz and L1+1 MHz, respectively.

Table 5.9: First Loss and Tracking Threshold under CWI

I/S [dB]	XTrac		Allstar	
Centre Frequency	First False Lock/Loss of XTrac	Tracking Threshold	First Lost	Tracking Threshold
L1+5 kHz	30	45	30	40
L1+500 kHz	35	50	35	45
L1+1 MHz	55	55	40	45

Table 5.10: Maximum Pseudorange Error under CWI

	XTrac		Allstar	
	Maximum Pseudorange Error [m]	I/S [dB]	Maximum Pseudorange Error [m]	I/S [dB]
L1+5 kHz	293.4	35	1.8	35
L1+500 kHz	754.1	40	5.3	40
L1+1 MHz	164.0	50	2.7	40
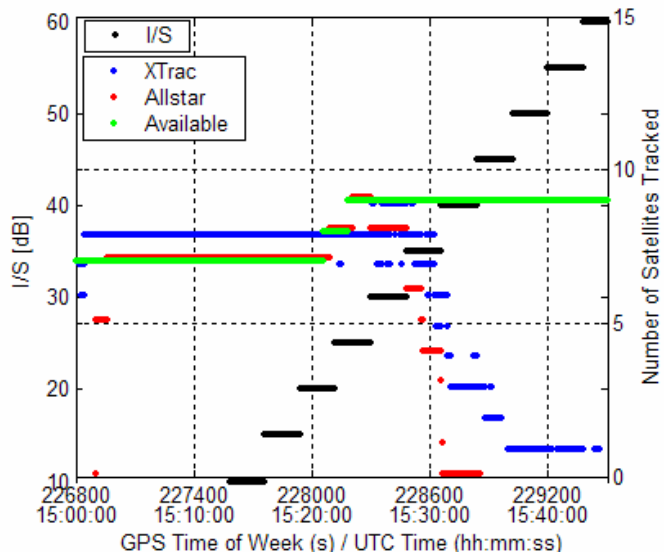
Figure 5.14: Number of Satellites Tracked during the CWI at L1+5 kHz Test
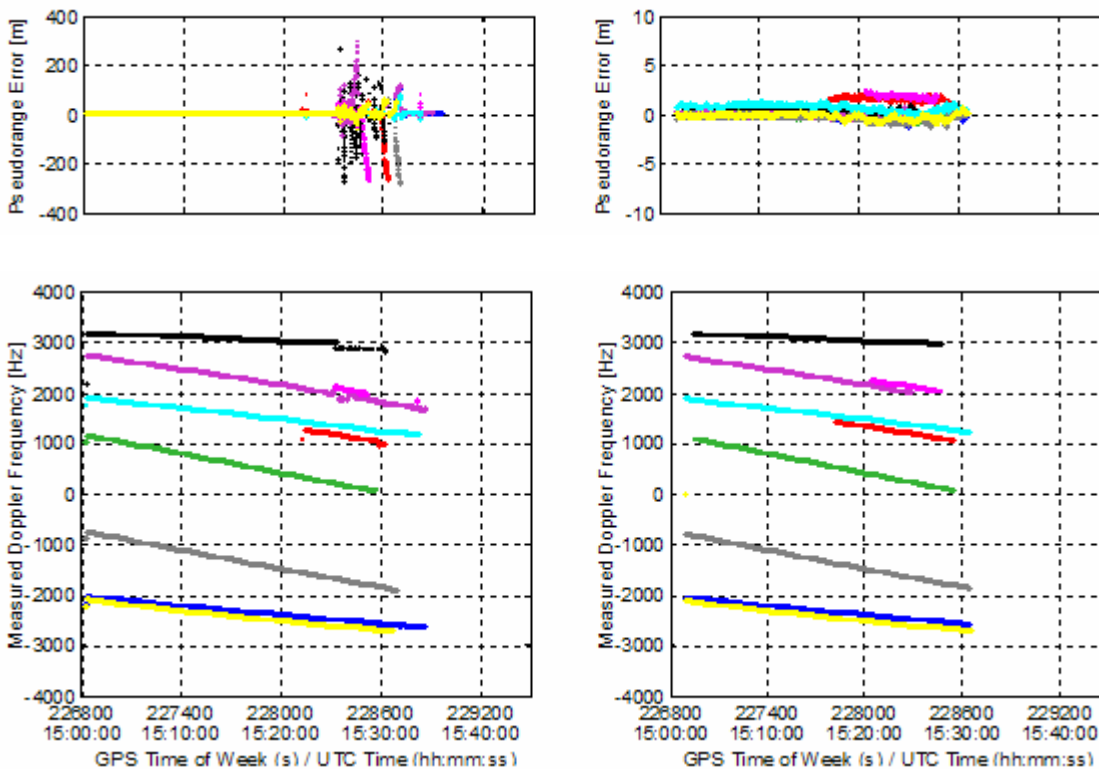
(a) XTrac Unit   (b) Allstar Unit

Figure 5.15: Pseudorange Errors and Doppler Measurements during the CWI Test at L1+5 kHz
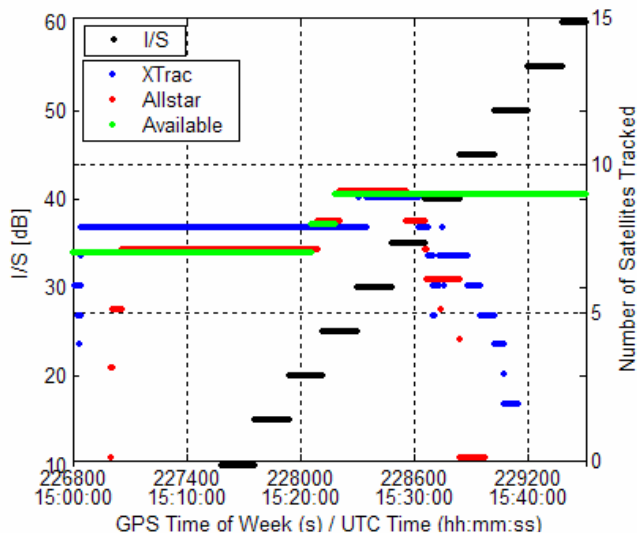
Figure 5.16: Number of Satellites Tracked during the CWI at L1+500 kHz Test

(a) XTrac Unit   (b) Allstar Unit
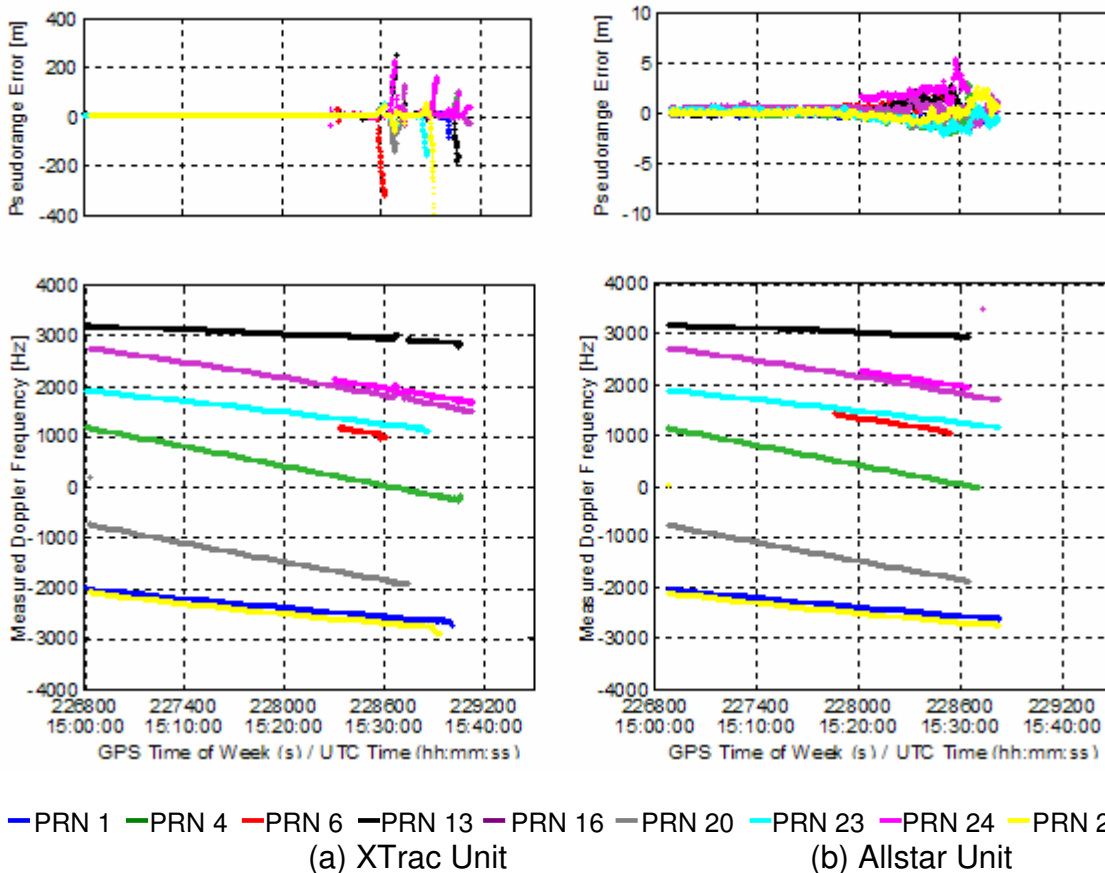
Figure 5.17: Pseudorange Errors and Doppler Measurements during the CWI Test at L1+500 kHz
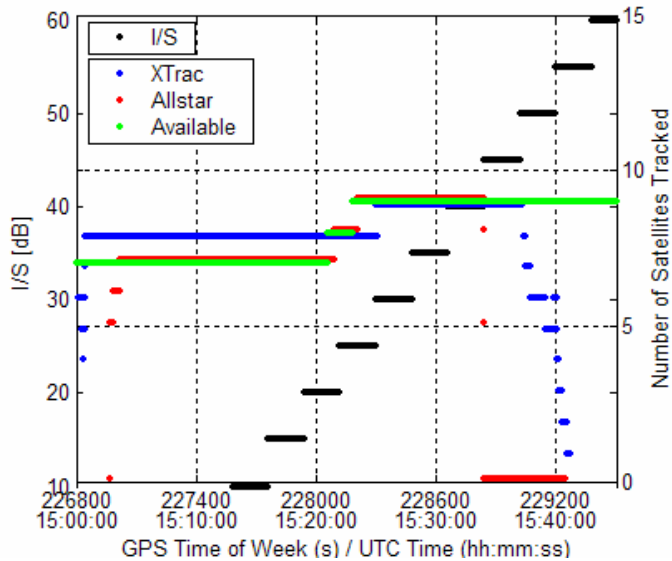
Figure 5.18: Number of Satellites Tracked during the CWI at L1+1 MHz Test

(a) XTrac Unit　　　　　　(b) Allstar Unit
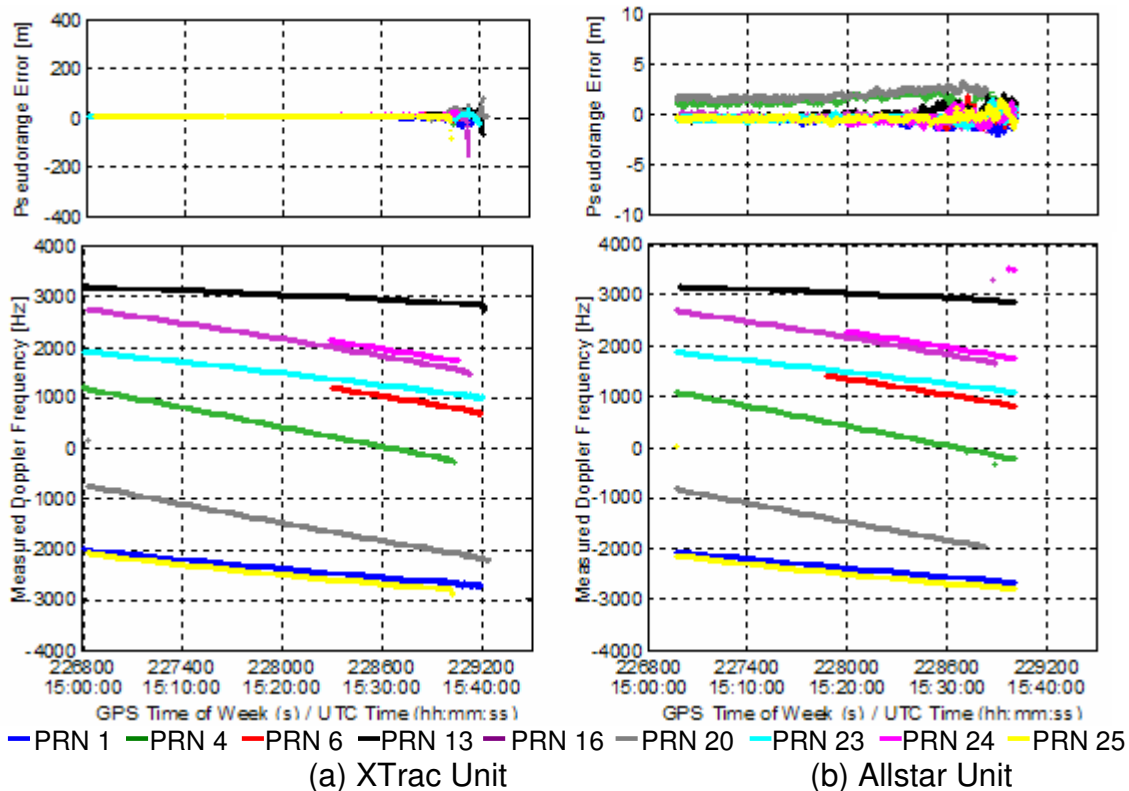
Figure 5.19: Pseudorange Errors and Doppler Measurements during the CWI Test at L1+1 MHz

Position errors

Figure 5.20 shows the 3D RMS position errors versus interference power during the CWI test. During this test, the largest position errors were measured with the CWI at L1+500 kHz for both receivers since this type of interference contains the larger pseudorange errors amongst the three centre frequencies. The corresponding maximum 3D RMS position errors were 3,580.4 m and 7.5 m for the XTrac and Allstar, respectively, as shown in Table 5.11.

(a) XTrac Unit

	-	0	10	15	20	25	30	35	40	45	50	55
■ L1+5 kHz	1.1	1.3	1.5	1.6	2.2	2.4	92.0	188.6	88.0			
■ L1+500 kHz	1.2	1.2	1.5	1.6	2.1	2.7	5.3	66.8	69.7	1111.5	1065.7	
■ L1+1 MHz	1.2	1.2	1.5	1.4	1.6	1.9	2.3	2.7	3.9	7.4	45.9	100.3

I/S [dB]

(b) Allstar Unit

	-	0	10	15	20	25	30	35	40	45
■ L1+5 kHz	0.8	1.2	1.3	1.5	1.5	1.5	1.5	1.7		
■ L1+500 kHz	0.6	0.7	0.4	0.7	1.2	2.6	4.2	4.6	4.7	
■ L1+1 MHz	1.3	1.1	1.2	1.6	2.1	2.4	3.0	3.5	3.6	2.3
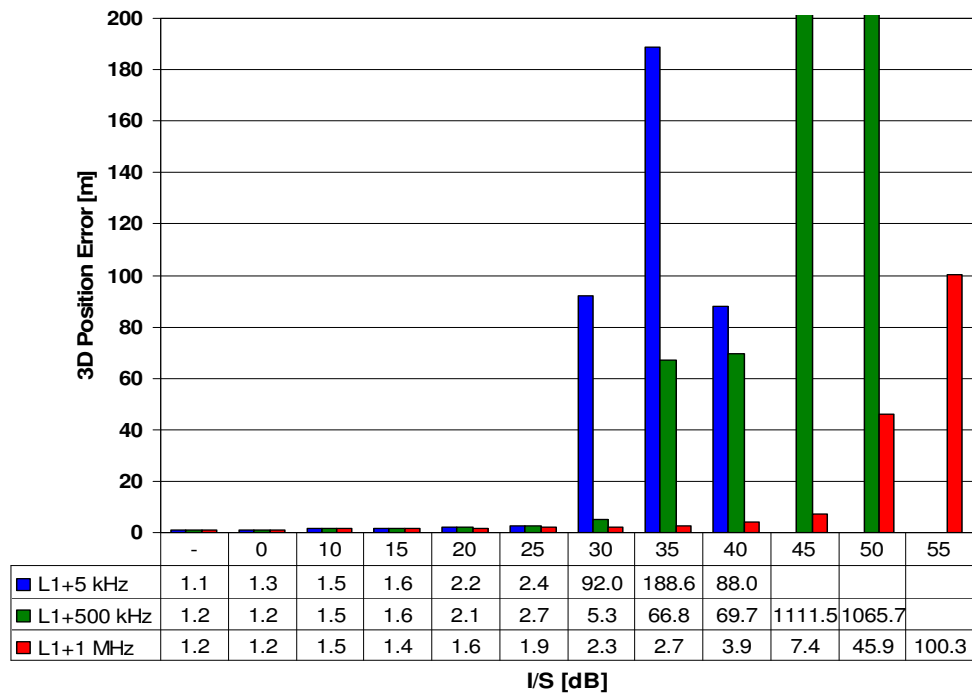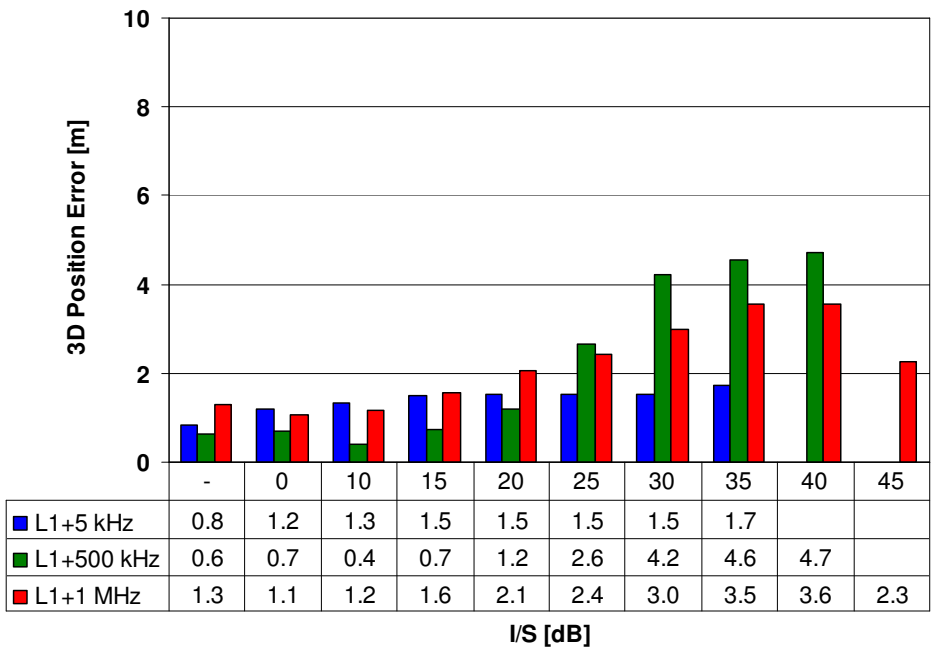
I/S [dB]

Figure 5.20: 3D RMS Position Errors under CWI

Table 5.11: Maximum 3D RMS Position Errors under CWI

		Max. 3D RMS Error [m]	I/S [dB]
	L1+5 kHz	625.1	35
Xtrac	L1+500 kHz	3580.4	45
	L1+1 MHz	133.7	55
	L1+5 kHz	2.6	35
Allstar	L1+500 kHz	7.5	40
	L1+1 MHz	4.3	45

5.4.6 CWI – Different Unjammed C/N_0

Objective and methodology

The aim of this test is to examine the effects of the unjammed C/N_0 on receiver performance under CWI. The centre frequency of CWI was set to L1+5 kHz, and the signal powers set to -160 dBW and –165 dBW after an initial 5-minute warm-up period. After 10 minutes, the interference generator was switched on at a level of –160 dBW and, following a 3-minute delay, the interference power was increased every 3 minutes in steps of 5 dB from –145 dBW.

C/N_0

The C/N_0 for three different unjammed C/N_0 values as a function of I/S are shown in Figure 5.21. The C/N_0 of the XTrac unit was affected by the unjammed C/N_0 untill I/S = 20 dB, while the C/N_0 of the Allstar unit was affected by the unjammed C/N_0 untill I/S = 40 dB.

(a) XTrac Unit   (b) Allstar Unit
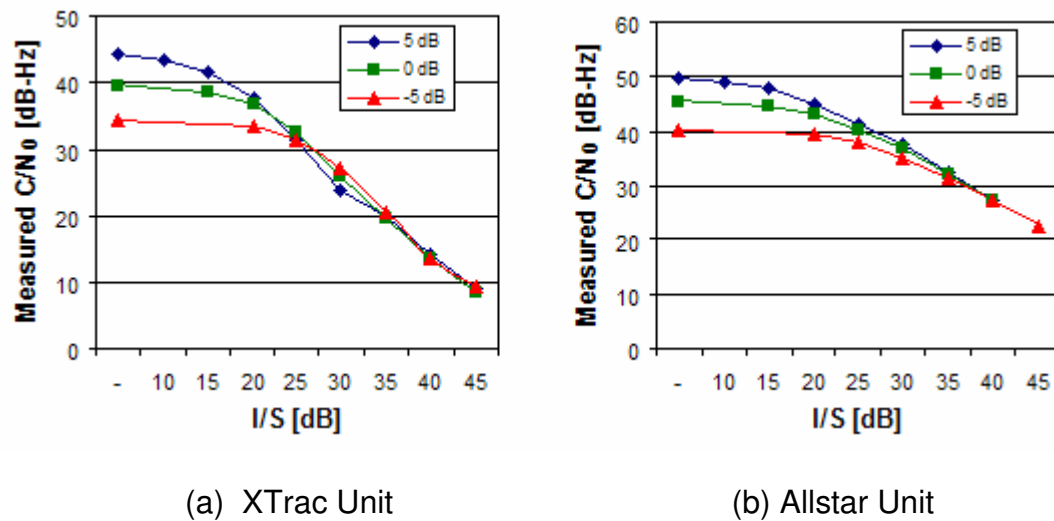
Figure 5.21: Mean C/N$_0$ under CWI at L1+5 kHz for Three Different Unjammed C/N$_0$ values

Tracking and raw measurements

As shown in Table 5.12, false locks and tracking loop losses appeared to commence at the same I/S as in the 30 dB case for the XTrac unit. Also, the raw measurements were available until I/S = 45 dB for three different unjammed C/N$_0$ values. The maximum pseudorange errors did not exceed 300 m under CWI at L1+5 kHz, as shown in Table 5.13. However, the Allstar unit began to lose satellites at 30 dB, 25 dB and 25 dB for three different unjammed C/N$_0$ values. Figure 5.22 and Figure 5.24 show the number of satellites tracked and Figure 5.23 and Figure 5.25 show pseudorange errors and Doppler measurements when the signal power equals -160 dBW and -165 dBW, respectively.

Table 5.12: First/Last Loss of Satellites (I/S [dB]) under CWI at L1+5 kHz for Three Different Unjammed C/N$_0$ values

Signal power relative to -160 [dBW]	XTrac		Allstar	
	First False Lock/Loss (I/S [dB])	Tracking Threshold (I/S [dB])	First Lost (I/S [dB])	Tracking Threshold (I/S [dB])
5 dB	30	45	30	40
0 dB	30	45	25	40
-5 dB	30	45	25	40

Table 5.13: Maximum Pseudorange Errors under CWI at L1+5 kHz for Three Different Unjammed C/N$_0$ values

Signal power relative to -160 [dBW]	XTrac		Allstar	
	Maximum Pseudorange Error [m]	I/S [dB]	Maximum Pseudorange Error [m]	I/S [dB]
5 dB	293.4	35	1.8	35
0 dB	282.3	35	1.3	35
-5 dB	288.9	40	1.7	40

Figure 5.22: Number of Satellites Tracked under CWI at L1+5 kHz When Signal Power = -160 dBW

(a) XTrac Unit   (b) Allstar Unit

Figure 5.23: Pseudorange Errors and Doppler Measurements under CWI at L1+5 kHz When Signal Power = -160 dBW

Figure 5.24: Number of Satellites Tracked under CWI at L1+5 kHz When Signal Power = -165 dBW

(a) XTrac Unit   (b) Allstar Unit

Figure 5.25: Pseudorange Errors and Doppler Measurements under CWI at L1+5 kHz When Signal Power = -165 dBW

Position errors

Figure 5.26 and Figure 5.27 show the 3D RMS position errors and GDOP for three different signal levels. Since the same geometry was not simulated with the same I/S in each case, the errors were not at comparable levels. However, the maximum position errors of the XTrac unit were observed with false locks and smaller than those of CWI at L1+500 kHz, as shown in Table 5.14.
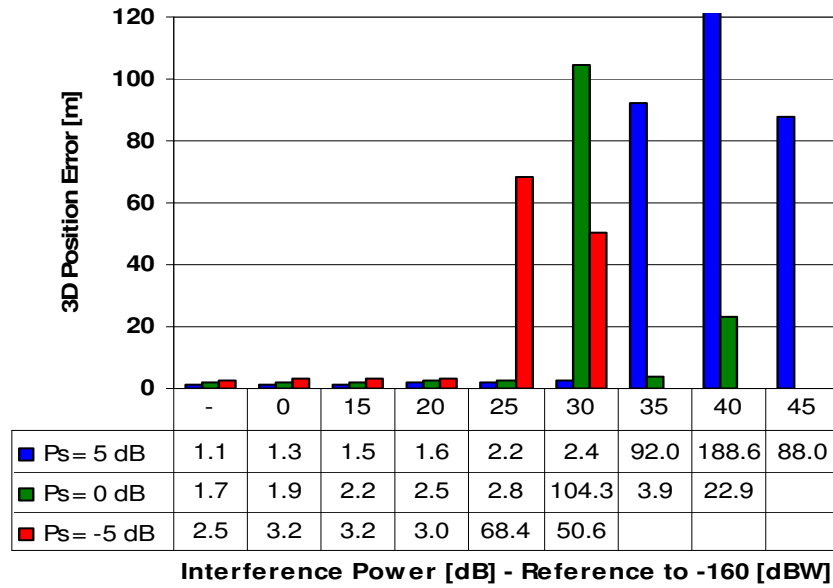
(a) XTrac Unit
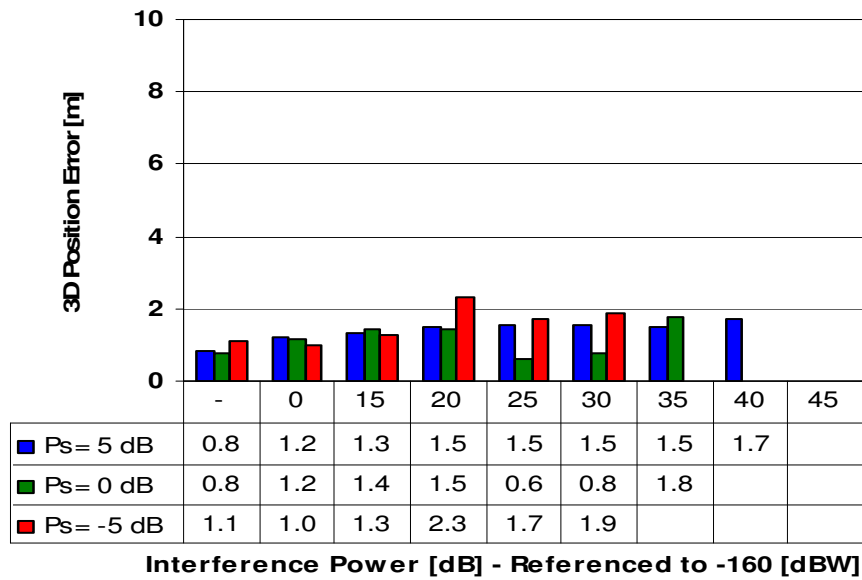
(b) Allstar Unit

Figure 5.26: 3D RMS Position Errors under CWI at L1+5 kHz for Three different Unjammed C/N$_0$

(a) XTrac Unit

(b) Allstar Unit
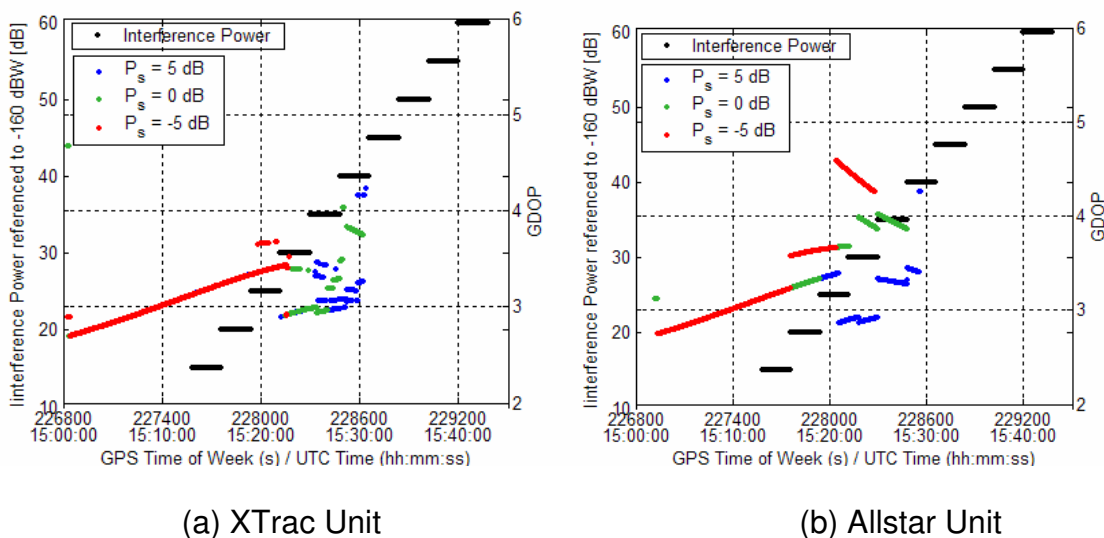
Figure 5.27: GDOP under CWI at L1+5 kHz for Three Different Unjammed C/N$_0$

Table 5.14: Maximum 3D RMS Position Errors during CWI at L1+5 kHz for Three Different Unjammed C/N$_0$

		Max. 3D RMS Error [m]	I/S [dB]
Xtrac	Ps = 5 dB	625.1	35
	Ps = 0 dB	311.4	30
	Ps = -5 dB	211.2	30
Allstar	Ps = 5 dB	2.6	35
	Ps = 0 dB	2.6	35
	Ps = -5 dB	4.4	35

5.4.7 BLWNI – Bandwidth Sweep

Objective and methodology

The aim of this test was to examine the bandwidth dependency of C/N_0 under BLWNI. The interference signal was centred at L1, and the bandwidths changed from 50 Hz to 20 MHz every 3 minutes following a 10-minute warm-up period. The signal power was set to –155 dBW and the interference power was set to –120 dBW after 10 minutes.

Results and discussion

Figure 5.28 shows the measured C/N_0 under 10 different bandwidths of BLWNI centred at L1. The narrower the bandwidth, the lower is the measured value of C/N_0 since the interference power is concentrated on the tracking loop pass-band.
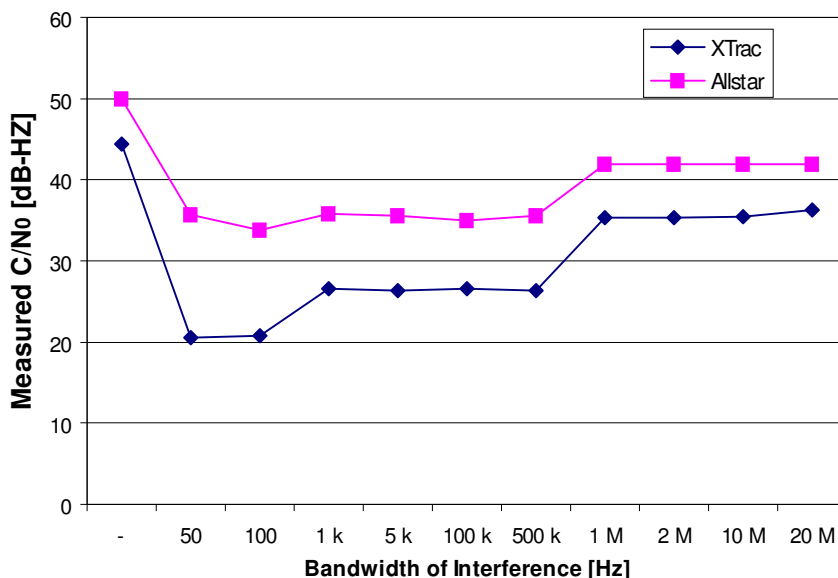
Figure 5.28: Bandwidth Dependency of C/N_0 under BLWNI

5.4.8 BLWNI with 1 kHz bandwidth centred at L1

Objective and methodology

This test assesses the tracking threshold, raw measurement errors and position errors under BLWNI. After the initial 10-minute warm-up period, the interference generator was switched on at a level of −160 dBW; as in previously described tests, a 3-minute delay ensued, after which the interference power was increased every 3 minutes in steps of 5 dB from the initial value of −145 dBW. The signal power was set to -155 dBW.

C/N_0

As the interference power increased, the measured C/N_0 values decreased, as shown in Figure 5.29 for both receivers. However, in a departure from the CWI test results, an abrupt increase of the C/N_0 was not observed under BLWNI since it has a flat spectrum within 1 kHz. In addition, the difference of the C/N_0 measured between satellites became larger as the interference power increased, since the effective power is proportional to the P_n, as shown in Table 2.1. The minimum C/N_0 values observed were 7.4 and 25.5 dB-Hz for the XTrac and Allstar unit, respectively, which are lower than in the white noise case.
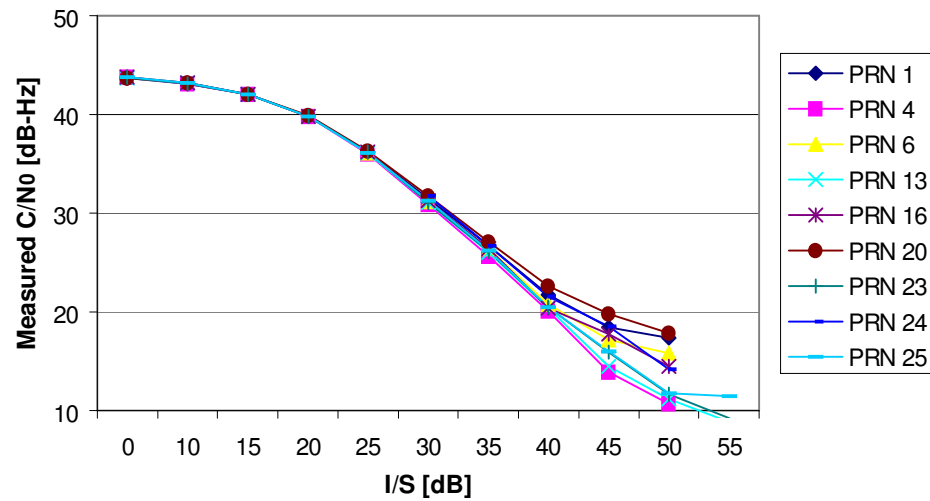
(a) XTrac Unit
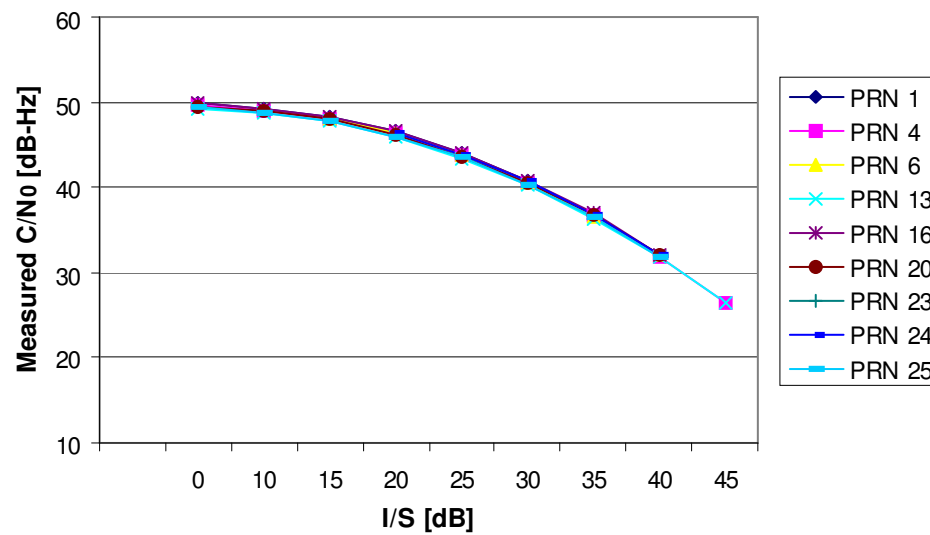
(b) Allstar Unit

Figure 5.29: C/N$_0$ during BLWNI with 1 kHz Bandwidth Test

Tracking and raw measurements

Figure 5.30 shows the number of satellites tracked and Figure 5.31 shows the raw measurement errors and Doppler measurements during this test. The raw measurements were available until I/S = 50 dB and 45 dB for the XTrac and Allstar, respectively, and the maximum pseudorange errors were 56.1 m and 3.6 m, respectively, for the two units. The large pseudorange errors for PRN 4 of the XTrac unit were measured for several epochs just before loss of tracking when three satellites were tracked. The C/N_0 observed for this satellite was the lowest among the satellites tracked. No false lock of tracking was observed with XTrac unit during this test. The Allstar provided the pseudorange measurements of PRN 4 and PRN 13 while the other satellites tracked were lost. For the XTrac unit, the measured C/N_0 values of these satellites were also low relative to the other satellites. This may indicate that the satellites with low C/N_0 values are less affected by this type of interference.

Figure 5.32 shows the 1-sigma values of pseudorange and Doppler measurements versus measured C/N_0 levels for white noise and BLWNI. For the same I/S, the tracking loop errors of satellites whose C/N_0 values were higher, were larger for the XTrac. In the case of the Allstar, however, the DLL tracking errors under BLWNI were higher than for the white noise case. Both DLL and PLL tracking errors are small, as compared to the XTrac.
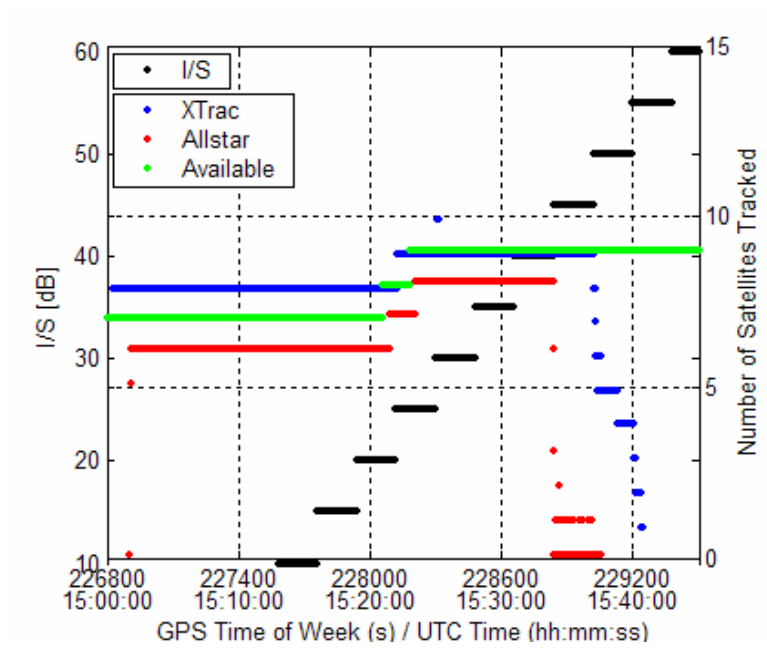
Figure 5.30: Number of Satellites Tracked during BLWNI Test
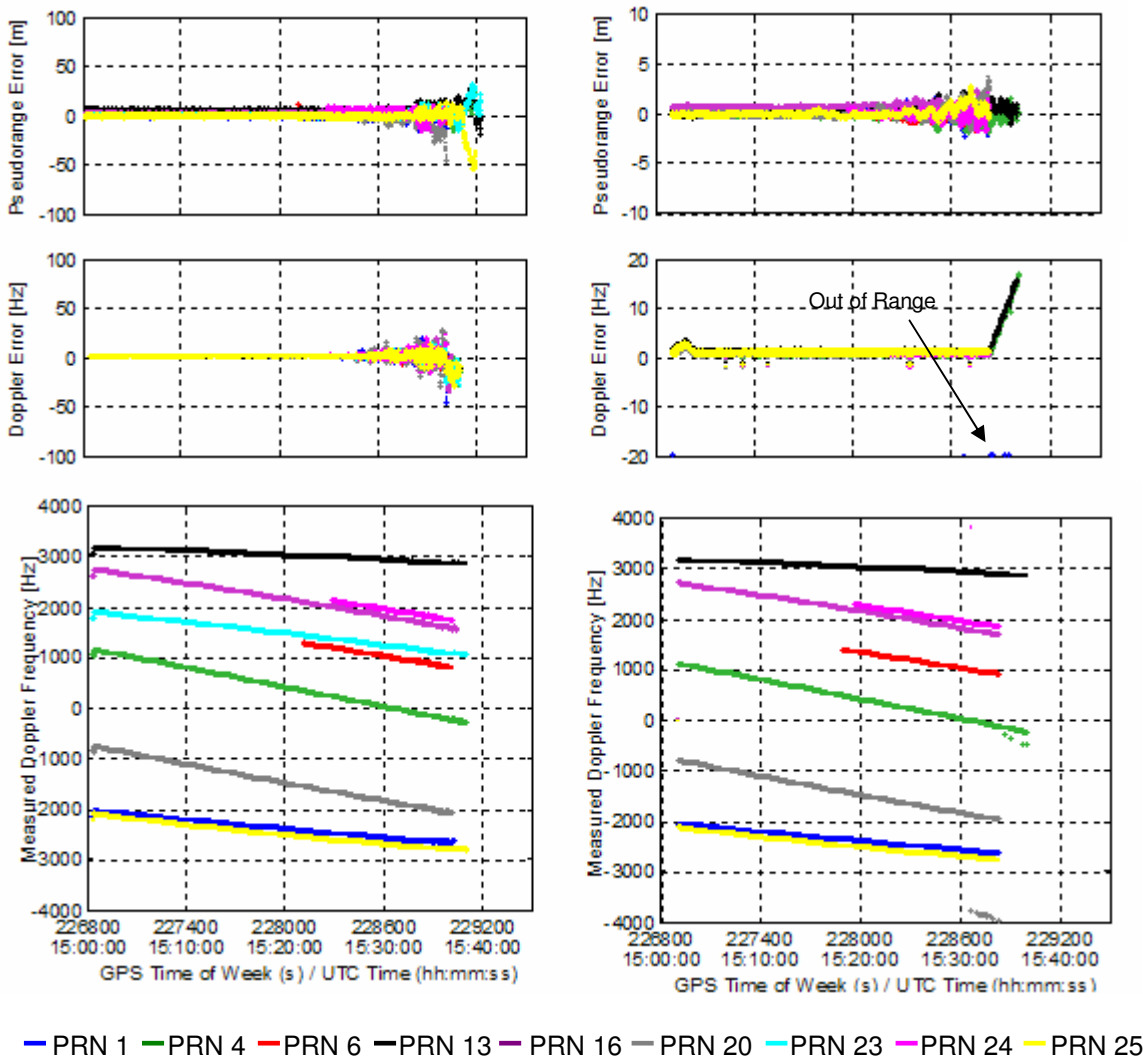
(a) XTrac   (b) Allstar

Figure 5.31: Raw Measurements Errors and Doppler Frequency Measurements during BLWNI Test

(a)-1 Pseudorange 1 σ of XTrac Unit (a)-2 Doppler 1 σ of XTrac Unit

(b)-1 Pseudorange 1 σ of Allstar Unit (b)-2 Doppler 1 σ of Allstar Unit
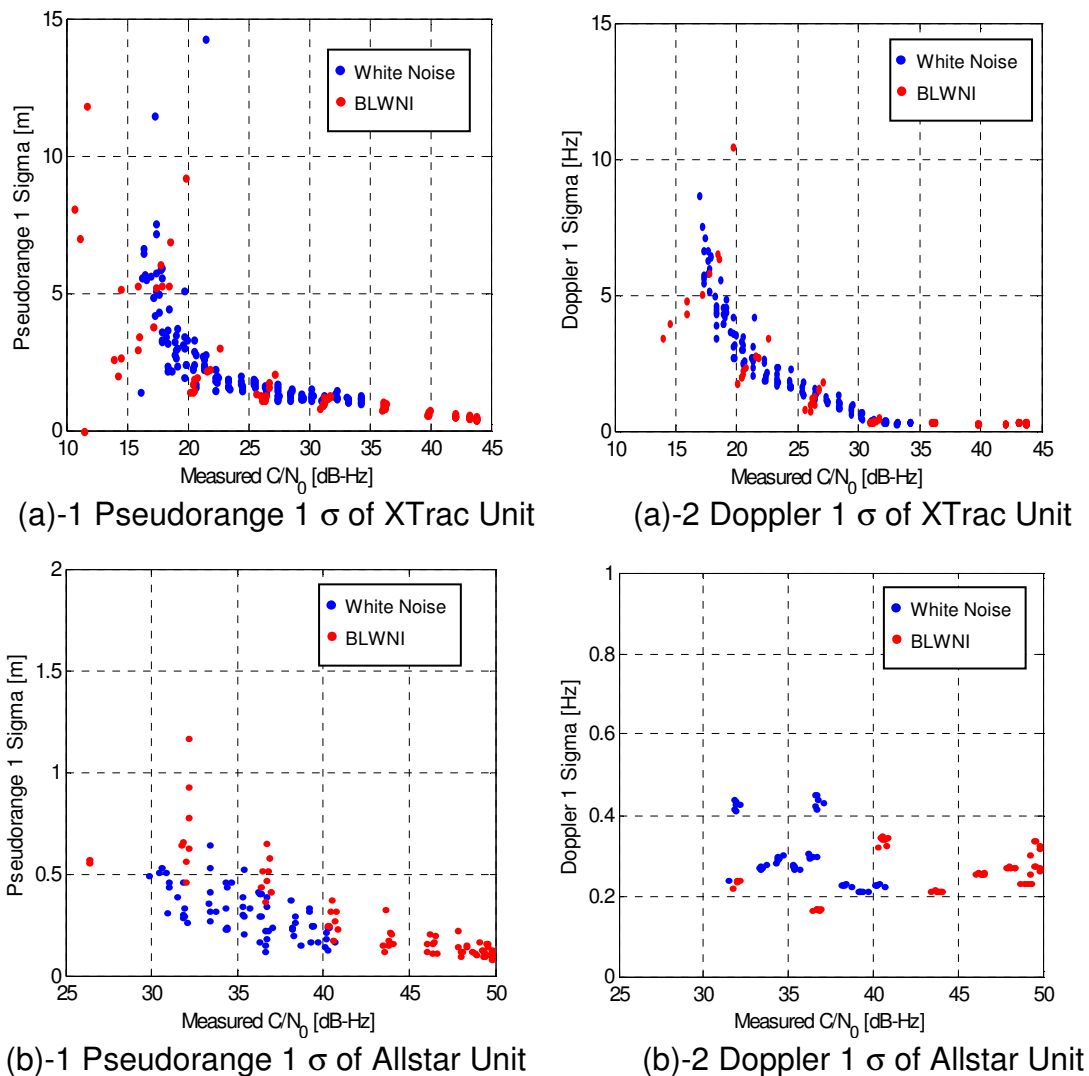
Figure 5.32: Comparisons of Tracking Errors between White Noise and BLWNI

Position errors

Figure 5.33 shows the 3D RMS position errors during the BLWNI test. These errors showed a similar trend compared to the trend under WN. The maximum position errors were observed with maximum interference power for both receivers, as shown in Table 5.15.
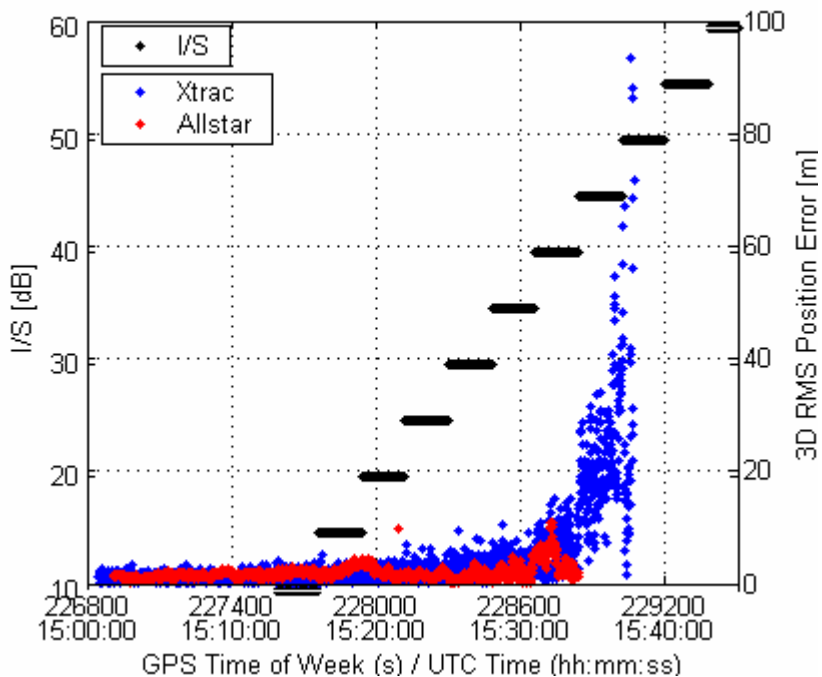
Figure 5.33: Position Errors during BLWNI Test

Table 5.15: Maximum 3D RMS Position Errors during BLWMI Test

	Max. 3D RMS Error [m]	I/S [dB]
XTrac	394.2	50
Allstar	10.8	40

5.4.9 BLWNI – Different Signal Strengths

Objective and methodology

The aim of this test was to examine the unjammed C/N_0 effects on receiver performance under BLWNI. The signal powers were set to -160 dBW and –165 dBW after the 5-minute warm-up. After 10 minutes, the interference generator was switched on at a level of –160 dBW; following a 3-minute delay, the

interference power was increased every 3 minutes in steps of 5 dBW from –

145 dBW.

C/N_0

Plots of the C/N_0 for three different unjammed C/N_0 values as a function of I/S

are shown in Figure 5.34. The C/N_0 of the XTrac unit was affected by the

unjammed C/N_0 until I/S = 30 dB, while the C/N_0 of the Allstar was affected by the

unjammed C/N_0 until I/S = 45 dB which is 5 dB higher than those under CWI.

(a) XTrac Unit   (b) Allstar Unit
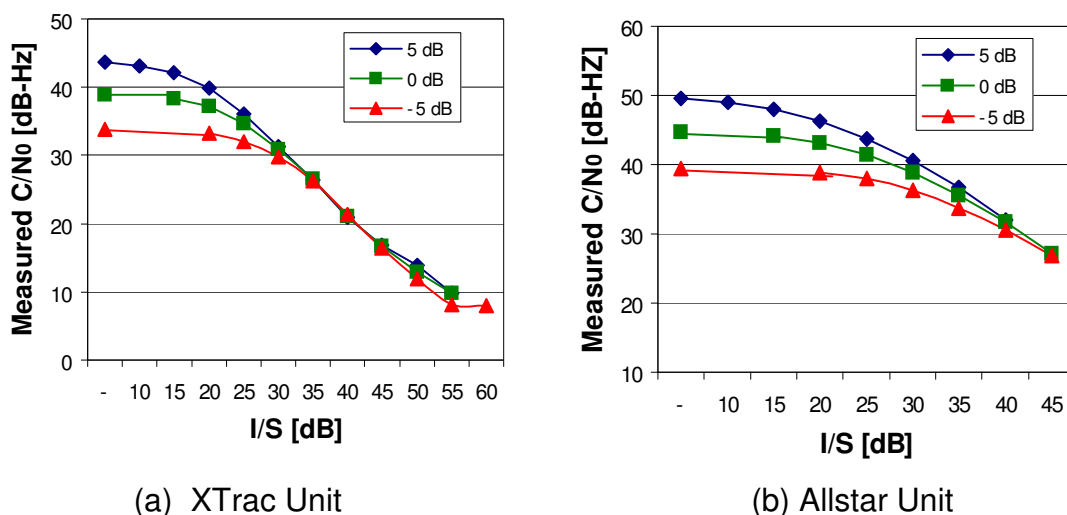
Figure 5.34: C/N_0 under BLWNI for Three Different Unjammed C/N_0 values

Tracking and raw measurements

Figure 5.35 and Figure 5.37 show the number of satellites tracked, while Figure

5.36 and Figure 5.38 show the raw measurement errors and Doppler

measurement for signal power levels of -160 dBW and -165 dBW, respectively.

The first loss of satellites and tracking threshold in terms of I/S are summerized

in Table 5.16. For both receivers, the last tracked satellites were PRN 4 and PRN 13, which is the same as for the 5 dB signal power test. As shown in Table 5.17, the maximum pseudorange errors for the Allstar were 3.6, 3.3 and 3.5 m for the three signal power levels, which were higher than the other tests with the exception of the test involving CWI at L1+500 kHz.
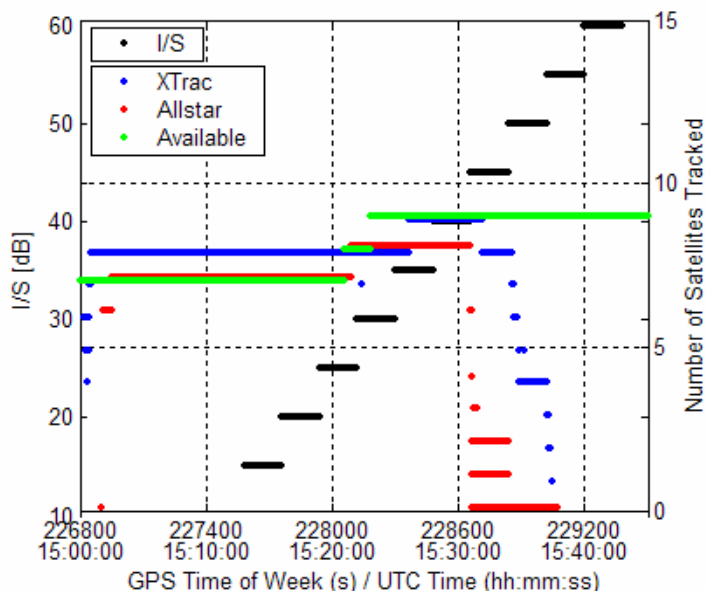
Figure 5.35: Number of Satellites Tracked under BLWNI when Signal Power = -160 dBW
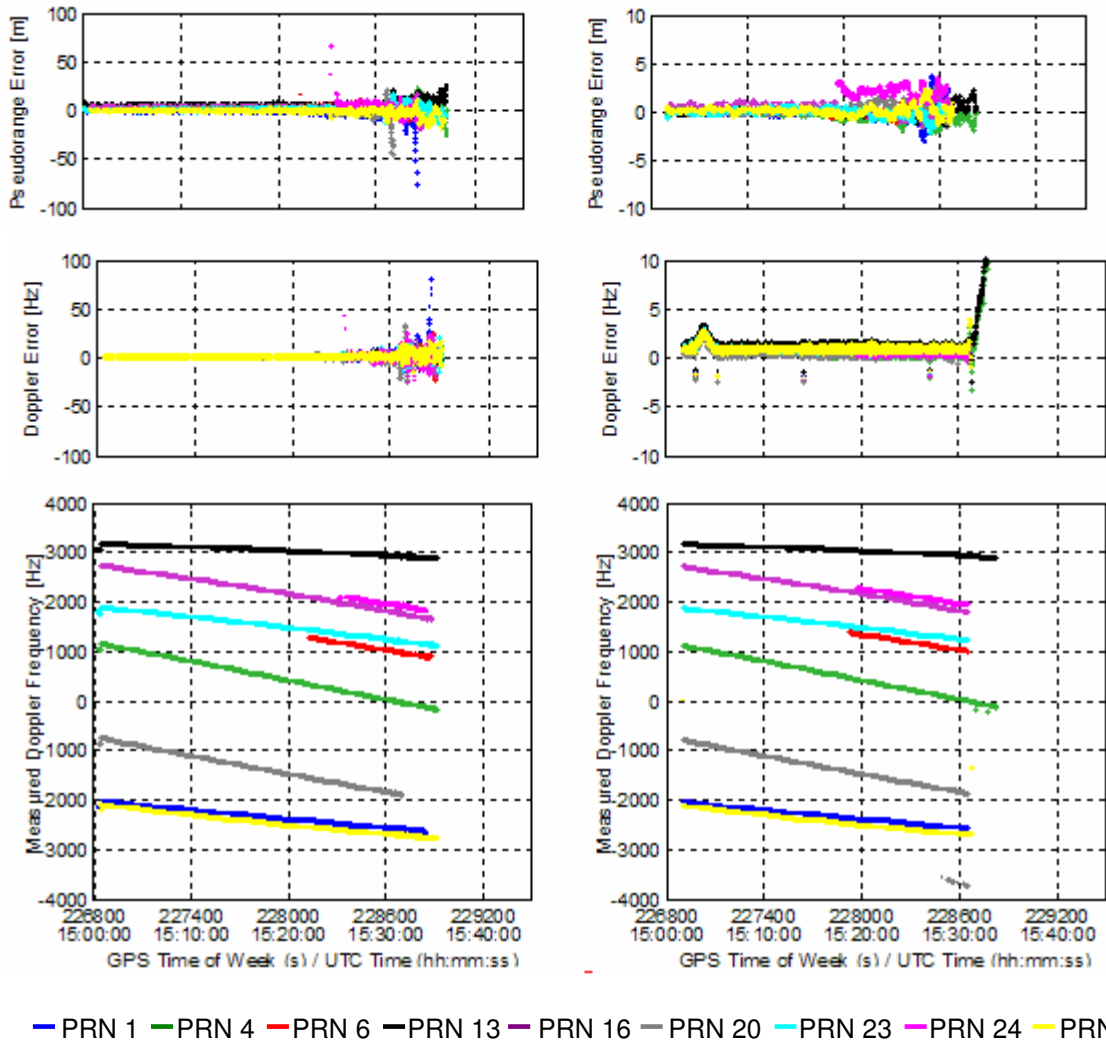
(a) XTrac (b) Allstar

Figure 5.36: Raw Measurements Errors and Doppler Frequency Measurements when Signal Power = -160 dBW
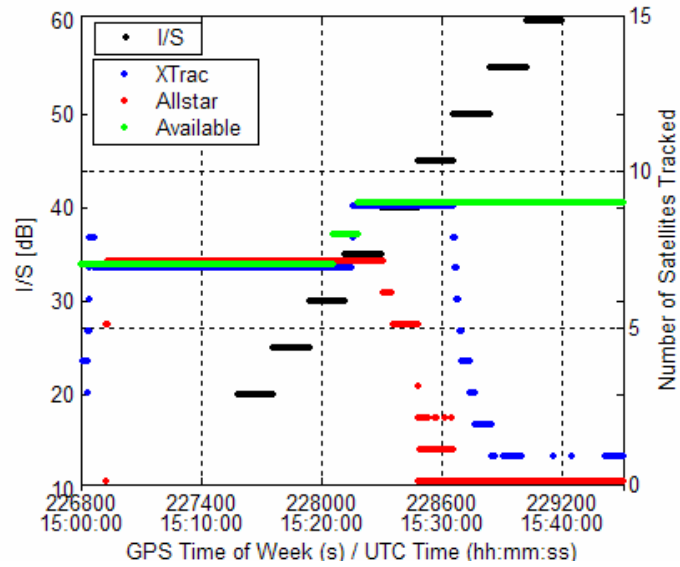
Figure 5.37: Number of Satellites Tracked under BLWNI when Signal Power = -165 dBW
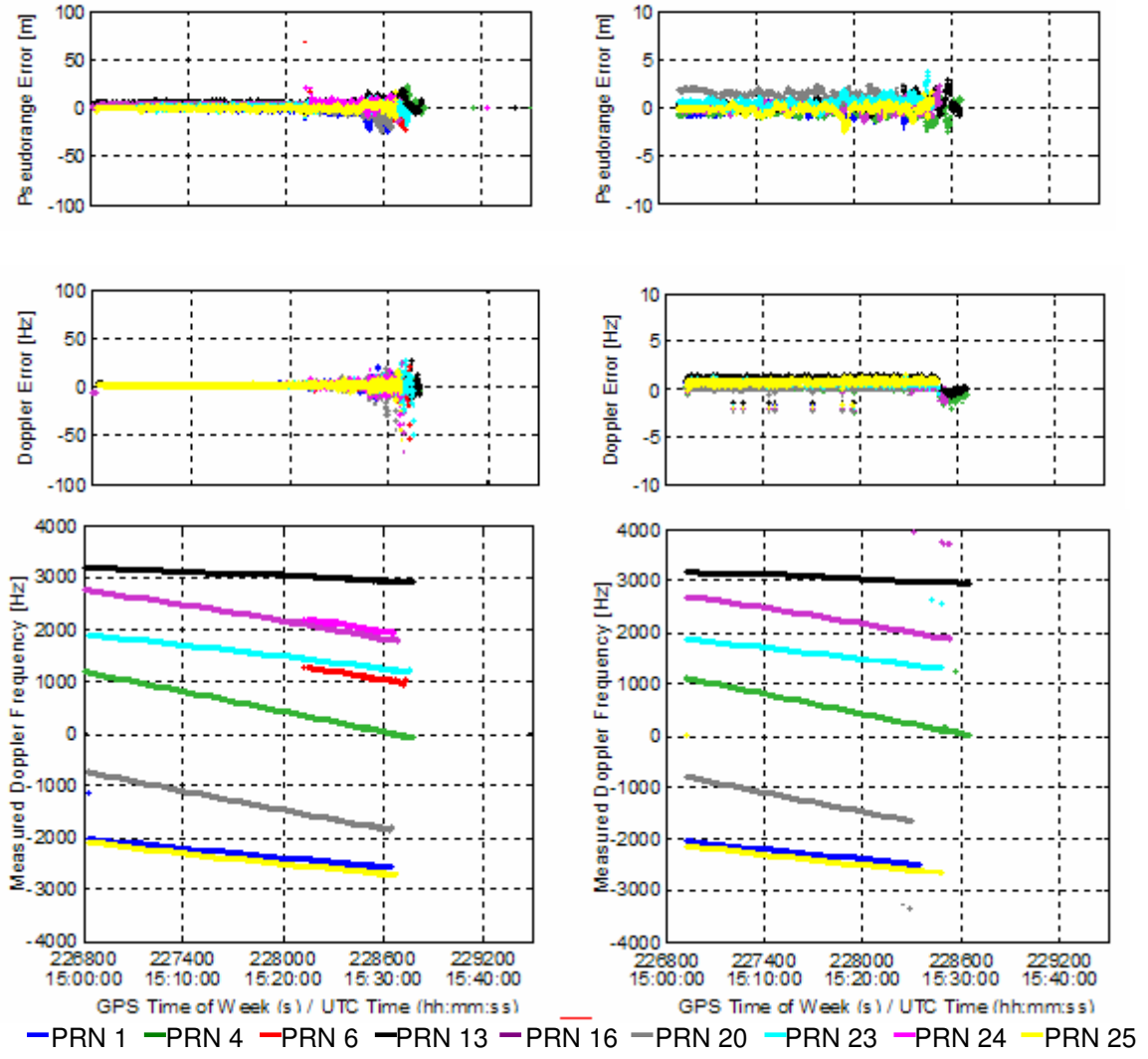
(a) XTrac Unit   (b) Allstar Unit

**Figure 5.38: Raw Measurements Errors and Doppler Frequency
Measurements when Signal Power = -165 dBW**

**Table 5.16: First Loss and Raw Measurements Availability (I/S [dB])
under BLWNI**

Signal power relative to -160 [dBW]	XTrac		Allstar	
	First Loss	Raw Measurements Availability	First Loss	Raw Measurements Availability
5 dB	45	50	40	45
0 dB	45	50	35	45
-5 dB	45	50	35	45

Table 5.17: Maximum Pseudorange Errors under BLWNI

Signal power relative to -160 [dBW]	XTrac		Allstar	
	Maximum Pseudorange Error [m]	I/S [dB]	Maximum Pseudorange error [m]	I/S [dB]
5 dB	56.1	50	3.6	45
0 dB	77.8	45	3.3	40
-5 dB	25.6	45	3.5	40

Position errors

Figure 5.39 shows the 3D RMS position errors versus interference power for three different signal power levels under BLWNI. Figure 5.40 shows the GDOP values calculated during this test. The maximum position errors for the XTrac unit were measured when I/S was at the highest interference power level tested herein, as shown in Table 5.18. In addition, the maximum errors were smaller than those measured with CWI. In the case of the Allstar unit, the position errors appeared to be related to the geometry of satellites rather than interference power, as observed with the other receiver.
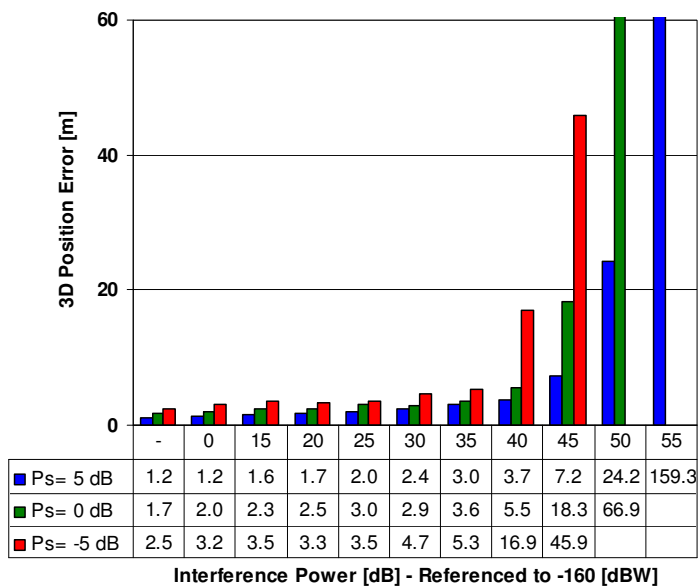
(a) XTrac Unit
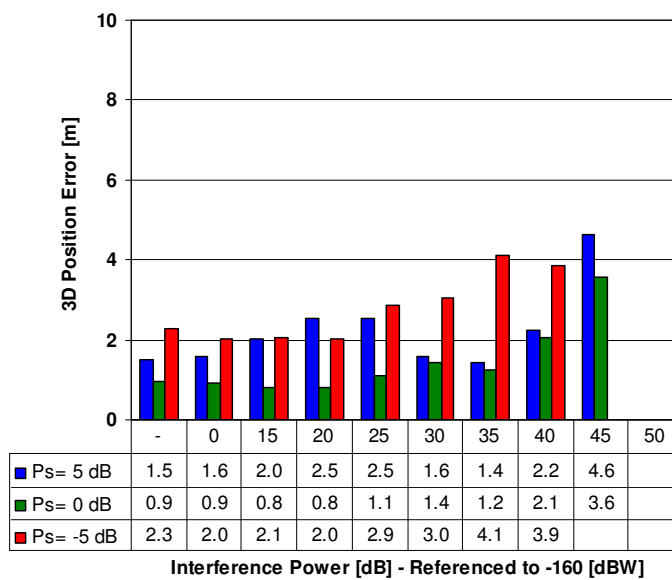
(b) Allstar Unit

Figure 5.39: 3D RMS Position Errors under BLWNI for Three different Unjammed C/N$_0$

(a) XTrac Unit   (b) Allstar Unit
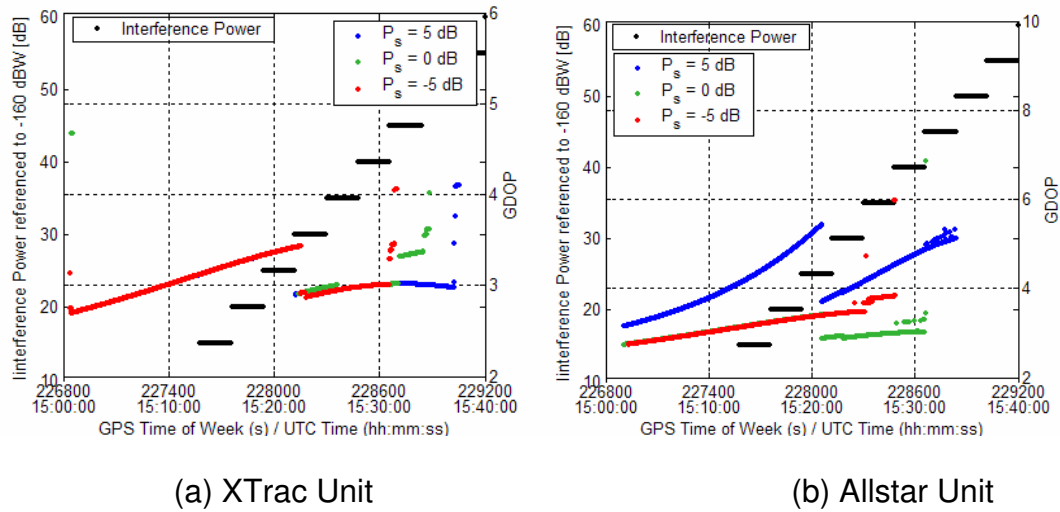
Figure 5.40: GDOP under BLWNI for Three Different Unjammed C/N$_0$

Table 5.18: Maximum 3D RMS Position Errors during BLWNI Test for Three Different Unjammed C/N$_0$

		Max. 3D RMS Error [m]	I/S [dB]
XTrac	Ps = 5 dB	394.2	50
	Ps = 0 dB	239.8	50
	Ps = -5 dB	123.4	50
Allstar	Ps = 5 dB	10.8	40
	Ps = 0 dB	6.2	45
	Ps = -5 dB	10.7	35

5.5 Dynamic Test

Since the dynamics of the vehicle produce Doppler shifts and tracking loop errors, this factor is expected to modify the observed effects on the receiver such as its tracking threshold. Since the variation in velocity causes Doppler change with

time, the northing velocity was changed from 0 to 50 m/s (=180 km/hr) for 1 minute and was decreased to 0 m/s for 1 minute. This cycling of velocity was repeated until the end of the test. During this test, the narrow band interference signals remained in the tracking loop for shorter periods, but more frequently than in the static test. Figure 5.41 shows the available PRN numbers during this test. The nominal number of satellites available was larger than in the static test.
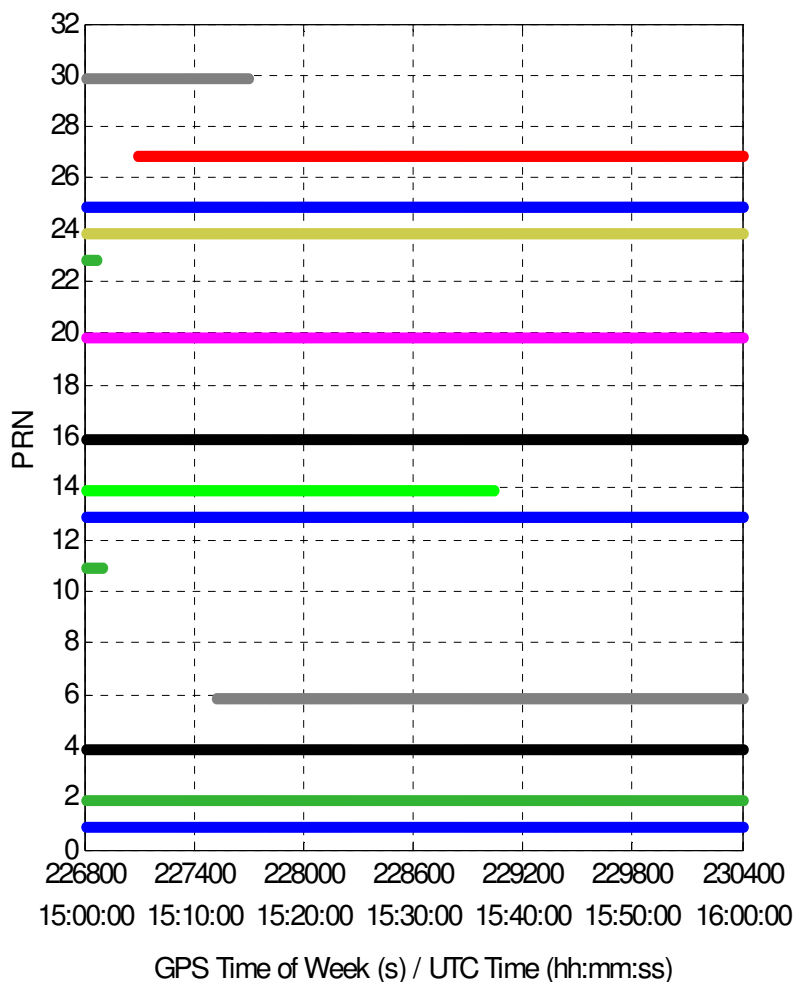
Figure 5.41: PRNs in View during Dynamic Test

5.5.1 Error-free Test

Objective and methodology

The aim of this test is to characterize the position errors of both receivers in the absence of pseudorange errors. The remaining errors include background noise, receiver noise, receiver clock error and dynamic induced errors. The signal power was maintained at –155 dB for 30 minutes.

C/N_0

The XTrac's measured C/N_0 is 5.9 dB lower than that of the Allstar, as shown in Table 5.19. Again, different C/N_0 values due to distinct estimation schemes were observed.

Table 5.19: Measured C/N_0 during the Error-free Dynamic Test

Unit :[dB-Hz]	Average	Min	Max
XTrac	43.2	42.9	43.8
Allstar	49.1	49.0	49.1

Tracking and position errors

The number of satellites tracked is shown in Figure 5.42. The simulated dynamics change only the latitudinal position. Larger latitudinal errors were observed compared to the static test for the XTrac unit, while the Allstar unit errors remained at a similar level, as shown in Table 5.20.
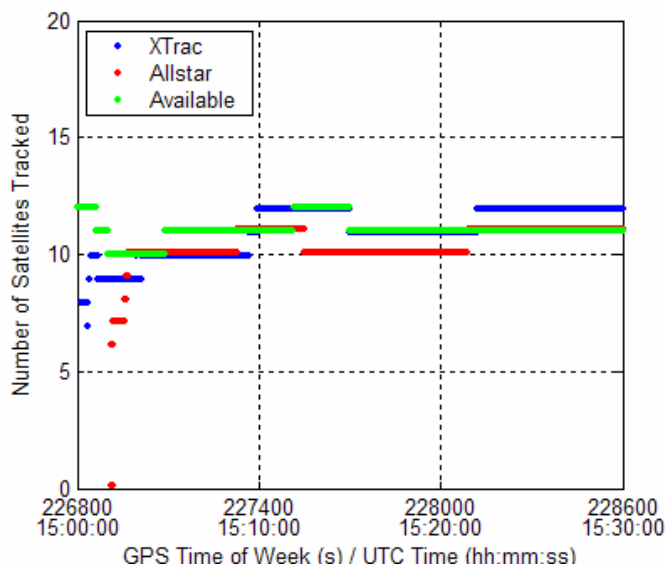
Figure 5.42: Number of Satellites Tracked during Error-free Dynamic Test

Table 5.20: Position Errors During the Error-free Dynamic Test

		Mean [m]	1 σ [m]	RMS [m]
XTrac	Latitude	1.3	1.2	1.7
	Longitude	0.0	0.3	0.3
	Height	-0.1	0.9	0.9
Allstar	Latitude	0.4	0.4	0.6
	Longitude	-0.0	0.1	0.1
	Height	1.0	0.6	1.2

5.5.2 White Noise

Objective and methodology

This test examines receiver performance under white noise conditions by changing the signal power of the simulator from +15 to -20 dB with respect to the initial level of -160 dBW. A 20 dB attenuator was connected between the

simulator and LNA to decrease the reference signal power from –160 dBW to –180 dBW. The dynamics of the vehicle was applied from the start of the test. The signal power was decreased in steps of 1 dB every 1 minute after an initial 10-minute warm-up period.

(a) C/N$_0$ (b) Number of Satellites Tracked
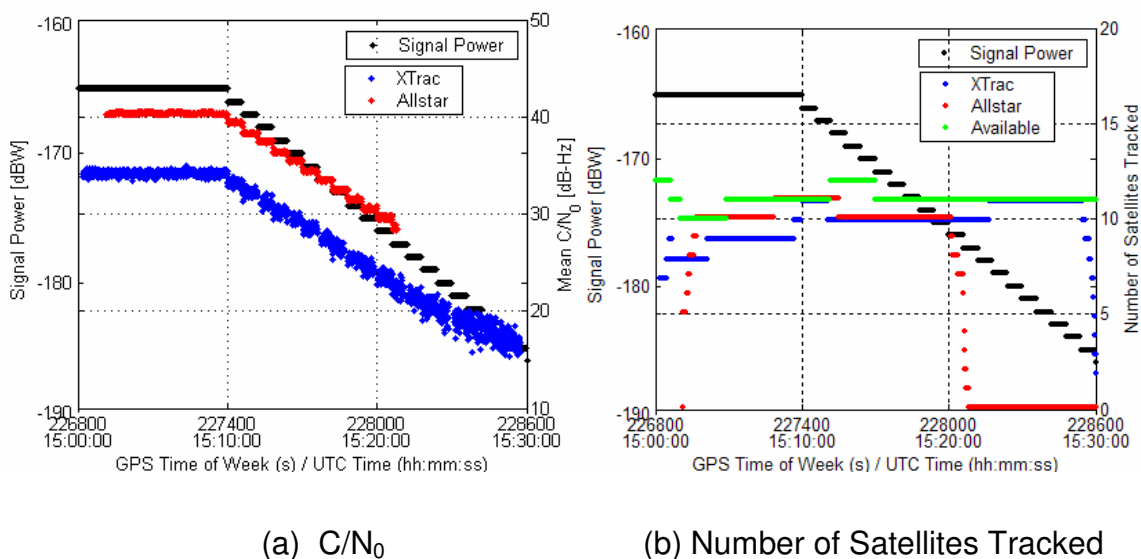
Figure 5.43: Measured C/N$_0$ and Number of Satellites Tracked during White Noise Dynamic Test

Tracking and raw measurement

Figure 5.43 shows the measured C/N$_0$ and number of satellites tracked during this test. Tracking thresholds were -185 dBW and -176 dBW for the XTrac and Allstar unit, the same as for the static test. Figure 5.44 shows the raw measurement errors and measured Doppler frequency during the test. The maximum pseudorange errors were larger than the static test for both receivers, as shown in Table 5.21. However, as shown in Figure 5.45, the 1 sigma of the

tracking errors remained at a similar level to that observed in the static test.

As a result, the tracking thresholds were the same as in the static test.
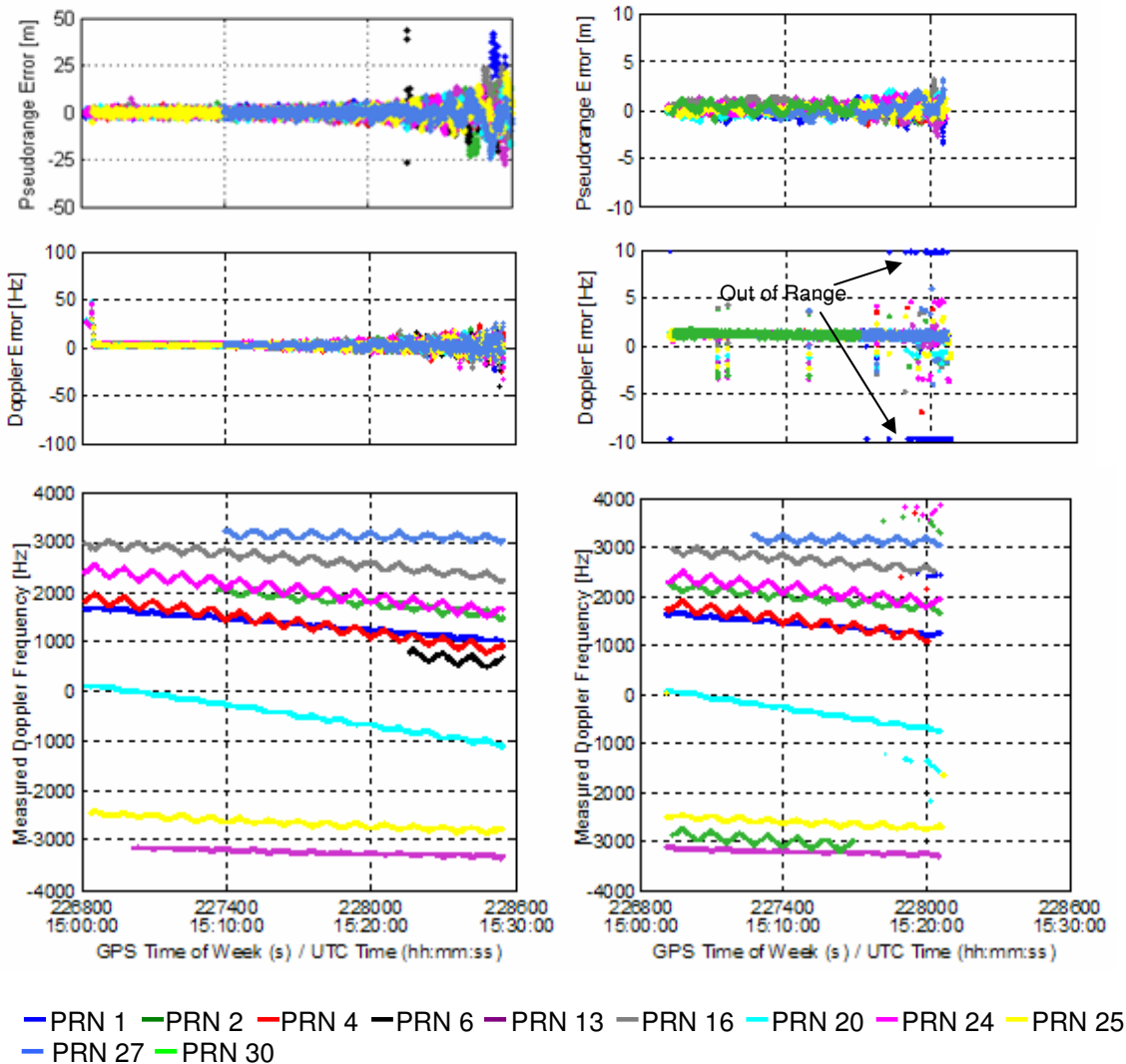
(a) XTrac Unit   (b) Allstar Unit

Figure 5.44: Raw Measurements Errors and Doppler Frequency Measurements during White Noise Dynamic Test

Table 5.21: Maximum Pseudorange Errors during White Noise Dynamic Test

	Max. Pseudorange Error [m]	Signal Power [dBW]
XTrac	28.7	-185
Allstar	3.1	-176
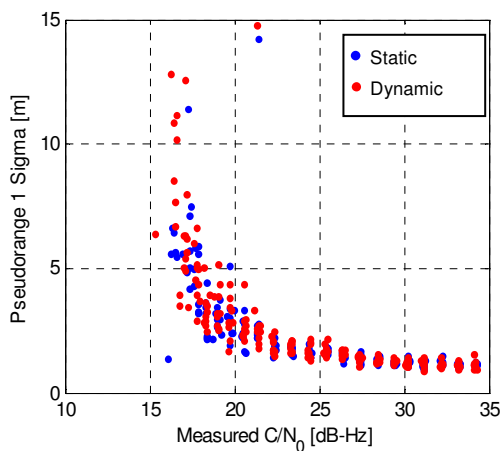
(a)-1 Pseudorange 1 σ of the XTrac unit   (a)-2 Doppler 1 σ of the XTrac unit
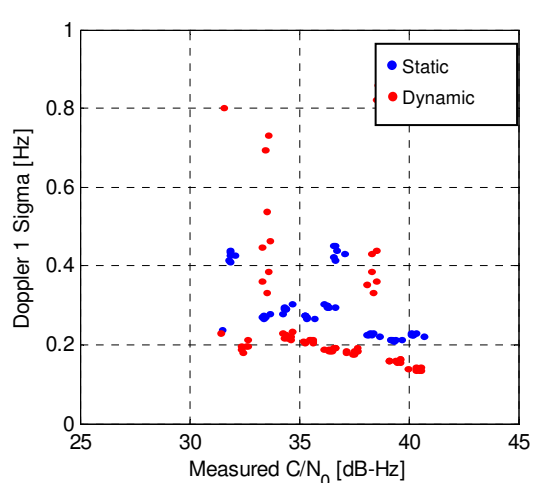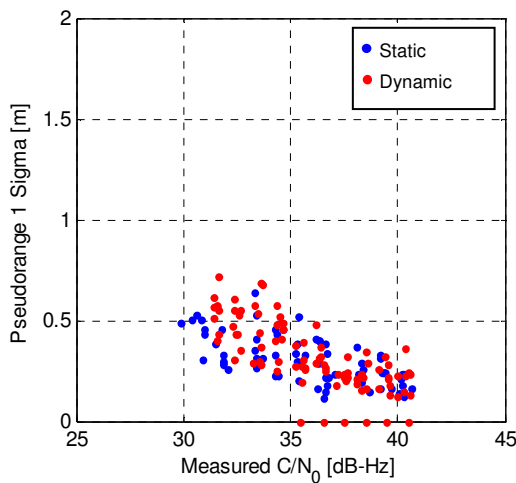
(b)-1 Pseudorange 1 σ of Allstar   (b)-2 Doppler 1 σ of Allstar

Figure 5.45: Comparisons of Tracking Errors between Static and Dynamic during White Noise Dynamic Test

Position errors

Figure 5.46 shows the position errors during the white noise test. The maximum 3D position errors were 142.2 m and 4.0 m measured with the minimum signal powers for the XTrac and Allstar receivers, respectively. The maximum error from the XTrac unit was slightly larger than that observed in the static test, as shown in Table 5.22.

(a)XTrac Unit   (b) Allstar Unit
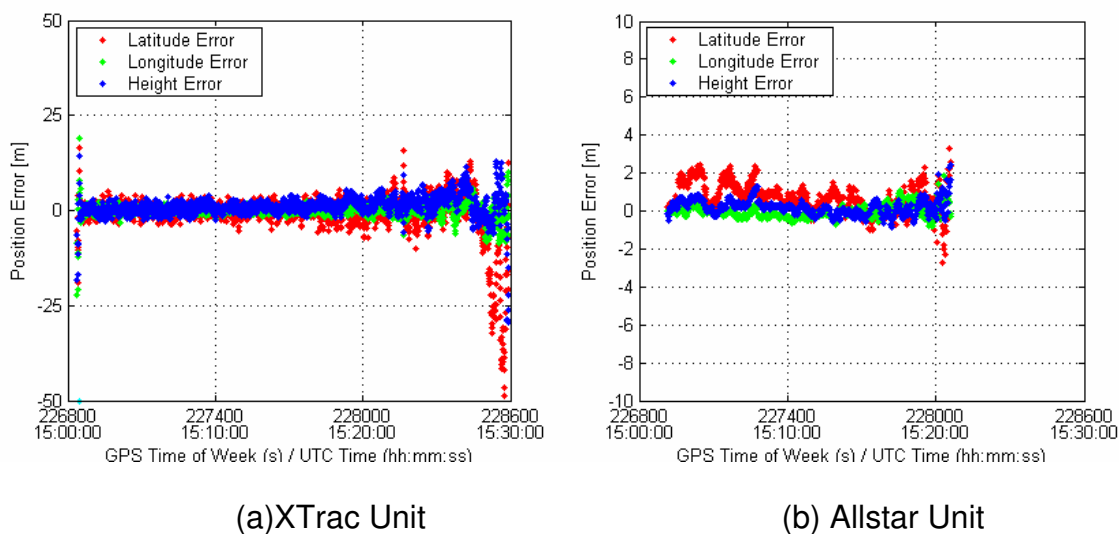
Figure 5.46: Position Errors during White Noise Dynamic Test

Table 5.22: Maximum 3D RMS Errors and Related Signal Power during White Noise Dynamic Test

	Signal Power [dBW]	Max. 3D RMS Error [m]
XTrac	-185	142.2
Allstar	-176	4.0

5.5.3 CWI within 1 kHz of δf

Objective & Methodology

This objective of this test is to examine the effects of CWI between the spectral lines of the C/A code. The satellite's signal power was set to 5, 3, 1 −1, -3, -5, -7 dB relative to the −160 dBW for PRN 1, 4, 13, 16, 20, 2, 25, respectively, after a 5-minute warm-up period. The interference power was set to −135 dBW after 5.5 min. This allows the I/S to range from 20 to 32 dB. The dynamics of the vehicle was applied from the start of the test. The centre frequency of CWI was L1+5 kHz.

Results

XTrac

Figure 5.47 shows the C/N_0, pseudorange error and Doppler measurements of the XTrac during this test. During the static test, the pseudorange error bursts with false lock were observed for the satellites whose signal power was equal to, or lower than, −163 dB. However, during the dynamic test, the false lock was not observed for PRN 25 whose power was the lowest among all of the satellites while, for PRN 16, whose signal power was −159 dB, a false lock was detected. The maximum pseudorange error was 1,115 m, which is larger than that of the static test, since the pseudorange changed due to the user dynamics while the phase-tracking loop was locked on a fixed frequency due to the interference signal.
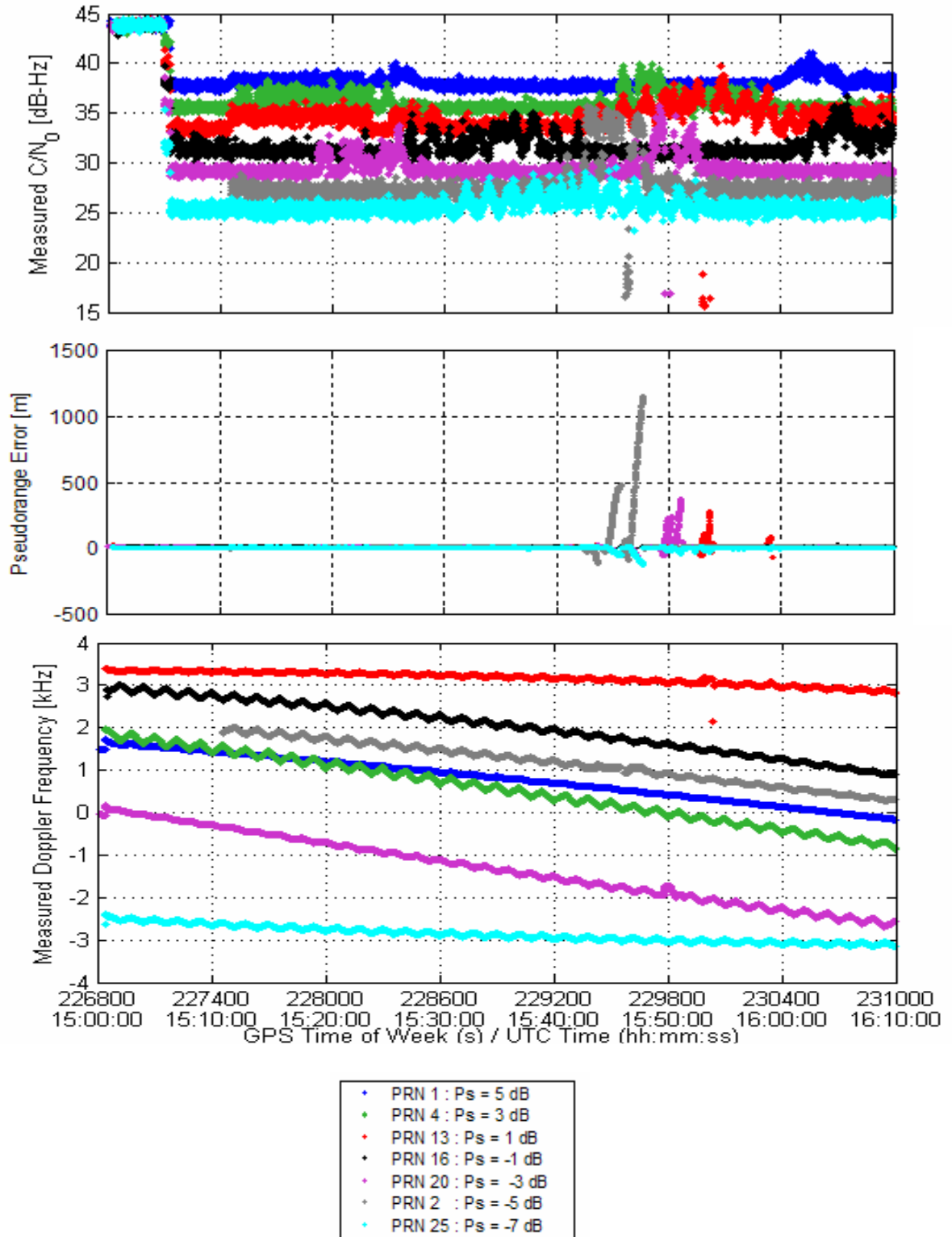
Figure 5.47: C/N$_0$ and Raw Measurements of the XTrac unit during CWI within 1 kHz of δf Dynamic Test

Allstar

Figure 5.48 shows the C/N$_0$, pseudorange error and Doppler measurements of the XTrac during this test. Tracking of PRN 13 and 16 was lost and subsequently reacquired, while that on PRN 20, 2 and 25 was lost and not reacquired. As compared to the static test, the signal powers of satellites which suffer those occurrences are 2 dB higher. However, similar to results observed in the static test, no pseudorange error burst due to false lock was observed.
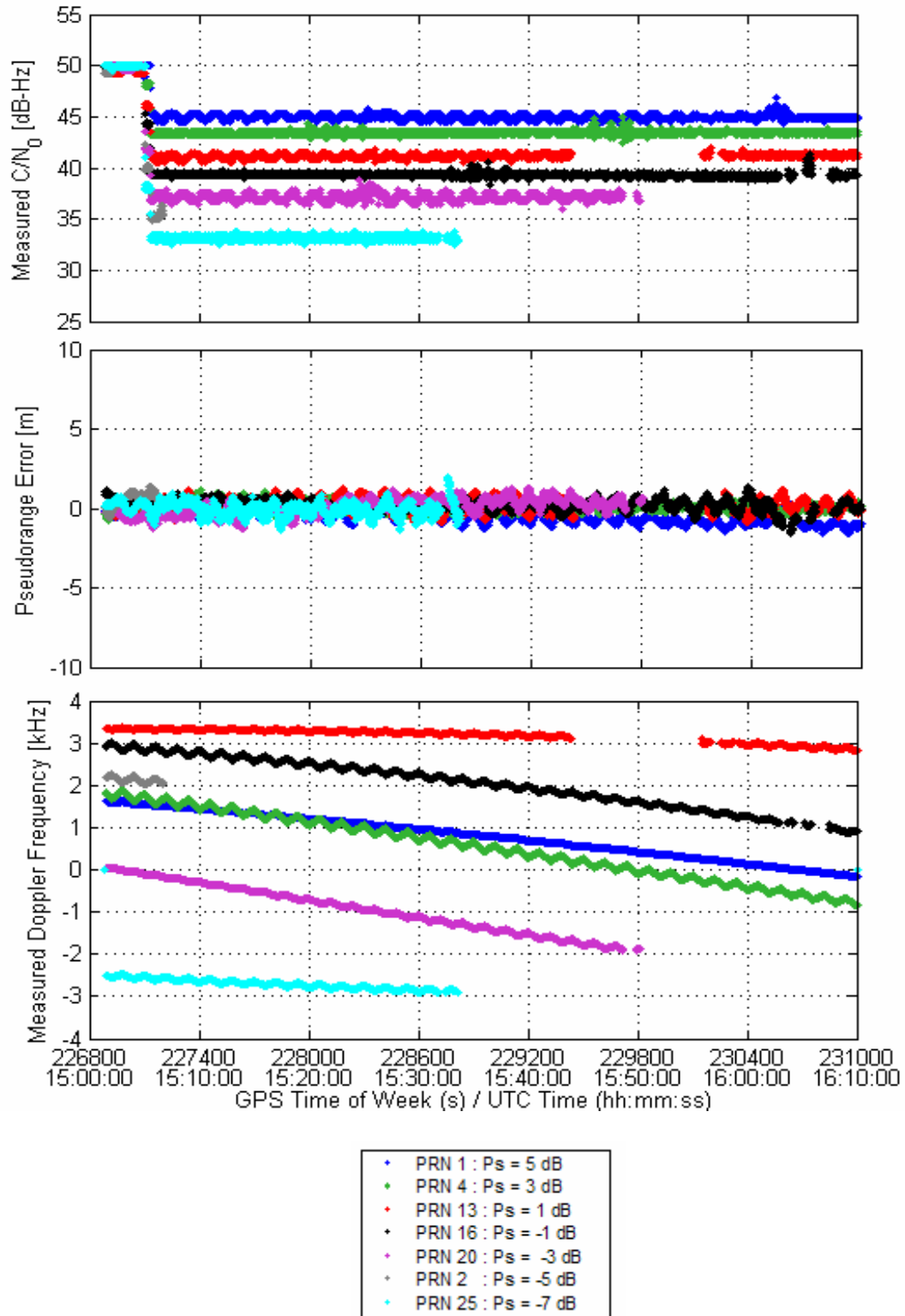
Figure 5.48: C/N₀ and Raw Measurements of the Allstar Unit during CWI within 1 kHz of δf Dynamic Test

5.5.4 CWI at L1+ 5 kHz

Objective and methodology

This test assesses the tracking threshold, raw measurement errors and position errors under CWI at L1+5 kHz. After the initial 10-minute warm-up period, the interference generator was switched on at a level of −160 dBW; following a 3-minute delay, the interference power was increased every 3 minutes by 5 dB from −145 dBW. The dynamics of the vehicle was applied from the start of the test. The signal power was set to -155 dBW

Tracking and raw measurements

The pseudorange measurements were available until the I/S = 45 dB for the XTrac receiver, which is 5 dB lower than that for the static test, while the Allstar's pseudorange measurements were available until the I/S = 40 dB, which is same as that for static test. However, both receivers lost the first satellite at 30 dB of I/S. The maximum pseudorange errors were larger than those observed in the static test, as shown in Table 5.23. Figure 5.49 and Figure 5.50 show number of satellite tracked and raw measurements during this test.

Table 5.23: Maximum Pseudorange Errors and First Lost under CWI at 5 kHz

	First Loss	Max. Pseudorange Error	
	I/S [dB]	[m]	I/S [dB]
XTrac	30	422.6	35
Allstar	30	2.1	35
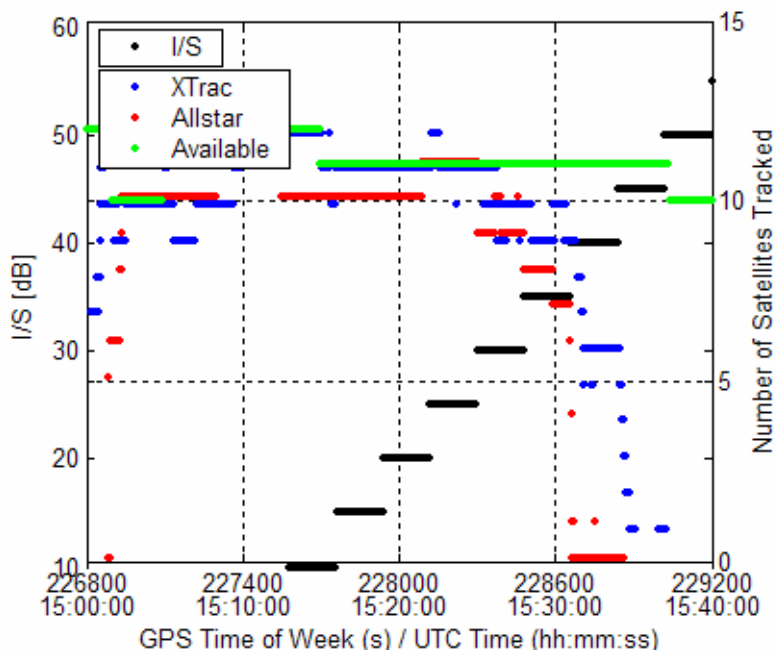
Figure 5.49: Number of Satellites Tracked during CWI at L1+5 kHz Dynamic Test
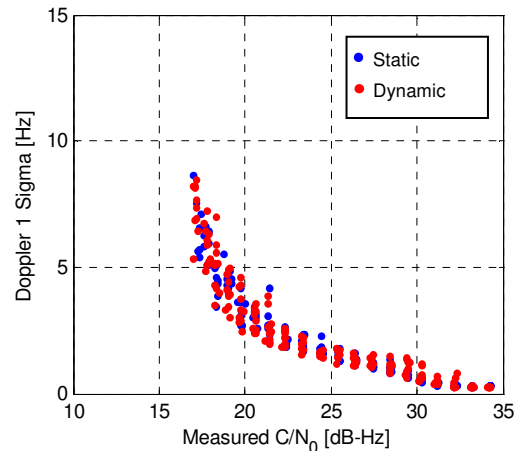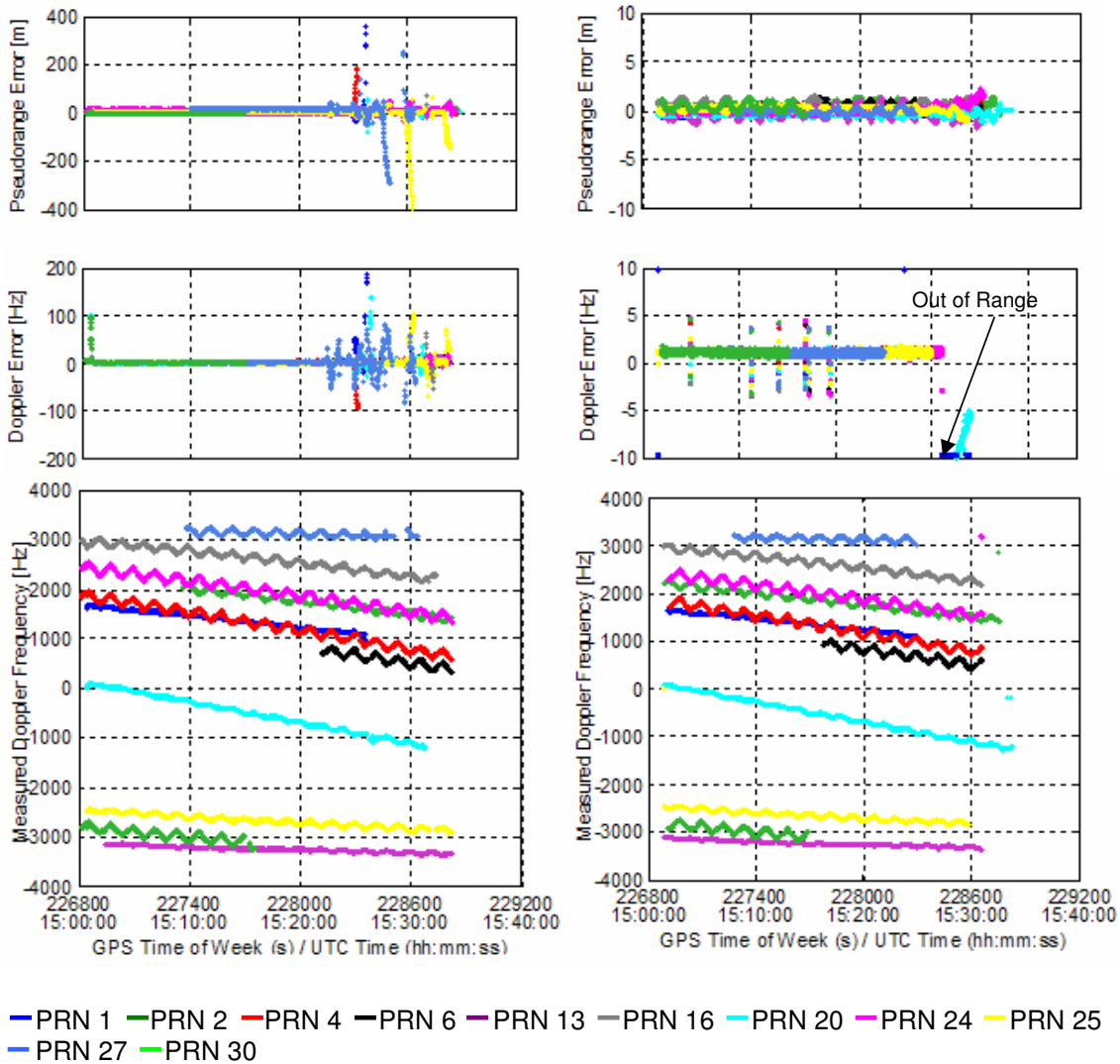
(a)XTrac Unit   (b) Allstar Unit

Figure 5.50: Raw Measurements during CWI at L1+5 kHz Dynamic Test

Position errors

The XTrac unit provided position solutions until the I/S reched 45 dB, while the maximum error occurred at 40 dB of I/S due to false lock, as shown in Figure 5.51 and Table 5.24.

<div align="center">

(a)XTrac Unit   (b) Allstar Unit
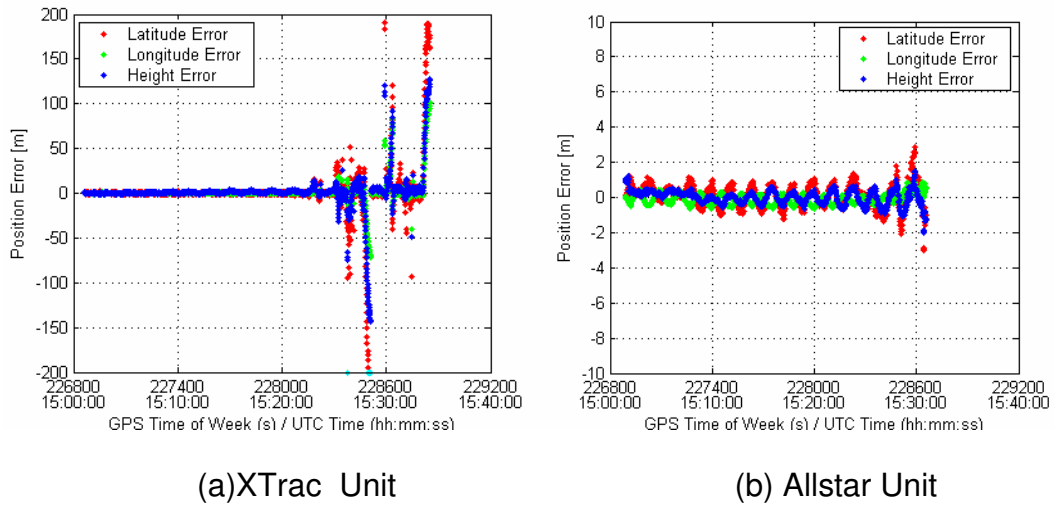
Figure 5.51: Position Errors during CWI at L1+5 kHz Dynamic Test

Table 5.24: Maximum 3D RMS Position Errors during CWI Dynamic Test

</div>

	Max. 3D RMS Error [m]	I/S [dB]
XTrac	295.2	40
Allstar	3.6	40

5.5.5 BLWNI with 1 kHz bandwidth centred at L1

Objective and methodology

This test verifies the tracking threshold, raw measurement error and position error under BLWNI. After the initial 10-minute warm-up, the interference generator was engaged at a level of −160 dBW; following a 3-minute waiting period, the interference power was increased every 3 minutes by 5 dB from −145 dBW. The dynamics of the vehicle was applied from the start of the test. The signal power was set to -155 dBW.

Tracking and raw measurements

The raw measurements were available until the I/S = 50 dB and 45 dB for the XTrac and Allstar receivers, respectively. The maximum pseudorange error of XTrac unit was observed to have the highest level of interference power, as shown in Table 5.25. Figure 5.52 and Figure 5.53 show the number of satellite tracked and raw measurements during this test.

Table 5.25 Maximum Pseudorange Errors during BLWNI Dynamic Test

	Max. Pseudorange Error [m]	I/S [dB]
XTrac	33.3	50
Allstar	4.9	40
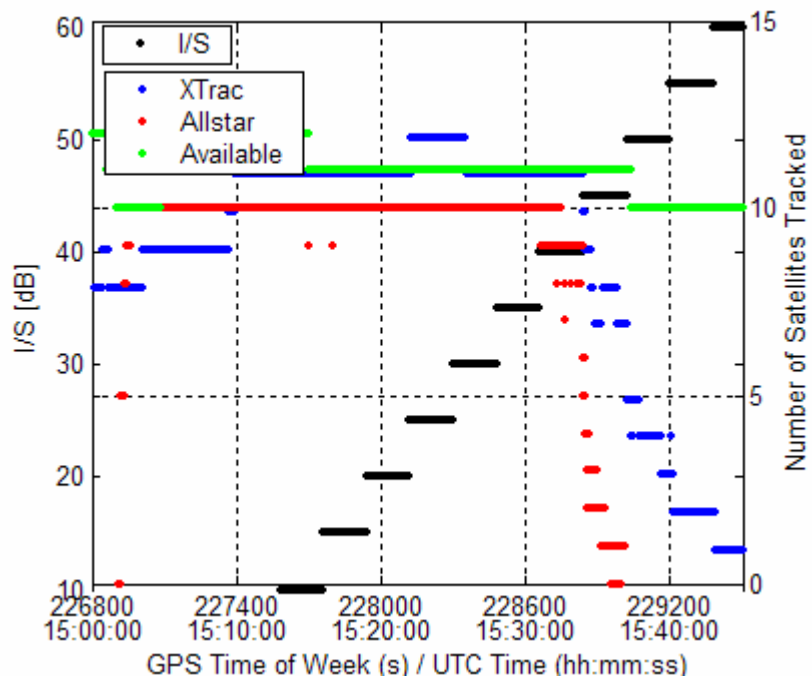
Figure 5.52: Number of Satellites Tracked during BLWNI Dynamic Test
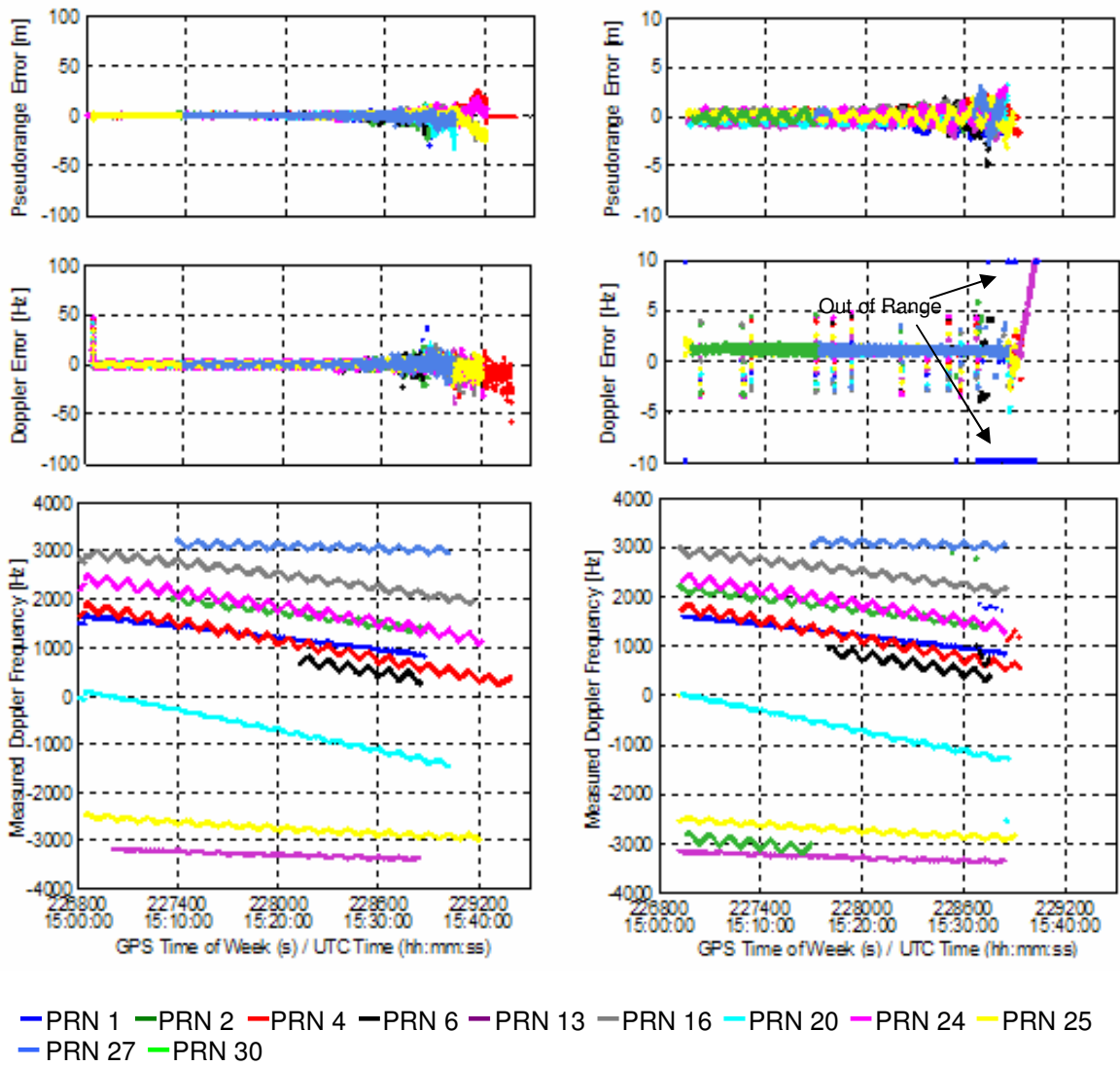
(a)XTrac Unit
(b) Allstar Unit

Figure 5.53: Raw Measurements during BLWNI Dynamic Test

Position errors

Position errors were available until the I/S reached 45 dB, 40 dB for the XTrac
and Allstar, which were 5 dB lower than those observed in the static test. The

maximum 3D position errors were 55.9 m and 31.9 m measured with maximum interference power for the XTrac and Allstar receivers, respectively, as shown in Table 5.26. The position errors during the BLWNI dynamic test are shown in Figure 5.54.

(a) XTrac Unit   (b) Allstar Unit
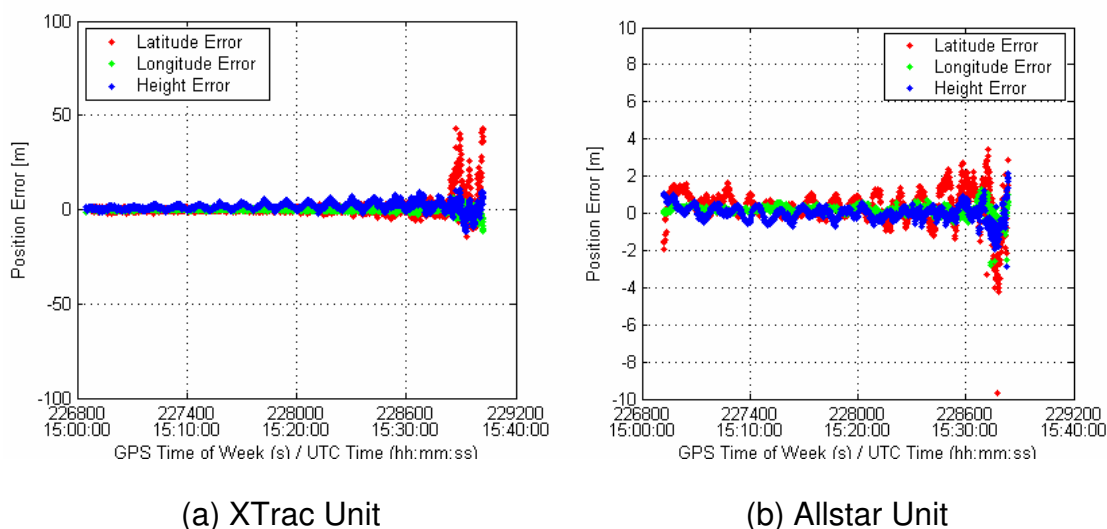
Figure 5.54 Position Errors During BLWNI Dynamic Test

Table 5.26 Maximum 3D RMS Position Errors during BLWNI DynamicTest

	Max. 3D RMS Error [m]	I/S [dB]
XTrac	55.9	45
Allstar	31.9	40

5.6 Conclusions

In this chapter, the tests results of two commercial receivers were presented. As the design targets and applications are different for the two receivers, the

interference effects on both receivers are different. The XTrac receiver out-performed the Allstar unit in terms of tracking performance, especially in respect of the XTrac's ability to quickly reacquire satellites which were lost due to low processing gain under CWI near the 1 kHz spectral line. Furthermore, the tracking threshold of this receiver under white noise interference is 9 to 10 dB lower than that of the Allstar unit in terms of simulated signal power, since the long integration time of this receiver decreases the tracking loop jitter to some extent. On the other hand, the Allstar receiver was observed to lose an interfered satellite signal with relatively low signal strength versus interference level, resulting in relatively small errors in position domain. Also, the pseudorange errors of the Allstar are weakly correlated with tracking loop jitters.

This chapter also studied the distinct reactions of the two receivers for different types of interference by examining the C/N_0 and raw measurements in static and dynamic modes. The processing gain under CWI with respect to the difference between the interference spectral line and interference frequency and the power spectral density of the associated spectral line were discussed. The results show that the first losses of tracking for both receivers are the same for CWI at L1+5 kHz and CWI at L1+500 kHz in static mode. Also, the first tracking losses for both receivers are the same for CWI at L1+5 kHz in dynamic mode.

CHAPTER SIX: RAIM UNDER CWI

6.1 Background

Receiver autonomous integrity monitoring (RAIM) has been developed as a means of improving the accuracy and reliability of GPS data processing through the use of integrity monitoring techniques adapted to GPS signal architecture. Under the assumptions that (i) there is at most one blunder (or gross error) present at a time and that (ii) the errors are normally distributed zero-mean variables, there are two aspects of statistical testing of interest in this methodology, namely, the global test and the local test. A global test is intended to detect the existence of a blunder, while a local test is used to identify and characterize the blunder. In the previous chapter, it was observed that the XTrac receiver often produced large position errors and may produce false lock of the tracking loop under CWI. In this chapter, the position domain errors are assessed with the use of traditional least-squares estimation under this type of interference, as augmented by the RAIM scheme.

6.2 Least-Squares and RAIM

6.2.1 GPS measurement equations

The least-squares method is a statistical approach to estimate an expected value from observations characterized by random errors by minimizing the sum of the

squares of the residuals. A set of linearized GPS measurement equations based on the parametric least-squares method may be expressed as follows (Kaplan 1996):

$$\mathbf{\Delta\rho} = \mathbf{H}\Delta\hat{\mathbf{x}} + \mathbf{\varepsilon} \tag{6.1}$$

$$\Delta\hat{\mathbf{x}} = \left(\mathbf{H}^{\mathsf{T}}\mathbf{C_l}^{-1}\mathbf{H}\right)^{-1}\mathbf{H}^{\mathsf{T}}\mathbf{C_l}^{-1}\mathbf{\Delta\rho} \tag{6.2}$$

where $\mathbf{\Delta\rho}$(or $\mathbf{l}$) : Misclosure vector (delta pseudo range)

H : Design matrix (geometry matrix)

X : [x y z –cdt] (Unknowns)

$\mathbf{C_l}$: Covariance matrix ($= \sigma_0^2\mathbf{P^{-1}} = \sigma_0^2\mathbf{Q}$)

The position estimates, $\hat{\mathbf{x}}$, are iteratively calculated until the norm of the incremental value is small enough to be accepted. The least-squares residual vector, $\hat{\mathbf{v}}$ is

$$\hat{\mathbf{v}} = \mathbf{H}\Delta\hat{\mathbf{x}} - \mathbf{\Delta\rho} = -\mathbf{C}_{\hat{r}}\mathbf{C_l}^{-1}\mathbf{\Delta\rho} \tag{6.3}$$

where $\mathbf{C}_{\hat{r}} = \mathbf{C_l} - \mathbf{H}(\mathbf{H}^{\mathsf{T}}\mathbf{C_l}^{-1}\mathbf{H})^{-1}\mathbf{H}^{\mathsf{T}}$

6.2.2 RAIM

Errors can be categorized into random errors, systematic errors and gross errors. Random errors are unavoidable and can be described statistically, while a

systematic error (or bias) is defined by the difference between the functional model and reality. A gross error is a result of a malfunctioning of the equipment or another unexpected phenomena. If the functional and statistical models correctly represent the data set, we can assume that systematic and gross errors are absent, and that only random errors exist. Based on this assumption, statistical testing theory can be used. The statistical test has two important components: the global test and the local test.

Global Test – Detection

A global test is a method of detecting the existence of blunders. Detection is based on the testing of residuals. Because the residual vector is assumed to have a normal distribution, from the law of propagation of errors, the estimated variance factor (the so-called '*a posteriori* variance factor') has a chi-squared distribution. The *a posteriori* variance factor, s_0^2 is expressed as follows (Caspary 1988):

$$s_0^2 = \frac{\hat{\mathbf{v}}^T \mathbf{P} \hat{\mathbf{v}}}{n - r} \quad : a\ posteriori\ \text{variance factor} \tag{6.4}$$

$$\text{where} \quad r: \text{Rank(H)}$$

In the case where no failure exists, H_0, the test statistic, T, should satisfy the following assumption:

$$T = \frac{\hat{\mathbf{v}}^{\mathbf{T}}\mathbf{P}\hat{\mathbf{v}}}{\sigma_o^2} \sim \chi^2(n-r) \,\big|H_0 \tag{6.5}$$

If blunders exist, H_a, the corrected measurement vector, $\bar{\mathbf{l}}$, can be rewritten as:

$$\bar{\mathbf{l}} = \mathbf{l} + \mathbf{C}\nabla \tag{6.6}$$

where $\mathbf{C}\nabla$: correction vector

The state estimation vector is then:

$$\hat{\bar{\mathbf{x}}} = \hat{\mathbf{x}} + (\mathbf{H}^{\mathbf{T}}\mathbf{PH})^{-1}\mathbf{H}^{\mathbf{T}}\mathbf{PC}\nabla \tag{6.7}$$

The residual vector is:

$$\hat{\bar{\mathbf{v}}} = \hat{\mathbf{v}} - \mathbf{Q}_{\hat{\mathbf{v}}}\mathbf{PC}\nabla$$
$$\text{where} \quad \mathbf{Q}_{\hat{\mathbf{v}}} = \mathbf{Q} - \mathbf{H}\mathbf{Q}_{\hat{\mathbf{x}}}\mathbf{H}^{\mathbf{T}} \tag{6.8}$$

$$\hat{\bar{\mathbf{v}}}^{\mathbf{T}}\mathbf{P}\hat{\bar{\mathbf{v}}} = \hat{\mathbf{v}}^{\mathbf{T}}\mathbf{P}\hat{\mathbf{v}} - \nabla^{\mathbf{T}}\mathbf{C}^{\mathbf{T}}\mathbf{PQ}_{\hat{\mathbf{v}}}\mathbf{PC}\nabla - \nabla^{\mathbf{T}}\mathbf{C}^{\mathbf{T}}\mathbf{PQ}_{\hat{\mathbf{v}}}\mathbf{P}\hat{\bar{\mathbf{v}}} - \bar{\mathbf{v}}^{\mathbf{T}}\mathbf{PQ}_{\hat{\mathbf{v}}}\mathbf{PC}\nabla \tag{6.9}$$

Assuming that $\bar{\mathbf{v}}$ and ∇ are independent,

$$\hat{\bar{\mathbf{v}}}^{\mathbf{T}}\mathbf{P}\hat{\bar{\mathbf{v}}} = \hat{\mathbf{v}}^{\mathbf{T}}\mathbf{P}\hat{\mathbf{v}} - \nabla^{\mathbf{T}}\mathbf{C}^{\mathbf{T}}\mathbf{PQ}_{\hat{\mathbf{v}}}\mathbf{PC}\nabla \tag{6.10}$$

The variance is then,

$$\sigma_o^2 = E(s_o^2) - \frac{E(\nabla^{\mathbf{T}}\mathbf{C}^{\mathbf{T}}\mathbf{PQ}_{\hat{\mathbf{v}}}\mathbf{PC}\nabla)}{n-r} \tag{6.11}$$

Thus, if the gross errors are taken into account, the expectation of the *a posteriori* variance factor is always larger than, or equal to, the true variance. Now, the test statistic of H_a has (n-r) degrees of freedom and a χ^2-distribution with a non-centrality parameter λ:

$$T = \frac{\hat{\mathbf{v}}^{\mathbf{T}}\mathbf{P}\hat{\mathbf{v}}}{\sigma_0^2} \sim \chi^2(n-r,\lambda) \,|H_a \qquad (6.12)$$

$$\text{where} \quad \lambda = \frac{\nabla^{\mathbf{T}}\mathbf{C}^{\mathbf{T}}\mathbf{P}\mathbf{Q}_{\hat{v}}\mathbf{P}\mathbf{C}\nabla}{\sigma_0^2}$$

The principle of the null hypothesis is testing of residuals, the so-called global test, and to determine whether an *a posteriori* variance factor, s_0^2, is centrally chi-squared distributed or not. The non-centrality parameter depends on the size of the blunders resulting in the *a posteriori* variance factor exceeding the threshold:

$$\begin{aligned} H_0 &: s_0^2 < \hat{\sigma}_{0,\,\text{threshold}}^2 \quad \text{(Global Test Fail)} \\ H_a &: s_0^2 \geq \hat{\sigma}_{0,\,\text{threshold}}^2 \quad \text{(Global Test Pass)} \end{aligned} \qquad (6.13)$$

Local Test – Identification

Once the existence of blunders from measurements has been detected, the identification of blunders should be made to exclude the outliers. Following verification of the existence of a blunder, the appropriate test statistic is:

$$T = \frac{\hat{\mathbf{v}}^T\mathbf{P}\hat{\mathbf{v}}}{\sigma_0^2} = T_{H_o} + \Delta T \tag{6.14}$$

$$\text{where } \Delta T = \frac{\hat{\mathbf{v}}^T\mathbf{PC}(\mathbf{C}^T\mathbf{PQ}_{\hat{v}}\mathbf{PC})^{-1}\mathbf{C}^T\mathbf{P}\hat{\mathbf{v}}}{\sigma_0^2}$$

The test statistic for an individual measurement is:

$$T_i = \frac{(\mathbf{e}_i^T\mathbf{P}\hat{\mathbf{v}})^2}{\sigma_0^2(\mathbf{e}_i^T\mathbf{PQ}_{\hat{v}}\mathbf{Pe}_i)} \sim \chi^2(\lambda) \tag{6.15}$$

$$\text{where } \mathbf{C} = \mathbf{e}_i = \begin{bmatrix} 0\,0...1\,0\,0 \end{bmatrix}^T$$

Then, the square-root of T_i is:

$$\sqrt{T_i} = w_i = \frac{\mathbf{e}_i^T\mathbf{P}\hat{\mathbf{v}}}{\sigma_0\sqrt{\mathbf{e}_i^T\mathbf{PQ}_{\hat{v}}\mathbf{Pe}_i}} \sim N(\lambda_o,1) \tag{6.16}$$

$$\text{where } \lambda_o = \sqrt{\lambda_i} = \sqrt{\frac{\nabla^T\mathbf{C}^T\mathbf{PQ}_{\hat{v}}\mathbf{PC}\nabla}{\sigma_0^2}}$$

The measurement with the largest standardized residual exceeding the threshold is regarded as an outlier and this measurement is excluded from the navigation solution (Teunissen 1998). The local test is based on the one blunder situation, seeks the maximum value of w and checks whether this value is within the confidence level or not:

$$
\begin{aligned}
H_{0,i} &: w_i < n_{1-\frac{\alpha_0}{2}} \quad (i \text{ acceptable }) \\
H_{a,i} &: w_i \geq n_{1-\frac{\alpha_0}{2}} \quad (i \text{ erroneous })
\end{aligned}
\tag{6.17}
$$

If two blunders exist, the impacts of the blunders on the residuals still follow equation (6.8) (Ryan 2002). Thus, the global test will detect the blunders with the boundary of the global ellipse, which is a function of the magnitudes of the blunders and non-centrality parameter. To isolate the multiple blunders from the local test, the test is repeated on the remaining measurements after the outlier is excluded (Kuusniemi & Lachapelle 2004).

When the statistical test is performed, two types of errors may occur. If the null hypothesis is true, the test statistic will reject the true hypothesis in α_0 of all cases, which means rejection of good data. This is often called a 'type-I error'. On the other hand, if the alternative hypothesis is true, the test statistic can fall in the region of no rejection. This 'type-II error' occurs with probability β_0. The

probability of $(1 - \beta_0)$ is called the power of the test. The α_0, β_0 value for the local test must be defined before performing the statistical test.

6.3 RAIM Methods and Results

In the current application, if the global test is a fail, the maximum blunder is excluded until the global test succeeds or the number of satellites is larger than 4, as shown in Figure 6.1. The α_0, β_0 parameters are set to 0.1% and 10%, respectively.

| # of Sat. > 4 | Global test $\hat{\sigma}_0^2 < \hat{\sigma}_{0,\text{threshold}}^2$? | Local Test $\left| w_j \right| \geq \left| w_i \right|$ for all i & $\left| w_j \right| \geq n_{1-\alpha_0/2}$ |

Global Test Pass?

Position Estimate With Warning

Reliable Position Estimate

Exclude j-th measurement

→ Yes
→ No
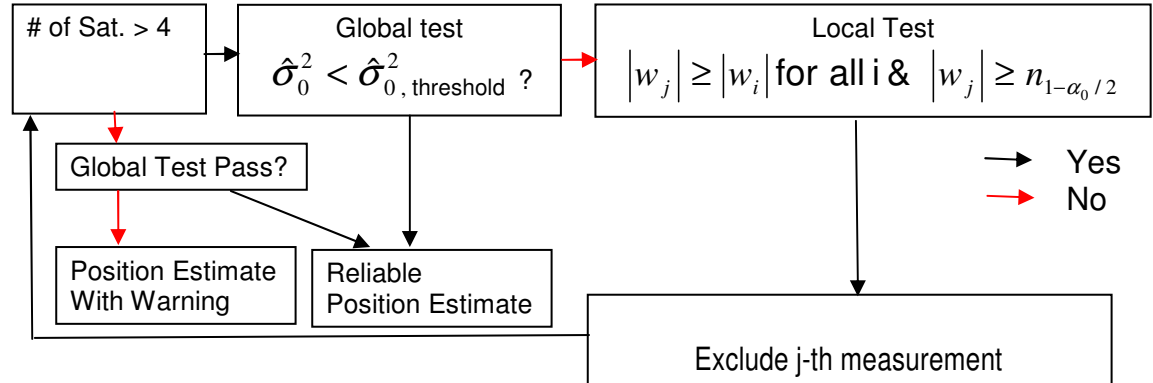
Figure 6.1: RAIM Procedure

6.3.1 CWI – Different I/S at the same time

In this section, the data obtained from the test described in Section 5.4.4 is analyzed. During this test, the GPS signals of seven satellites were simulated, whose I/S were set from 20 dB to 32 dB with 2 dB increments between each satellite. During this test, false lock occurred on PRN 20, 23 and 25 due to

interference, causing pseudorange errors up to 300 m, while the rest of the satellites were not affected. In addition, during this test only one satellite was affected at a time.

As shown in Figure 6.2, the 3D RMS position errors were up to 786.6 m without RAIM, while the errors were less than 60 m with RAIM implemented. As shown in Figure 6.3, the measurements with large pseudorange errors under this condition were largely excluded from the position estimation. The average GDOP with RAIM implemented was 3.3, which was slightly higher than the corresponding GDOP without RAIM, which was 3.1. The increase is due to the exclusion of the satellites on which measurements were deemed faulty.
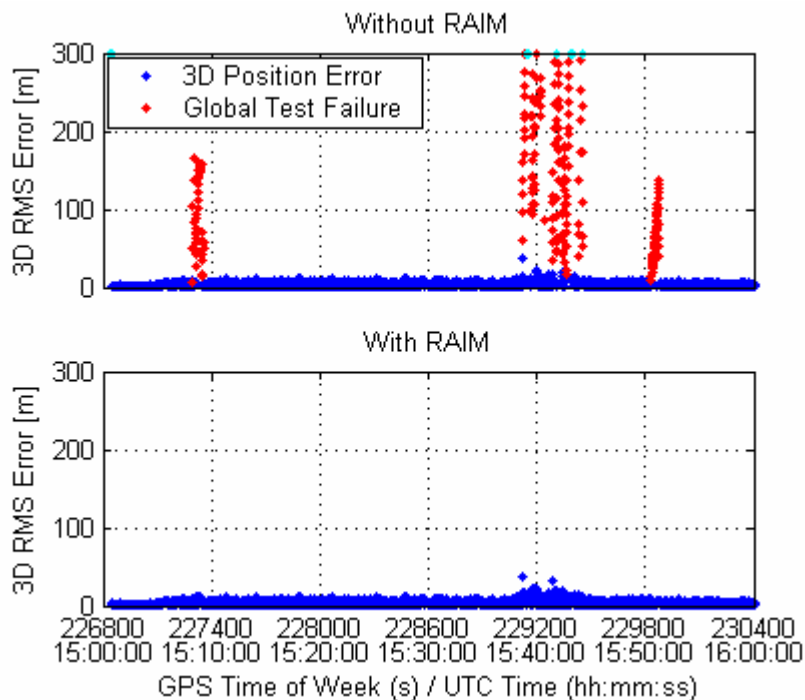
Figure 6.2: 3D RMS Position Errors without/with RAIM under CWI - Different I/S at the same time
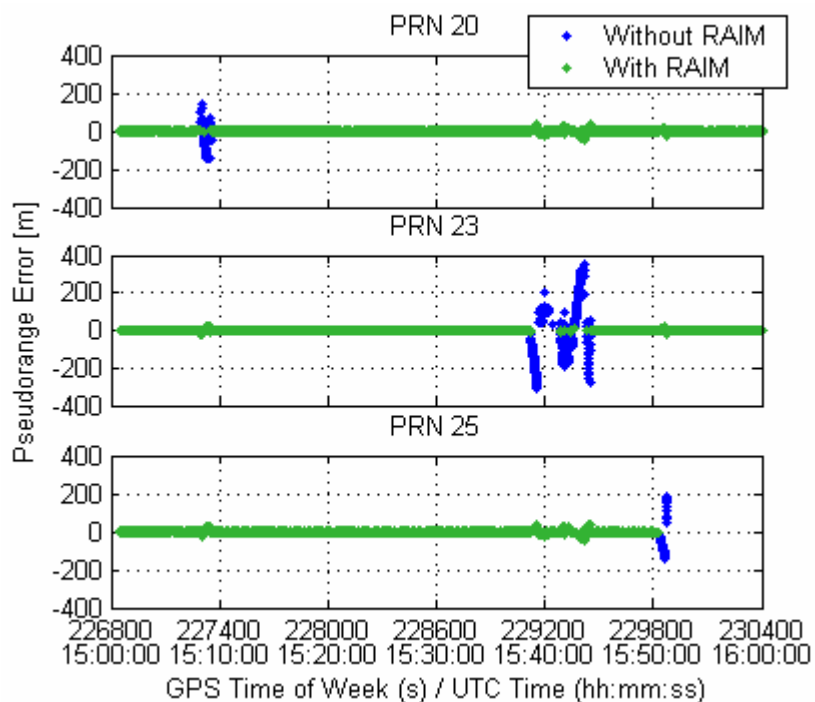
Figure 6.3: Pseudorange Measurements used for Position Solutions under CWI, without/with RAIM– Different I/S at the same time

6.3.2 CWI – Different I/S

In this section, the data obtained from the test under CWI at L1+5 kHz in Section 5.4.5 is analyzed. The I/S was increased by 5 dB every three minutes from 10 dB to 45 dB.

Figure 6.4 shows the 3D RMS errors versus time, while Figure 6.5 shows the pseudorange utilization without and with RAIM implemented. When the I/S was 30 dB, the position errors decreased with RAIM by excluding up to four faulty satellite measurements, as shown in Figure 6.6. However, when the I/S was 35

dB, improvements in the position domain by using this scheme were limited; position errors in excess of 100 m were not often detected by the global test. This is the result of a combination of poor measurement accuracy as well as low measurement redundancy, as discussed by Kuusniemi & Lachapelle (2004) for the indoor environment case. Also, the maximum errors without and with RAIM are shown in Table 6.1. The mean GDOP with RAIM was 1.8, which was slightly higher than GDOP without RAIM which was 1.7. Improvements with RAIM implementation are remarkable until an I/S of 35 dB is reached in which case the improvement inevitably decreases due to interference. An I/S between 30 and 35 dB is obviously the critical threshold in this case.
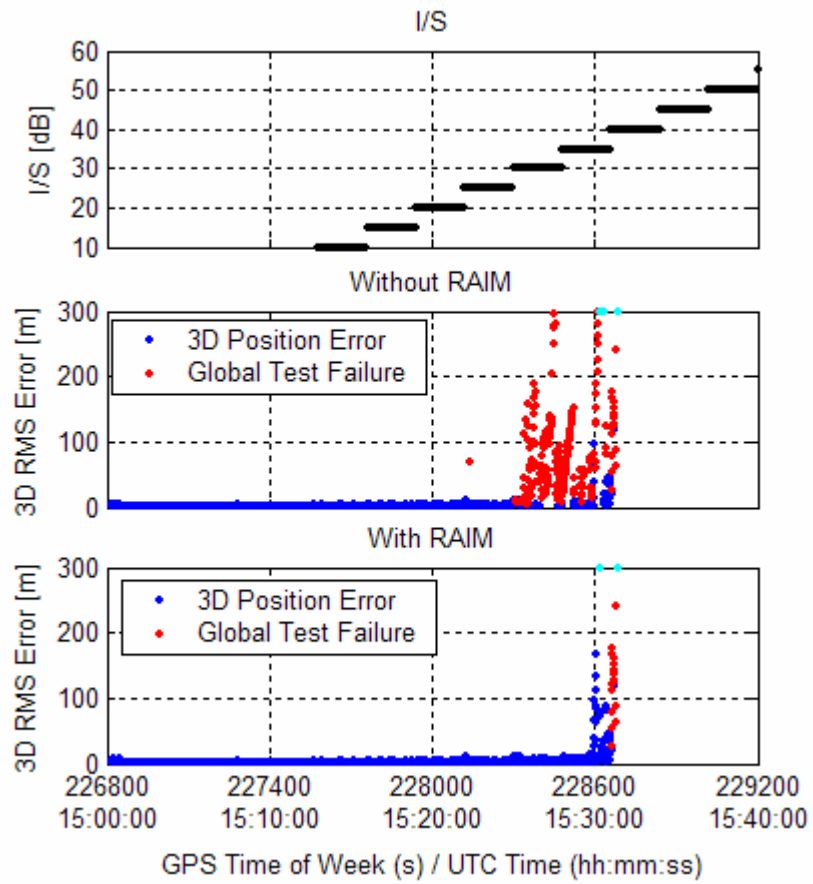
Figure 6.4: 3D RMS Position Errors under CWI - Different I/S, without/with RAIM
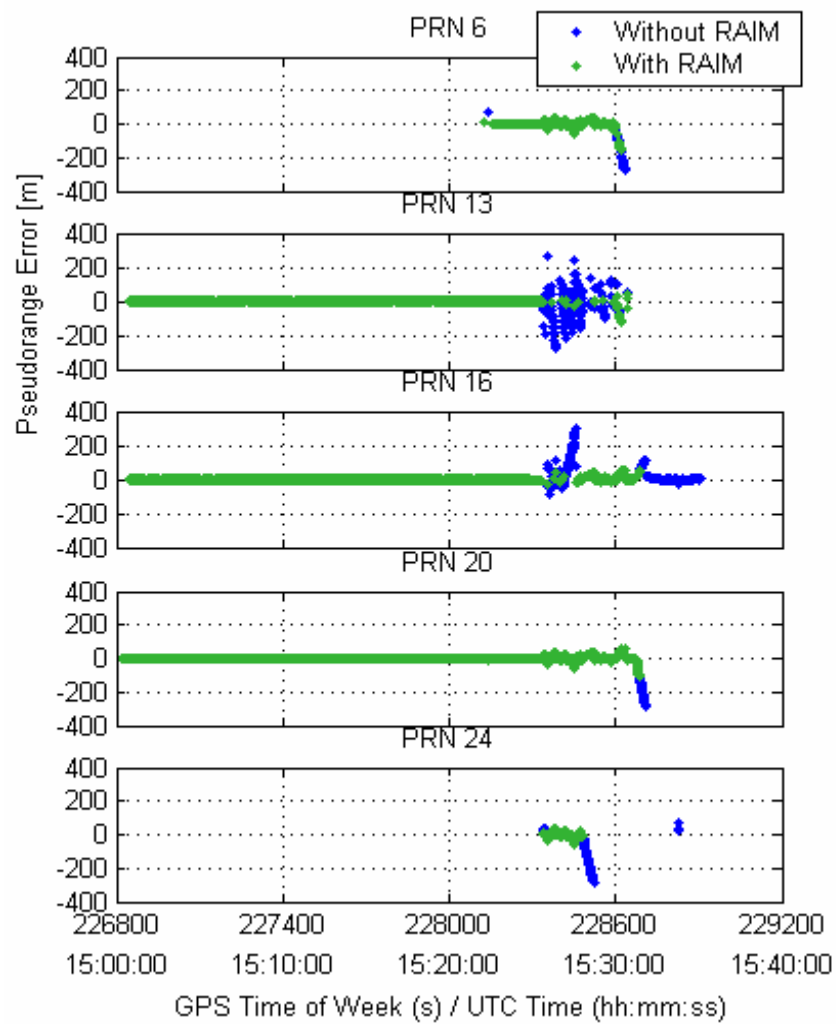
**Figure 6.5: Pseudorange Utilization for Position Solution under CWI –
Different I/S, without/with RAIM**
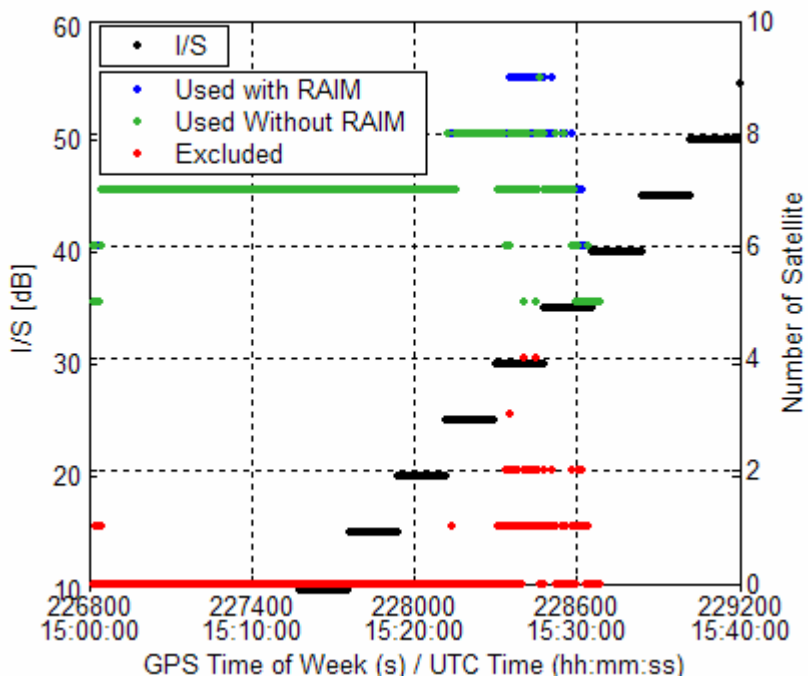
**Figure 6.6: Number of Satellites Used and Excluded for Position Solution
under CWI – Different I/S**

Table 6.1: Maximum 3D RMS Position Errors

I/S [dB]	Without RAIM	With RAIM
No	3.5	3.5
10	3.9	3.9
15	3.5	3.5
20	6.0	6.0
25	70.3	9.6
30	342.9	12.0
35	625.1	459.2

6.4 Conclusions

In this chapter, position error reduction under CWI using RAIM for the XTrac unit is studied. Since only some of the satellites are highly affected by this type of interference, the CWI effects on position estimation are considerably reduced when the required number of satellites is available. However, similar to other degraded environments, when the I/S is higher than about 30 dB, improvements are limited due to poor accuracy and lack of redundancy.

CHAPTER SEVEN: CONCLUSIONS AND RECOMMANDATIONS

7.1 Conclusions

This research has studied the performance of selected GPS receivers under interference conditions through two distinct strategies. To explore theoretical concerns, the first part of this analysis employed a software receiver. In order to test the impact of interference on actual commercial receivers, two commercial units were selected, including one high sensitivity unit that has the capability to operate under attenuated signal conditions. Hardware-in-the-loop tests were completed using a state of the art GNSS signal simulator. From these two tests, the followings are concluded: A CWI whose frequency is close to the L1 frequency causes false locks which may lead to large pseudorange errors and thus cause loss of tracking. Also, the effects due to narrowband interference are different for each satellite contributing to the particular position solution, due to different Doppler shifts and GPS C/A code line spectra. The interference lowers the C/N_0, which is a function of effective jamming power. Theoretically, the C/N_0 changes are very small when the CWI is near the first null of the GPS signal spectrum, i.e. L1+1 MHz. Although the test results show that the measured C/N_0 has a centre frequency dependency, it is weaker than the theoretical values, which may be caused by an increase in background noise due to interference.

Also, from these tests, it was observed that narrowband interference - regarded as signal power due to leakage - raises the measured values of C/N_0.

Use of the software receiver approach allows an investigation of tracking loop performance as well as other performances at various receiver settings. The following conclusions can be drawn from this approach:

1. Integration time: A longer integration time improves tracking performance under white noise conditions by effectively decreasing tracking loop jitter. However, under narrowband interference, improvements are limited because relatively low tracking jitter is observed.

2. Number of quantization bits: Under white noise interference conditions, the degradation of measured C/N_0 with 3 bits is approximately 0.5 dB, which is 1.8 dB higher than comparable test results for 1-bit quantization. Under CWI, the difference between these two quantizers increased with an increase in interference power.

3. DLL bandwidth: Two DLL bandwidths were investigated: 0.2 Hz and 2 Hz. The wide bandwidth tends to be locked on a false frequency more frequently. On the other hand, when using the same adaptive PLL, improvements in tracking jitters were not significant.

4. Correlator spacing: Based on the knowledge that the DLL tracking loop

jitter of a narrow correlator is less than that of a wide correlator, it follows that narrow correlators provide more accurate pseudorange estimates than those produced from wide correlators. However, in the case of a 2-MHz front-end bandwidth and the same adaptive PLL, the narrow correlator did not improve tracking thresholds.

5. Tracking loop errors: It was observed that the DLL tracking loop jitter under coloured noise interference was lower than that produced in the presence of white noise interference. The results also show that CWI centred near L1+500 kHz is associated with larger DLL tracking loop errors.

The performance of the XTrac and Allstar receivers were assessed under various interference conditions. The XTrac outperformed the Allstar under the tested interference scenarios in terms of both tracking and reacquisition performance. On the other hand, the Allstar performed better in terms of the accuracy of the tracking loop while maintaining tracking behaviour sufficient for positioning purposes.

The C/N_0 dependency on the centre frequency under CWI was investigated. When the I/S was 25 dB, the C/N_0 estimates for the XTrac varied from 31 dB-Hz to 37.5 dB-Hz for the range of CWI from L1 to L1+1 MHz; C/N_0 values for the Allstar varied from 40.8 dB-Hz to 42.3 dB-Hz. It was observed that the C/N_0

estimates within 1 kHz spectral depends on three factors: (i) unjammed C/N_0; (ii) the magnitude of line spectrum; and (iii) the frequency difference between centre frequency of both the interference imposed and of the line spectrum.

Raw measurements errors, tracking thresholds and position errors were also assessed under white noise conditions, CWI with three different centre frequencies, and BLWNI with 1 kHz bandwidth. The pseudorange errors for the XTrac unit increased to approximately 293 m and 754 m under CWI at L1 and L1+500 kHz, respectively, due to false locks, while the pseudorange errors of the Allstar unit did not exceed 6 m as this receiver tends to lose track entirely, rather than locking onto a false frequency. Pseudorange errors under white noise are less than 25 m and 2 m for the XTrac and Allstar, respectively.

Three different unjammed C/N_0 values were also investigated. The unjammed C/N_0 affected the XTrac unit up to levels of 30 dB and 35 dB of I/S for CWI at L1+5 kHz and BLWNI, respectively; by comparison, the unjammed C/N_0 affected the Allstar receiver up to levels of 40 dB to 45 dB of I/S for CWI at L1+5 kHz and BLWNI, respectively. Since the Doppler shift is a function of dynamics, under CWI, the interference signal remains in the tracking loop for less time, but more often. This changes the processing gain inside the receiver, and thereby produces changes in its tolerance to interference. During CWI at L1+5 kHz test,

PRN 25 (whose I/S = 32 dB) was falsely locked in static mode, while it was not falsely locked in dynamic mode for the XTrac unit.

Since only one or two of the satellites in view were highly affected at a particular time by CWI due to large processing gain changes, it was observed that RAIM is capable of improving the precision of position estimates in cases where large pseudorange errors occur with false locks and provided redundant measurements in an appropriate geometry are available.

7.2 Recommendations

All of the tests in this research were conducted using simulated interference sources without atmospheric errors. As discussed in Chapter 3, the interference sources simulated herein were not actually detected in the real world. Since interference sources are routinely reported throughout the world (and, hence, amidst actual and widely varying conditions), interference tests using actual sources of interference such as UWB interference, as well as an actual GPS signal, are recommended.

This research has sought to characterize the receiver's reaction to interference related to the DLL loop bandwidth and correlator spacing. However, a PLL is known to be a weaker link than a DLL. It is recommended that future research be

undertaken towards a performance analysis of GPS receivers under interference depending on PLL bandwidth.

Further research with a wider bandwidth of front-end filter and a higher sampling rate is recommended. Especially, since band-limiting rounds the correlation peak, a wider bandwidth of the front-end is required for the narrow correlator. However, to widen this bandwidth, a higher sampling rate is necessary, resulting in high computational burden.

As demonstrated in this study, the effects of interference could be explained with respect to the spectral characteristics of the GPS signal. Future signal architectures, such as GPS L2C, L5 and Galileo, employ various coding methods with different modulation frequencies. Thus, an analysis of new receiver behaviour using these signals under interference conditions will be most interesting.

REFERENCES

AGNSSCC (2001). Study of Interference to Civil GNSS Applications by out of Band Interference. Australian Global Navigation Satellite System Coordination Committee. November 2001.

Betz, J. W. (2002). Effect of Narrowband interference on GPS Code Tracking Accuracy. Proceedings of ION NTM-2000, January 26-28, 2000, Anaheim, California, pages 16-27.

Butsch, B. M., Dafesh P. A., Stansell T. A. (2002). Assessing Ultra Wide Band (UWB) Interference to GPS Receivers. Proceedings of ION GPS-2002, September 24-27, 2002, Portland, Oregon, Pages 1251-1259.

Caspary W.F. (1988). Concepts of Network and Deformation Analysis. The University of New South Wales, Australia, School of Surveying, Monograph, 11.

Deshpande, S.M. (2004). Study of Interference Effects on GPS Signal Acquisition. MSc Thesis, UCGE Report No. 20199, Department of Geomatics Engineering, University of Calgary.

Dong, L., C. Ma and G. Lachapelle (2004). Implementation and Verification of a Software-Based IF GPS Signal Simulator. Proceedings of ION NTM-2004, Institute of Navigation, January 26-28 2004, San Diego, California, pages 378-389.

FCC Report (2003). Report and Order and Second Furthuer Notice of Proposed Rule Making, Report No. FCC 03-290, Washington DC. Available at: http://hraunfoss.fcc.gov/edocs_public/attachmatch/FCC-03-290A1.pdf.

Forsell, B., Olsen T. B. (2003). Jamming GPS. GPS World, January 1, 2003, available at: http://www.gpsworld.com/gpsworld/article/articleDetail.jsp

Godefroy, B. (2004). Analysis of Potential CW Interference Effects Caused by UWB Devices on GNSS Receivers. Proceedings of International Technical Meetings of the Satellite Division, September 21-24, 2004, Long Beach, California, pages 187-196.

Hegarty, C. H., Tran M., Lee, Y. (2002). Simplified Techniques for Analyzing the Effects of Non-white Interference on GPS Receivers. Proceedings of ION GPS-2002, September 24-27, 2002, Portland, Oregon, pages 620-629.

IS-GPS-200D (2004). IS-GPS-200 Revision D dated 7 Dec 04. Navstar Global Positioning System Joint Program Office, Dec. 2004, pages 15-16, available at: http://www.navcen.uscg.gov/gps/geninfo/IS-GPS-200D.pdf

Jong, K. D. (2002). GPS Limitation and Vulnerabilities. GEO INFORMATICS, April/May 2002,available at: http://www.geoinformatics.com.

Jwo, D.J. (2001). Optimization and sensitivity analysis of GPS receiver tracking loops in dynamic environments. IEE Proceedings online no. 20010429, 2001.

Kaplan, E. (1995). GPS Satellite Signal Characteristics, Understanding GPS Signal Characteristics. Artech House, Inc.

Karunanayake, M. D., Cannon, M. E., Lachapelle, G. (2002). Effect of Kinematics and Interference on Assisted GPS (AGPS). Proceedings of ION NTM-2005, January 24-26, 2005, San Diego, California, pages 1071-1081.

Klinker, F., Pietersen, O. B. M. (2000). Interference of GPS signals: Influence of

Licenced Transmitters on the GPS Signal Quality in the Netherlands' Airspace. Proceedings of ION NTM-2000, January 26-28, 2000, San Diego, California, pages 260-267.

Kuusniemi, H., Lachapelle G. (2004). GNSS Signal Reliability Testing in Urban and Indoor Environiments. Proceedings of ION NTM-2004, Institute of Navigation, January 26-28 2004, San Diego, California, pages 210-224.

Luo, M., Akos, D., Pullen, S., Enge, P., Erlanson, B., Frodge, S. (2000). Interference to GPS from UWB Transmitters. Proceedings of ION GPS-2000, September 19-22, 2000, Salt Lake, Utah, pages 981-992.

Ma, C., G. Lachapelle, and M.E. Cannon (2004). Implementation of a Software GPS Receiver. In Proceedings of ION GNSS-2004,,Long Beach, California. September 21-24, 2004. pages 956-970.

Macabiau, C., Julien, O., Chartre, E. (2001). Use of Multicorrelator Techniques for Interference Detection. Proceedings of ION NTM-2001, January 22-24, 2001, Long Beach, California, pages 353-363.

MacGougan, G.D. (2003). High Sensitivity GPS Performance Analysis in Degraded Signal Environments. MSc. thesis, UCGE Report No. 20176, Department of Geomatics Engineering, University of Calgary.

Nguyen, T., Ely, J.J. (2004). DETERMINATION OF RECEIVER SUSCEPTIBILITY TO RADIO FREQUENCY INTERFERENCE FROM PORTABLE ELECTRONIC DEVICES. available at: http://techreports.larc.nasa.gov/ltrs/PDF/2002/mtg/NASA-2002-21dasc-txn.pdf

Phacas, M., Bickerstaff J., Haddrell T. (2004). GPS Jamming –the Enemy Inside! Proceedings of International Technical Meetings of the Satellite Division, September 21-24, 2004, Long Beach, California, pages 156-165.

Raquet, J.F. (2004). Engo 699.10 Lecture note: GPS receiver design. Department of Geomatics Engineering, The University of Calgary.

Ray, J. (2005). Engo 699.73 Lecture note: Advanced GPS Receiver Technology. Department of Geomatics Engineering, The University of Calgary.

Ryan, S. (2002). Augumentation of DGPS for Marine Navigation. Ph.D. Thesis, UCGE Report No. 20164, Department of Geomatics Engineering, University of Calgary.

Spirent communications limited (2003). SimGEN (Including SimLOCATE) user manual. Software for the Spirent range of satellite navigation simulator products.

Spliker, J.J. Jr. and Natali, F.D. (1996). Interference Effects and Mitigation Techniques, Global Positioning System: Theory and Applications Volume 1. American Institute of Aeronautics and Astronautics, Inc.

Teunissen P.J.G. (1998). Quality Control and GPS, Chapter 7 in GPS for Geodesy, 2nd Edition, Springer, New York, NY.

Titus B. M., Dafesh, P.A., Stansell T.A. (2002). Assessing Ultra Wide Band (UWB) Interference to GPS receivers. Proceedings of ION GPS-2002, September 24-27, 2002, Portland, Oregon, pages 1251-1259.

USCG (2002). SAFETY ALERT-TELEVISION ANTENNAE INTERFERENCE WITH GPS. available at: http://www.uscg.mil/HQ/G-M/MOA/DOCS/11-02.HTM

Van Dierendonck (1996). GPS receivers, Global Positioning System: Theory and Applications Volume 1. American Institute of Aeronautics and Astronautics, Inc.

Volpe Report (2001). Vulnerability Assessment of the Transportation Infrastructure relying on the Global Positioning System. John A. Volpe National Transportation Systems Center, August 29, 2001.

Zhodzishsky, M., Cherniavsky, D., Kirsanov, M., Vorobiev M., Prasolov V., Zhdanov A., Ashjaee J. (2002). In-band Interference Suppression for GPS/GLONASS. 2002 Javad Positioning Systems.